Acoustic Backscattering from Sea Ice at 10 - 100 kHz

by Dale P. Winebrenner

Technical Report
APL-UW TR 9017
January 1991

Applied Physics Laboratory University of Washington
1013 NE 40th Street Seattle, Washington 98105-6698

Contract N00039-88-C-0054

Report Documentation Page

Form Approved
OMB No. 0704-0188

1. REPORT DATE	2. REPORT TYPE	3. DATES COVERED
01 JAN 1991	**N/A**	**-**

4. TITLE AND SUBTITLE
Acoustic Backscattering from Sea Ice at 10-100kHz

5a. CONTRACT NUMBER
SPAWAR Contract N00039-88-C-0054

5b. GRANT NUMBER

5c. PROGRAM ELEMENT NUMBER
62435N

6. AUTHOR(S)
Dale P. Winebrenner

5d. PROJECT NUMBER

5e. TASK NUMBER

5f. WORK UNIT NUMBER

7. PERFORMING ORGANIZATION NAME(S) AND ADDRESS(ES)
Applied Physics Laboratory University of Washington 1013 NE 40th St. Seattle, WA. 98105-6698

8. PERFORMING ORGANIZATION REPORT NUMBER

9. SPONSORING/MONITORING AGENCY NAME(S) AND ADDRESS(ES)
Naval Oceanographic & Atmospheric Researh Laboratory, Code 242 Stennis Space Center, MS. 39529-5004

10. SPONSOR/MONITOR'S ACRONYM(S)

11. SPONSOR/MONITOR'S REPORT NUMBER(S)

12. DISTRIBUTION/AVAILABILITY STATEMENT
Approved for public release, distribution unlimited

13. SUPPLEMENTARY NOTES

14. ABSTRACT
This report considers high frequency (10-100 kHz) acoustic backscattering from the underside of sea ice from a fundamental physical point of view. The underice acoustic backscatter problem involves serveral issues in wave propagation and scattering not typically encountered in backscattering from other geophysical media (e.g., the ocean surface and floor). It is thus of instrinsic scientific interest, as well as being of vital interest in underwater acoustic applications.

15. SUBJECT TERMS
Arctic Beaufort Sea Ice Keels Acoustic Reflections Acoustic Scattering Sonar Ice Properties

16. SECURITY CLASSIFICATION OF:			17. LIMITATION OF ABSTRACT	18. NUMBER OF PAGES	19a. NAME OF RESPONSIBLE PERSON
a. REPORT	b. ABSTRACT	c. THIS PAGE			
unclassified	**unclassified**	**unclassified**	**SAR**	**118**	

ACKNOWLEDGMENTS

Many researchers at APL contributed time and effort in discussing aspects of the work in this report and helping to generate certain results. I would especially like to thank R.E. Francois, G.R. Garrison, R.P. Stein, T. Wen, D.R. Jackson, E.I. Thorsos, D.B. Percival, K.L. Williams, and J.C. Luby for valuable discussions and for their comments on all or parts of the manuscript. W.L.J. Fox and P.D. Mourad pitched in to help generate some of the more important results in Appendix 4A and Chapter 5, respectively. C.M. Bader assisted with programming and numerical analysis for the results in Chapter 5. R.D. Light and E.A. Pence provided input on plausible capabilities for an underwater vehicle suggested in Chapter 4. F.G. Olson contributed qualitative but valuable firsthand observations of underice morphology, and librarians P.T. Schneider and J.R. Doggett tracked obscure references above and beyond the call of duty. Finally, I am grateful to C.G. Sienkiewicz for initiating and supporting this research and for his patience in waiting for the final report.

ABSTRACT

This report examines the problem of acoustic backscattering from the underside of sea ice at frequencies between approximately 10 and 100 kHz. The approach is from the viewpoint of fundamental scattering physics. I begin with an examination of existing experimental results for clues to the basic processes involved. Based on this examination, I propose a partition of the backscattering problem into three component processes, namely direct backscattering from ice keels, forward reflection and/or scattering from flat ice, and modulation of the first two processes by the effects of ice-water transition layers. I then further examine experimental results bearing on the individual component processes, develop or explain some theoretical background where necessary, and propose experiments on a conceptual level to address key questions. The report concludes with some thoughts on future research directions under differing scenarios for scientific or application-oriented priorities.

CONTENTS

LIST OF FIGURES

Page

Chapter 1: INTRODUCTION

This report considers high frequency (≈ 10–100 kHz) acoustic backscattering from the underside of sea ice from a fundamental physical point of view. The underice acoustic backscatter problem involves several issues in wave propagation and scattering not typically encountered in backscattering from other geophysical media (e.g., the ocean surface and floor). It is thus of intrinsic scientific interest, as well as being of vital interest in underwater acoustic applications.

The purpose of this report is to specify measurements and analysis of ice and acoustic field properties that support development of practical scattering models. Physically based scattering models for acoustic reverberation simulations, as well as other applications in the general domain of exploratory development, are of particular interest. In what follows, I will pay special attention to issues of importance in high-frequency acoustic reverberation simulations (see Goddard [1986] and Miyamoto [1986], among others). Most applications at present involve sea ice in the Arctic rather than the Antarctic; thus I will concentrate on acoustic scattering from the types of sea ice and sea ice formations characteristic of the Arctic. Nonetheless, I hope that the work presented here will prove useful to a wide variety of people working on fundamental and applied underice acoustics problems in many environments.

Over approximately the past 25 years, a number of investigations have produced limited sets of underice reflection and scattering measurements in the Arctic. These investigations were often undertaken with rather specialized measurement goals. Taken together, the results of this work allow some qualitative understanding of the underice scattering problem. However, fundamental questions remain as to the nature of underice scattering processes, and the data necessary for quantitative modeling of these processes are not yet in hand.

In this report, I assume some general familiarity with the ice cover in the Arctic and its basic physical structure and properties. An excellent introduction to these topics is provided by Maykut [1985]. I begin by using the results of previous studies to conceptually partition the problem of high frequency acoustic backscattering under ice into three practical subproblems, each concerned with a particular fundamental reflection or scattering mechanism or physical effect. This is the subject of the next chapter. In the following three chapters, I assess what is known about the physics of each subproblem and discuss measurements and analyses that will contribute toward qualitatively and quantitatively understanding these phenomenon for the purposes of modeling. I also suggest conceptual designs for experiments to acquire the necessary measurements.

The final chapter provides a concise summary of my findings and inferences, and some thoughts on priorities for future work based on scientific considerations.

Chapter 2: BACKSCATTERING AS A COMBINATION OF PHYSICAL PROCESSES

Section 2.1: Introduction

This chapter is a survey of what is presently known and can be inferred about high frequency underice backscattering, based on experimental evidence to date. Its purpose is to identify and clarify areas on which to focus further research. The outcome of this survey will be the identification of three distinct physical effects which apparently act together to produce the backscattering observed under ice. The three following chapters consider the individual subproblems in detail and develop strategies for further investigation of their most immediately relevant aspects.

Some elaboration on this approach may be in order. As noted in Chapter 1, the purpose of this report is to identify those experimental and analytical investigations that would most strongly contribute to modeling of underice backscattering. The scattering models whose development is to be supported are to be physically based, but may not build directly on first principles in all their parts. This suggests an approach in which we first address the most *primary questions* regarding the physical processes involved. For example: What are the roles of scattering and reflection from physically differing types of ice (ridged, relatively undeformed, etc.)? Is scattering from a particular type of ice due to surface scattering, volume scattering, some combination of these two, or some other type of mechanism? Answers to these questions would help to identify the relevant *refined questions*, which might include: What are the dependencies of compressional and shear wave speeds, density, absorption, and their vertical profiles on the ice temperature and salinity profiles, especially in the lower ice–water transition layer? What effect do these dependencies have on the reflection coefficient of the water–ice interface? Investigation of these *refined questions* should, in turn, help to better understand primary issues, and perhaps raise new *primary questions*. Thus, a kind of dialectic can begin between investigation of *primary* and more *refined questions* within the province of "basic research."

It will become clear in this chapter that many primary questions on underice backscattering presently remain open. Thus, I will concentrate most attention in this report on primary questions, on the premise that this is the best place to begin both scientifically and from the standpoint of simulation. I will provide entry points into the literature on more refined questions where appropriate, but the reader will find relatively little discussion of such questions in this initial investigation.

Section 2.2 introduces the broad outlines of the present physical understanding of underice backscattering by taking a primarily historical approach. Section 2.3 considers existing observations in sufficient detail to motivate and support a proposed partition of the backscattering problem into subproblems, each concerned with a distinct physical reflection or scattering effect. Detailed reviews of what is presently known about individual subproblems are, however, left to the chapters concerned with those subproblems.

Section 2.2: Background

When sea ice freezes, it is relatively flat, and its lower surface displays only small amplitude (order 1–100 cm) variations in draft on fairly long (order 1–100 m) horizontal scales. Relative motion of ice floes due to forcing by winds and currents pulls ice apart to expose open water, and shears or compresses ice into piles of broken rubble on the topside and undersides of floes at their boundaries. The open water areas are known as leads. The topside and underside ice features are known, respectively, as ridges and keels. Keels can extend tens of meters below the sea surface and are the major contributors to underice roughness. The horizontal length scales associated with keels and the spacing between them are typically hundreds to thousands of meters. The underice surface is thus a composite of features that arise from very different physical processes: relatively flat areas on the undersides of undeformed ice (or ice which has not been deformed very much) and rubble piles of deformed ice. Further distinctions in ice types that may be relevant to acoustics involve the age of the ice or ice feature. Relatively new ice in a frozen lead may have different surface properties and roughness from older, undeformed first-year ice, and undeformed multiyear ice may differ from both of the younger ice types. Relatively jagged, newly formed ice keels may scatter sound quite differently from older, consolidated keels. Leads constitute gaps in the ice cover, in which the air–water interface is likely to be wind-roughened. (Maykut [1985] discusses this in greater detail, giving many references.) This, very briefly, is the scattering medium which gives rise to underice backscattering.

Section 2.2.1: Measurements with explosive sources

Attempts to characterize and study underice acoustic reverberation at frequencies approaching high frequencies evidently began in the early 1960s. The first group of studies used explosive charges as sound sources. Receiving hydrophones and banks of filters were used to record (most typically) the backscattered signal within frequency bands over a wide range of frequencies. Ray tracing and deconvolution of the source spectrum were then used to estimate the backscattering strength of the underice surface as a function of frequency and grazing angle. Both the source and the receiving hydrophones were typically omnidirectional in azimuth, so an azimuthal average of the backscattered signal over a rather large area was actually recorded. This experimental technique had previously proven useful in characterizing acoustic reverberation from the open ocean surface. Such studies were undertaken by several investigators at a number of locations in the Arctic during several seasons.

The first such study of which I am aware is that of Mellen and Marsh [1963], in which bistatic scattering was characterized at a number of locations over a frequency range from 40 to 8000 Hz. This study produced the often-quoted comment, "Ice causes reverberation levels as much as 40 dB greater than those encountered from the ice-free sea surface." Brown [1964] measured backscattering strength in 1 octave bands from 1.28 to 2.56 kHz and from 5.12 to 10.24 kHz for summer sea ice in the Canadian Archipelago. His reported backscattering strengths are 10–20 dB lower than those indicated

by the work of Mellen and Marsh [1963] and are similar in both absolute level and in their dependence on grazing angle and frequency to backscattering strengths observed for an open sea roughened by a 30 knot wind. Milne [1964] measured backscattering between 12 Hz and 4 kHz from broken and packed first-year ice in the Canadian Arctic in April. He reported only a weak dependence of backscattering strength on grazing angle (between 5° and 14°) at kilohertz frequencies. He also reported an absolute level comparable to that reported by Mellen and Marsh [1963], and thus up to 20 dB higher than that reported by Brown [1964]. Chapman and Scott [1964] reported backscattering strengths for young first-year ice in the Gulf of St. Lawrence, for grazing angles from 15° to 70° and frequencies from 400 Hz to 25.6 kHz. Their results show little frequency dependence and tend to be a few decibels below those reported by Brown [1964]. Thus they are much lower than those reported by Milne [1964]. Brown and Brown [1966] measured backscattering strengths in octave bands between 1.28 and 10.24 kHz for grazing angles from 10° to 70° under uniform, melting, first-year ice in the Canadian Archipelago. Their values for backscattering strength fall significantly below even those of Brown [1964]. Finally, Brown and Milne [1967] reported backscattering strength measurements of ridged, first-year ice in the Beaufort Sea taken in April, for frequencies between 40 Hz and 10.24 kHz and grazing angles between approximately 5° and 70°. They find little frequency dependence and levels comparable to those reported by Milne [1964] and Mellen and Marsh [1963].

Taken together, these studies suggest at least two things. The first of these is that the overall level of underice backscatter depends strongly on underice roughness, and thus on the amount of deformed ice in the ensonified region. At low acoustic frequencies where the roughness is relatively small compared with the radiation wavelength, we might expect backscatter models based on perturbation theory to apply. However, even in this case, Mellen [1966] found that the underice surface roughness spectrum inferred from backscatter measurements using perturbation theory was in poor agreement with independent measurements of the actual roughness spectrum. This suggests that the physics of the underice backscatter problem may differ from that of other backscatter problems (e.g., backscatter from the ocean surface) where scattering from homogeneous surface roughness is the primary effect.

The second thing suggested by these studies is that seasonal changes in underice properties may strongly affect backscatter. However, seasonal variations in the water column are also likely to strongly affect the backscatter observed and to confound any other seasonal effects. Thus this second inference is weak when based only on the studies reviewed so far.

These initial studies provided a "zeroth-order" look at underice backscatter, establishing its large strength, variability, and connection with underice roughness. However, later research has made it clear that the methods used by this first group of investigators also tended to obscure elements of the physics of the problem in several ways.

As noted above, underice roughness consists of distinct kinds of features (keels, relatively flat ice) that are formed by very different physical processes. There is every reason to suspect (and experiments reviewed below confirm) that each kind of feature

scatters sound differently. As was noted above, the measured backscattered intensity was typically an azimuthal average over an annulus on the underside of the ice, and this annulus contained one or more types of roughness. The samples of backscattered intensity were thus likely to be averages over backscattering from distinct kinds of roughness. Such an average obscures the differing natures of backscattering from the different roughness types and is of limited use in understanding how an observer using a directional sonar would perceive underice backscattering. Note that this difficulty does not occur in cases where the surface roughness is statistically homogeneous within the ensonified area, as for example is typically the case in sea surface scattering experiments using the method of the studies reviewed above.

Milne [1964] has also noted that explosive sources may excite flexural waves in the ice cover. Such waves could cause reradiation from ice discontinuities that would be indistinguishable from acoustic backscattering. There is thus no guarantee that measurements made using explosive sources are comparable to those made with directional sonars. However, this may be less of a problem at the high frequencies of interest in this report.

Section 2.2.2: Studies using directional sonars

The second group of studies began in the early 1970s and has continued to the present. The common feature of this group is the use of high frequency directional sonars to characterize underice backscattering.

The first of these is apparently that of Berkson et al. [1973], in which a sonar operating at 48 kHz with a narrow (1.5°) horizontal and wide (51°) vertical beam was used. The pulse length was 1 ms. The transducer was lowered to a depth of 8.8 m through a hole in 1.5 m of first-year ice in a frozen lead surrounded by ridges. The maximum range was evidently between 275 and 550 m. Thus the nominal grazing angles in this experiment were much smaller than those typical of the explosive source experiments, ranging between approximately 1° and 20°.

The experiment took place approximately 175 km north northeast of Barrow, Alaska, in May 1972. By rotating the transducer, the experimenters produced a qualitative range–azimuth map of relative backscattering strength (for the relatively small grazing angles used in this experiment). When the range–azimuth sonar map is compared with an aerial photograph of the experimental area, the degree of coincidence between regions of strong backscatter and ridged ice is striking. Backscattering from resolution cells in intervening regions of undeformed ice is at least 20 dB lower than that of many cells below visible surface ridges. However, the spatial extent and distribution of regions within keels that produce strong returns are unclear from these data because horizontal beamwidth and azimuthal sampling interval were both large enough to obscure direct observation of these quantities.

These qualitative results generally agree with those from an experiment conducted using the same sonar near Fletcher's Ice Island (T-3) in April 1972 [Kan et al., 1974] (though performed before the experiment near Barrow, this experiment was reported later). A notable feature in this experiment was the observation of a fairly linear ridge

(presumably with an associated keel) on the surface that did not appear on the sonar survey. This may have been because the angle between the mean line of the keel and the sonar line of sight, i.e., the aspect angle, was relatively small in contrast to other cases where the angle was fairly close to 90°.

The results of measurements reported by Garrison et al. [1974] further confirmed the relationship between deformed ice and strong backscattering and provided better quantitative characterization. The acoustic frequency was 60 kHz, the horizontal transducer beamwidth was approximately 7°, and a 4 ms pulse was used. These measurements were made during March and April 1973 in the Bering Sea. Independent measurements showed that the sound speed in the water column under the ice was very uniform with depth; ray traces based on the sound speed measurements showed little refraction for the ranges involved in these measurements. The authors present range–azimuth maps of the backscattering strength of individual resolution cells. Very uniform flat ice, 75–80 cm thick, under which the sonar transducer was suspended, produced resolution cell target strengths of less than –27 dB. However, ice in resolution cells under large ridges routinely displayed target strengths of 0 to +12 dB. Regions of strong backscattering on the maps appear as circular arcs, centered on the transducer position, lying roughly along and at the range of deformed ice features. Such arcs could result from azimuthal smearing of localized backscattering regions by the transducer beam pattern. Alternatively, arcs would also be observed if the backscattering regions of ice subtend a large horizontal angle at the transducer. It is unclear from the data as presented whether the arcs observed result from one cause or the other. It is also unclear from these data whether apparent regions of low backscattering between arcs of strong backscattering could, in some cases, have been caused by shadowing of the ice rather than by its backscattering properties.

Garrison et al. [1976a and b] report similar but more extensive backscattering measurements, made, respectively, in the Beaufort Sea in April 1974 and in the Chukchi Sea in April 1975. Sound speed conditions in the Beaufort were strongly upward-refracting, while those in the Chukchi were nearly nonrefracting. Measurements were made at 20 and 60 kHz, using pulse lengths of 1 and (apparently, at times) 4 ms. The horizontal beamwidth of the 20 kHz transducer was approximately 10°. Both new deformation features and the undersides of old, hummock-covered ice produced strong backscattering. Figure 2.1 (reproduced from Garrison et al. [1976a]) shows the raw observed backscattering at 60 kHz.

Garrison et al. [1976a] selected the peak target strength for each distinct arc of strong backscattering and plotted the position of these peaks on a range–azimuth map. This is reasonable if one suspects that azimuthal smearing of localized strongly backscattering regions is taking place. The results are shown for 20 and 60 kHz, respectively, in Figures 2.2 and 2.3 (also reproduced from Garrison et al. [1976a]). The apparent spatial clustering of strongly backscattering ice around deformed ice is much tighter than in, for example, Figure 2.1. Thus the spatial association of strong backscattering with deformed ice is strengthened further, and there is some indication that backscattering arises from spatially localized regions within areas of deformed ice. Note that the target

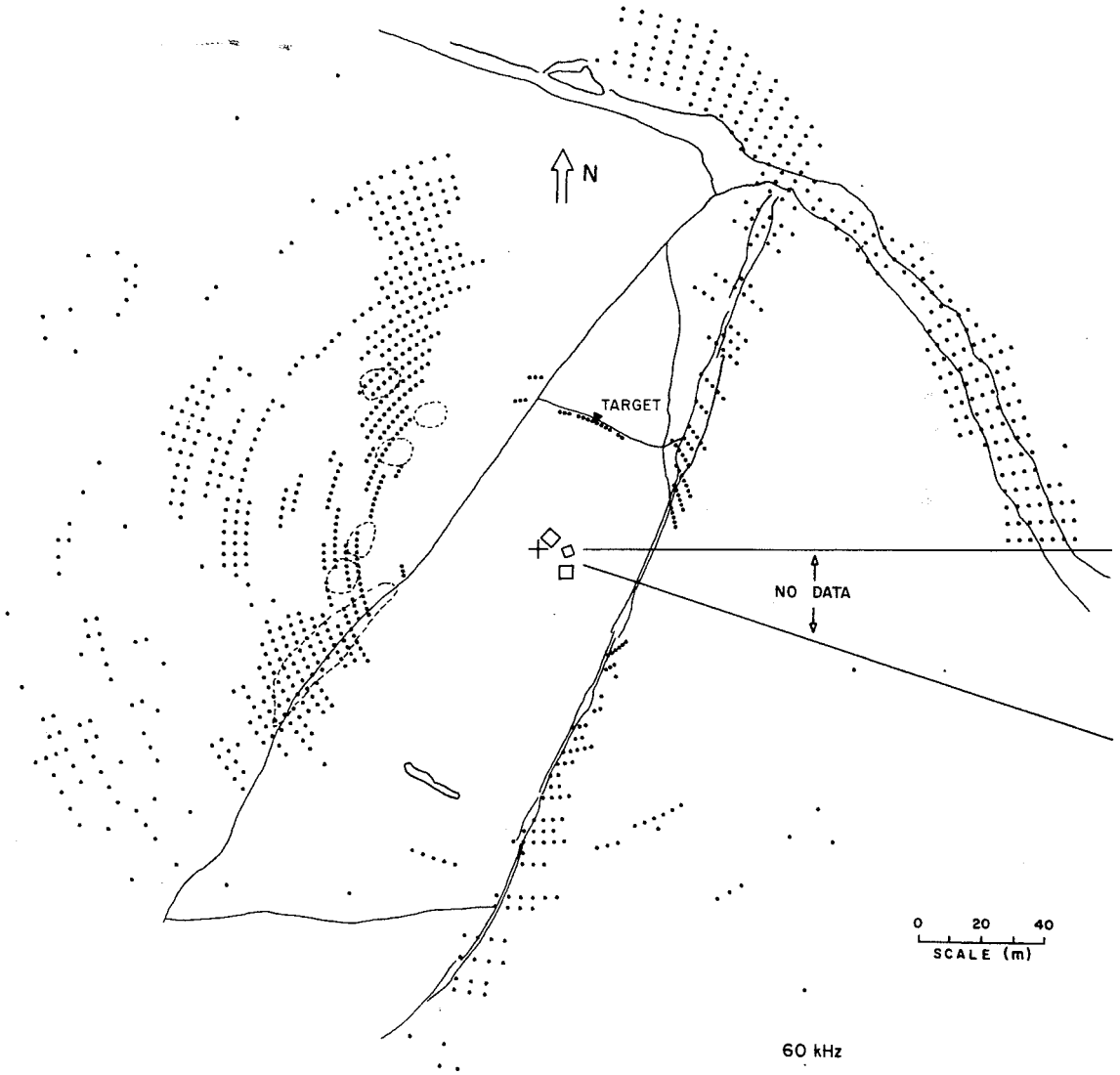

Figure 2.1. Reflections from underice features with target strengths exceeding −35 dB.

strengths in Figures 2.2 and 2.3 are generally higher for the new ridge than for the old, hummock-covered ice, but that the difference between ice types is smaller at 20 kHz than at 60 kHz. Note also that there appear to be fewer but stronger targets at 20 kHz versus 60 kHz. This suggests a nontrivial frequency dependence for backscattering. (However, there was apparently an unresolved 6–9 dB calibration problem at 60 kHz, and a 1–3 dB problem at 20 kHz. Thus the target strengths given may vary systematically from their true values by these amounts, and the difference in calibration errors may confound the true frequency dependence of backscattering.)

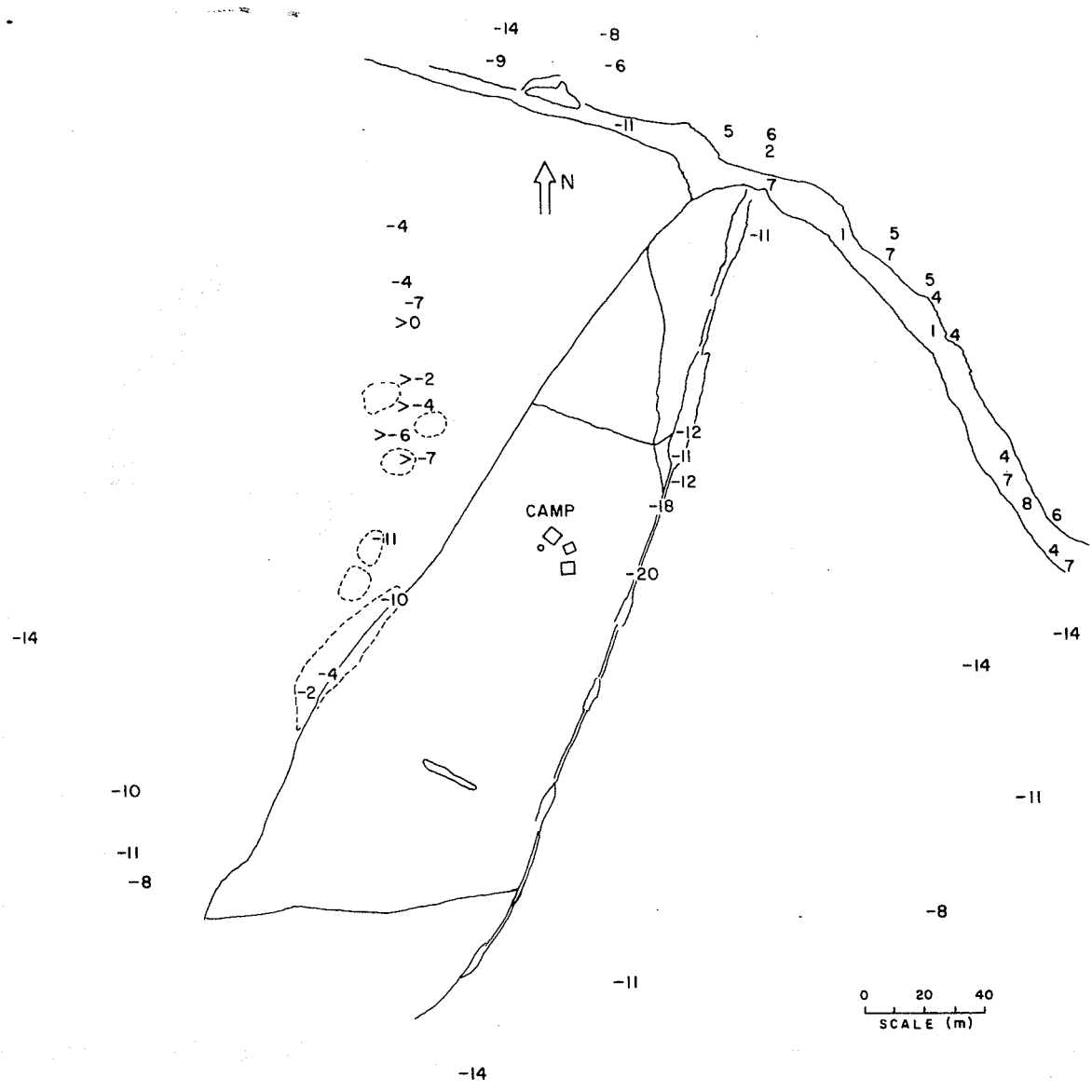

Figure 2.2. Peak target size of underice features at 20 kHz.

Results from an experiment reported by Francois et al. [1981] confirm and extend earlier results. This experiment took place northeast of Barrow, Alaska, in June and July 1977, and used essentially the same frequencies and equipment as previous experiments. Sound speed conditions in the water column were highly variable and refracting. The authors used two methods in an attempt to better observe localization of backscattering features.

First, they examined backscattered intensity versus transducer azimuthal angle (i.e., the so-called scan azimuth angle) in angular neighborhoods around large backscattered

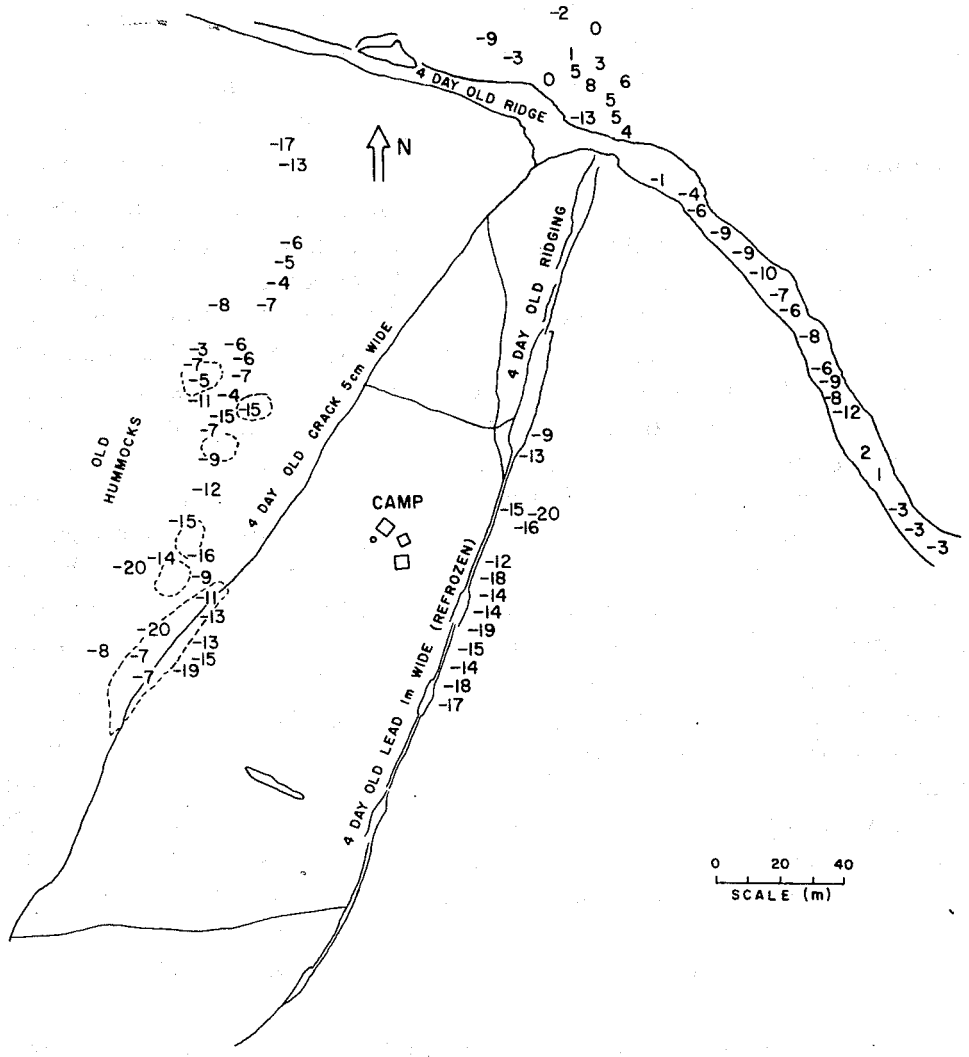

Figure 2.3. Peak target size of underice features at 60 kHz.

returns. The angular increment between pulses was 2°, which was considerably smaller than the horizontal beamwidths of the transducers. In approximately half the cases observed, the backscattered intensity as a function of transducer azimuthal angle had almost exactly the shape of the horizontal transducer beam pattern as a function of angle. The other half of the observations showed a structure similar to overlapping transducer beam patterns and, in a few cases, simply a broad angular spread. The maximum of the intensity versus scan azimuth curve provides an estimate of the azimuthal location of the backscatterer.

Second, the authors computed the apparent azimuthal location of nine large returns using the difference in phase of the received signal between the left and right halves of

the transducer array. The results show considerable scatter from ping to ping, but support the estimate of azimuthal angle based on beam pattern matching to within approximately 4° (see Figure 54 of Francois et al. [1981]). Data for both horizontal phase angle and intensity versus scan azimuth for a similar experiment are shown in Figure 2.4, which is reproduced from a later report by Garrison et al. [1986a] (see Section 3.2).

From these two lines of evidence, it appears that many strong backscattered returns originated from areas that subtended angular widths at the transducer which were narrow compared with the horizontal transducer beamwidth (approximately 10° at 20 kHz). At the ranges of 100–200 m used in this experiment, a 1° subtended angle corresponds to 1.75–3.5 m in horizontal extent. The evidence certainly does not exclude the possibility that even those returns for which azimuthal scans of the transducer trace out replicas of the transducer beam pattern could originate from areas subtending angles at the transducer on the order of the beamwidth. For example, scanning past a large, acoustically flat, appropriately oriented ice face could produce a trace of the transducer beam pattern. It would be necessary, however, that the ice face be large enough to fill the beam during most of the scan past and/or that no comparably strong scatterers exist on either side of the ice face within a distance subtending an angle of approximately one beamwidth (the latter would produce interfering returns at the beginning and/or end of the scan past the face and distort the trace of the beam pattern). In fact, scanning any configuration of coherently interacting scattering centers (and thus, a configuration that itself has a well-defined beam pattern) would, under the same conditions, produce a trace of the transducer beam pattern. The key question is the likelihood of satisfying the necessary conditions. The highly disorganized configuration of ice in keels would seem to make the satisfaction of such conditions too improbable to explain the observed frequency of cases displaying good replicas of the beam pattern. It thus appears more likely that the regions of ice responsible for the returns observed in the experiments above were indeed, in many cases, localized within areas having characteristic horizontal dimensions of 10 m or less.

The proportion of returns originating from highly localized regions to the total number of returns (including those that show overlapping beam patterns or no beam pattern), however, remains poorly determined. Furthermore, an experiment discussed in Section 3.2 suggests that the scattering centers observed in long range experiments may in fact be clusters of yet more highly localized scattering centers. The characteristic scale of such clustering and whether clustering of clusters (i.e., multiscale clustering) occurs remain unknown. Nonetheless, later observations tend to support the general view of scattering from localized regions in keels. Before discussing later work, it is worthwhile to consider the implications of the experiments reviewed so far, and to focus further investigation on the basis of these implications.

The paradigm of isolated backscattering regions led to the development of empirical target strength distributions per unit area, corrected to a degree for the effects of transducer beamwidth and pulse length [Garrison et al., 1984]. However, it was found that these empirical distributions are strongly dependent on geographical location (or, more directly, on the nature of the local ice cover) and on the refractive conditions present in the water column.

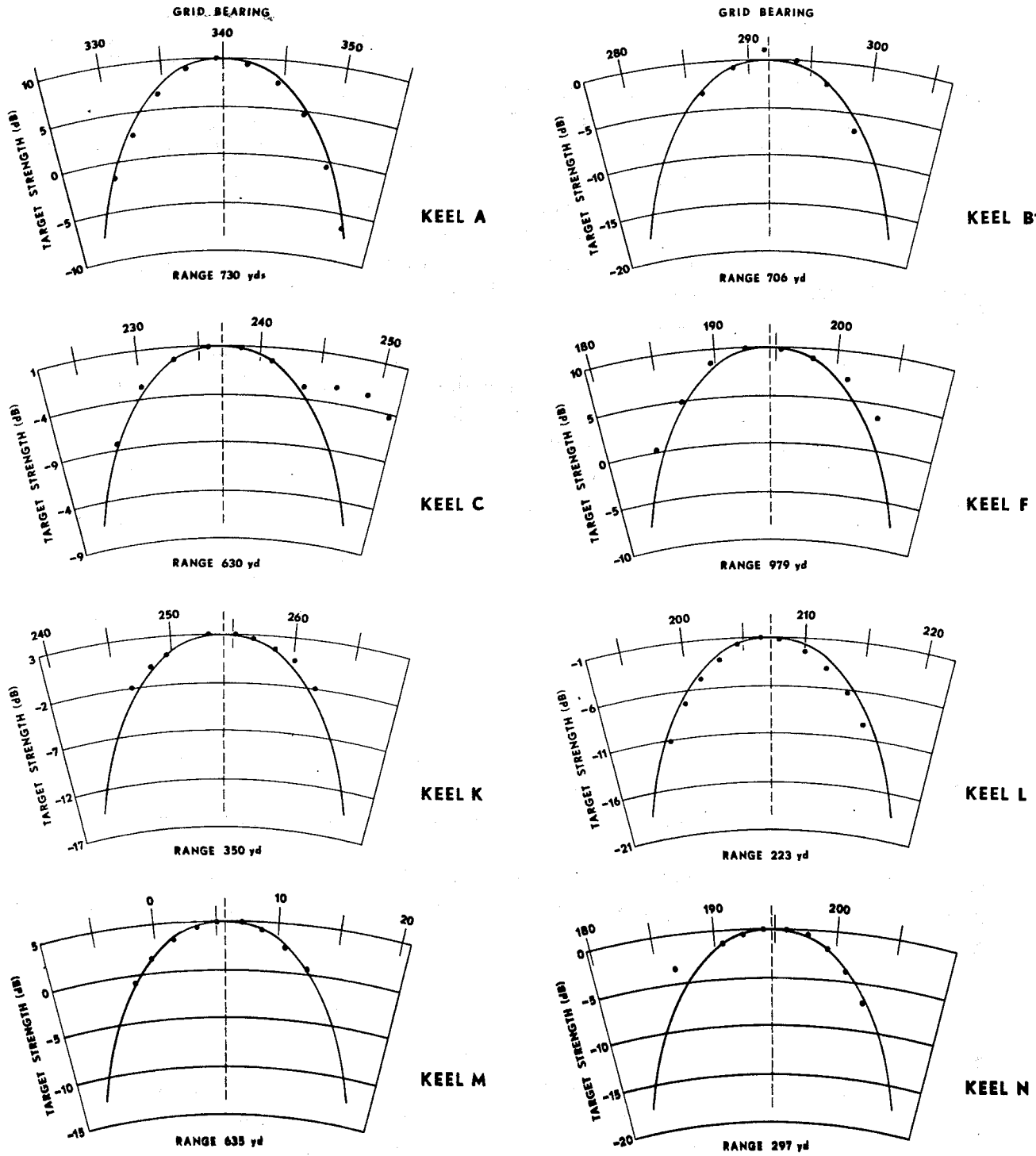

Figure 2.4. The returns from eight selected keels as the transducer scanned past. The match to the transducer pattern (solid line) indicates the point-like nature of the reflector.

This latter observation points up another fundamental limitation of the types of experiments reviewed so far. All of them were performed in such a way that several distinct physical effects may have contributed to the backscattering observed. For example, acoustic refraction in the ocean beneath the ice can be very strong and variable. Upwardly refracting conditions can increase backscattering by bringing rays up to the underice surface nearly vertically, and can produce shadow zones and other effects as well. Forward reflection and/or scattering of sound propagating between a transducer and an ice keel may lengthen backscattered returns in time and alter other characteristics of backscattering. In turn, the character of forward reflection and scattering may be affected by properties of the ice–water transition layer, which may vary with ice type, thickness, temperature profile, etc.

Experiments such as those just reviewed are clearly needed to illuminate the "big picture" of underice backscattering and directions for further research. Indeed, the results of these experiments are the basis of the following discussion. Such experiments are also needed to provide data for tests of theories or simulations concerning backscattering. However, in order to really understand the complete, complex problem, it seems useful to conceptually partition the problem into component effects, each of which involves fewer variables than the problem as a whole. With a quantitative, physical understanding of the individual components, a solid, testable theory of the composite backscattering phenomenon can then be constructed. An argument for a particular partition of the backscattering problem, based on a directed review of more recent experimental data, is the subject of the next section.

Section 2.3: A Proposed Partition of the Backscattering Problem

From this point on, this report will be concerned as much as possible with only those physical effects contributing to backscattering which involve the sea ice cover itself. In particular, I will not attempt to consider the effects on backscattering of refraction and scintillation caused by sound speed variations in the water beneath the ice. In discussing experimental evidence, I will try to avoid basing inferences on results that may be confounded by this or any other physical effects not directly connected to the ice cover.

Section 2.3.1: Scattering from localized regions in ice keels

From the previous section, it is clear that the primary cause of high frequency underice backscattering is scattering from regions of grossly deformed ice, i.e., from ice keels. That deformed ice displays distinctive scattering behavior is not very surprising; deformed ice features are extremely disordered because of the physical processes at work in their formation. These processes are very different from the processes of frazil and congelation ice production. The morphological changes of deformed ice are also likely to differ strongly from those of other ice types [Weeks and Ackley, 1982], causing changes in acoustic behavior over time that are distinct from those of other ice types.

Thus, backscattering, and perhaps bistatic scattering (see below), from ice keels is the first physical process that I propose as an element of the backscattering process. Existing observations indicate that the nature of this element is complex, and much about it remains to be examined, even empirically. Given that the significance of this process is already well established, I will defer further review of the present knowledge of this element to Chapter 3. For completeness, note also that there is some evidence that, in summer, melt ponds which have melted completely through the ice also give rise to significant direct backscattering [Francois et al., 1981]. However, the relative rarity of melt ponds extending all the way through the ice would seem to make this a secondary effect.

Scattering and reflection from ice that displays no gross deformation features stand in contrast to scattering from keels. Throughout the remainder of this report, I will refer to the former type of ice, in partial accordance with previous terminology, as "relatively flat ice." This term, however, does require some further definition, since presently available data suggest that the underside of sea ice is rough on many spatial scales [Rothrock and Thorndike, 1980]. A working definition for high frequency under-ice acoustics is proposed at the beginning of Chapter 4.

Direct backscattering from relatively flat ice has been shown to be very small in comparison with backscattering caused by keels. The first measurements of this effect of which of I am aware are reported by Garrison et al. [1974]. The large-scale (deformed and undeformed ice) backscattering measurements discussed above indicated target strengths for resolution cells of relatively flat ice to be less than –27 dB at 60 kHz and small grazing angles. The authors made further measurements of backscattering from very uniform ice approximately 90 cm thick, which "... must have frozen without disturbance." These measurements were made at four separate locations, also at 60 kHz, and using the same apparatus used previously. The grazing angle ranged between approximately 5° and 45°. The observed amplitude distribution of backscattering (based on 100 samples, each the average of 10 correlated measurements) was non-Rayleigh (cf. Chapter 4 and references therein). The deviation from Rayleigh statistics was due to a larger than expected relative frequency (approximately 5%) of amplitudes much greater than the mean. The authors assumed that these samples were caused by backscattering from deformed ice and discarded them when estimating backscattering strength versus grazing angle. (Although this procedure warrants further examination, a reading of the data report suggests that the conclusions below are unlikely to be significantly altered in any event.) Garrison et al. [1976a and b] report data at 20 and 60 kHz obtained using essentially the same procedure. These authors state, but do not show, that the 20 kHz amplitude data are more nearly Rayleigh distributed than the 60 kHz data, and that data at grazing angles greater than 30° are more nearly Rayleigh-distributed than those at lower angles. All the data just mentioned involve late winter or early spring ice that showed no signs of melting. (For completeness, note also that backscattering data at much higher frequencies of 100–300 kHz for relatively flat ice are reported by Garrison et al. [1984].)

A summary of backscattering strength per unit area versus grazing angle at 60 kHz is shown in Figure 2.5, which is reproduced from Garrison et al. [1976b]. Backscattering per unit area from cold, relatively flat ice is evidently very weak in comparison with backscattering from deformed ice. Its level and angular behavior are fairly similar to acoustic scattering from an air–water interface with relatively small, wind-induced

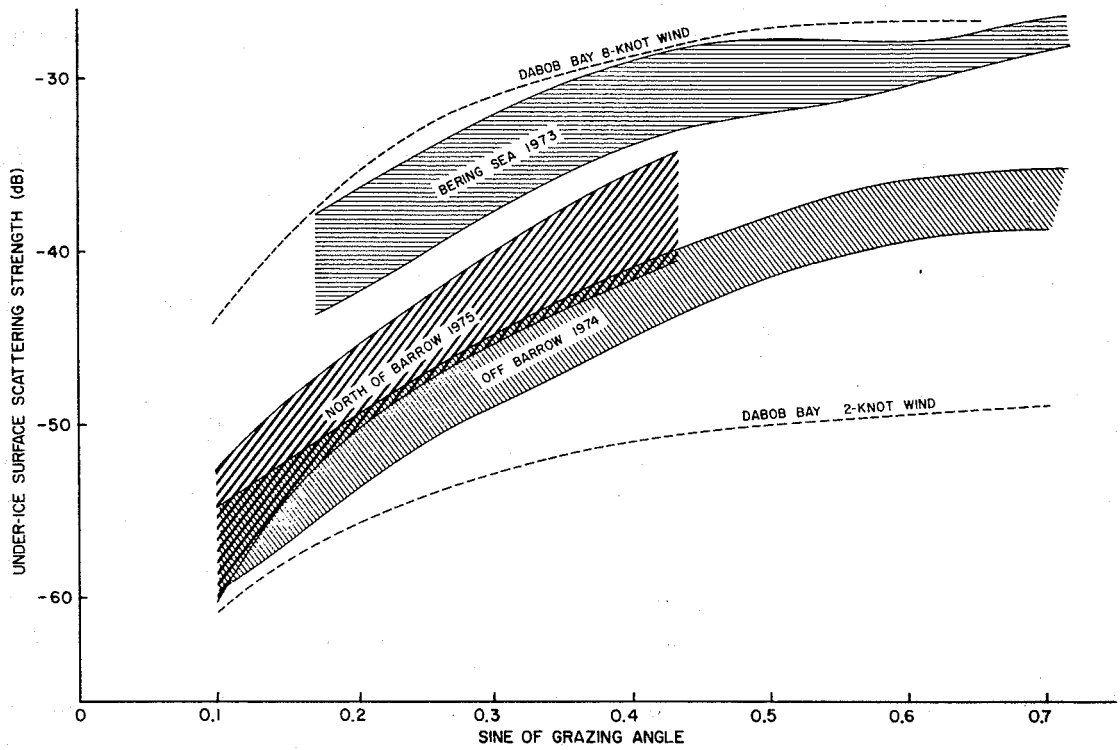

Figure 2.5. Underice backscattering strength measurements at 60 kHz.

roughness. This suggests that backscattering from relatively flat ice may be nearly indistinguishable from backscattering from open leads. Because it is relatively weak and apparently otherwise unremarkable, I argue, with one caveat, that this physical effect is a minor element of the total backscattering problem. The caveat is that it has not been shown that this type of backscattering is small for all ice conditions. Under certain seasonal and/or melting conditions, this argument may need to be revised. With this noted, I will leave further consideration of this physical effect for later, more refined work, and will not discuss it further in this report.

Section 2.3.2: Forward reflection and/or scattering

There is reason to think that another, potentially significant, though less obvious, element of the backscattering problem exists. Suppose that the scattering from keels occurs not only in the backward direction, but also bistatically into some range of directions. Radiation scattered upward may then be reflected and/or scattered again back to the sonar by relatively flat ice and would thus contribute to the total backscattered return. The significance of such a contribution would depend on the typical directions and angular pattern of radiation scattered from the keel, and on what fraction of energy incident on the relatively flat ice is redirected back into the water. To my knowledge, the first discussion of this scattering process in the literature appears in a report by Garrison et al. [1984].

Consider Figure 2.6, in which an ice keel is ensonified by a sonar from a typical range of 800 m and depth of 40 m below the undeformed ice–water interface. Assume that there is no ray-bending in the water beneath the ice. Undeformed, i.e., relatively flat, ice lies between the sonar and the ice keel. Suppose a localized scatterer exists within the keel 5 m below the level of the undeformed ice–water interface. Then radiation scattered bistatically into an angle 6° from the ensonifying direction, in the direction toward the relatively flat ice, could be specularly reflected or scattered back to the sonar.

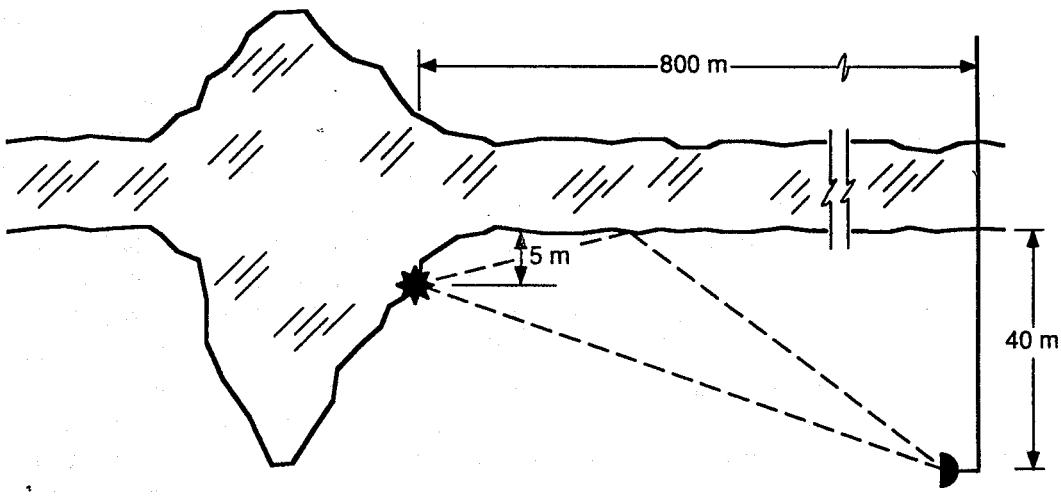

Figure 2.6. An ice keel ensonified by a sonar from a range of 800 m and a depth of 40 m below the undeformed ice–water interface.

Existing measurements indicate that much of whatever energy is scattered toward relatively flat ice is reflected and/or scattered back into the water, at least at grazing angles like those in the example of Figure 2.6. The intensity of sound redirected into the water from relatively flat ice at these angles, although highly variable, is on average diminished by 3 dB or less from incident intensity. (A thorough review of existing measurements of this phenomenon is given in Section 4.2.) Thus, one of the conditions necessary for forward reflection and/or scattering to be important appears to be met.

There is also some direct experimental evidence that sound is often scattered bistatically by keels up toward the relatively flat ice. Garrison et al. [1986a] report measurements made in November 1984 in the Beaufort Sea. Sound speed conditions were very uniform, and the measurements were made at ranges of less than 150 m; thus refractive effects were minimal. Monostatic and bistatic scattering from a one month old keel were measured at 20 kHz, using a receiving transducer array that allowed estimation of the vertical and horizontal arrival angles of signals (using the phase difference between halves of the array). The array depth was 12 m. The vertical angles of arrival in monostatic measurements indicated an apparent vertical distribution of localized keel scatterers between 3 and 7 m depth. At the short range in this experiment, there were no monostatic observations of vertical arrival angles, which would indicate that the return arrived via the relatively flat ice surface. The authors performed bistatic measurements, varying the depth of a transmitter with broad directionality near the keel between 1.5 and 12 m. The receiver depth was apparently held constant at 12 m. The vertical arrival angles at the receiver of bistatically scattered signals indicated that, in a large majority of cases (at least 85%), the signals had been forward reflected and/or scattered from the relatively flat ice. Assuming specular reflection from the relatively flat ice, a distribution of vertical keel scatter positions was deduced which agreed well with the analogous distribution estimated from the monostatic data. There were, however, some unresolved mysteries regarding the estimated vertical arrival angle for the direct pulse [see pages 27–29 of Garrison et al., 1986a], which could have affected the estimation of vertical arrival angle for scattered returns.

Suppose that the angular distribution of radiation from an ice keel scatterer is broad enough to include the backscattering direction, as well as the direction of a return path via the relatively flat ice surface. Then the directly backscattered and surface path returns would, if they overlap in time, interfere at the sonar location. The measurements of Garrison et al. [1986a] indicate widths of the bistatic scattering pattern for keel scatterers of 2–6°. Widths at the upper end of this range would produce interference between direct and surface bounce paths in the example in Figure 2.6. However, measurements reported by McDaniel [1986] indicate a smaller angular width. These measurements were made in the Beaufort Sea in October 1984 in a region of heavily ridged ice. A directional, split-beam receiver at 65 m depth was used in conjunction with a near omnidirectional source, the depth of which was varied between 50 and 75 m. The horizontal range between source and receiver was 240 m, but the range from either transducer to the keel being studied evidently varied up to something on the order of 1 km. Ray tracing based on measured sound speed profiles indicated that refraction was negligible over the ranges in this experiment. The acoustic frequency was 20 kHz, and 2 ms pulses were used. Individual scatterer observations were selected on the basis of stable horizontal arrival angle at the receiver, as the source was raised and lowered. The observations appear to show bistatic vertical scattering pattern widths on the order of 1°. This width is too small to cause interference in the example of Figure 2.6. Thus, a small proportion of the existing data indicate that interference between direct and surface path returns can occur. The data suggest that wide vertical beamwidths are not common, but inferences based on the present data are necessarily weak because the data set is small and the measurements are difficult.

To summarize, the geometries of the underice surface and typical sonar positions lead to consideration of backscattered returns that have been forward reflected and/or scattered from the underside of relatively flat ice. Present data on the fractional intensity of sound forward reflected or scattered from relatively flat ice support the likely significance of this mechanism. There is also one data set supporting the contention that ice keels scatterers often redirect radiation up toward the relatively flat ice to undergo forward reflection or scattering, though some unsettling mysteries in this data set remain. Present data on vertical scattering pattern widths of ice keel scatterers are very limited. Thus while it appears that forward reflection and/or scattering could well contribute to backscattering, the experimental evidence for this contention is inconclusive at best.

The practical implications of such a mechanism would, however, be highly significant in a number of applications, particularly those involving low grazing angles. Briefly, these could include broadening of backscattered pulses or the creation of double and triple backscattered pulses, the introduction of considerable noise in vertical arrival angle estimation (i.e., glint noise), and changes in the spreading loss of amplitude or intensity with range. These implications are reviewed in Chapter 4 (Section 4.4), where sufficient background is given to support detailed discussion.

Because of the potential implications of forward reflection and/or scattering, I argue for its inclusion as an element of the complete backscattering problem worthy of further investigation. Secondary reasons for considering this element may include its possible significance and implications in backscattering from objects other than ice keels, and the fundamental insight into acoustic interaction with ice that we would gain.

Section 2.3.3: Transition layer effects

The last proposed element of the backscatter problem arises from small scale observations of the ice–water interface and acoustic reflection, rather than from the large scale observations reviewed above. Comprising this element is the physical effect of the porous, ice–water transition layer on reflection and/or scattering from ice. The existence of this transition layer has been known for some time. For example, Weeks and Ackley [1982] discuss the thermodynamics of the formation of this layer, referencing work on sea ice or sodium chloride ice as far back as 1963. Francois et al. [1981] report on casts of the underside of sea ice. These clearly show the dendritic, sometimes spongy character of the ice–water interface, at least for summer sea ice. The penetration of a thin solution of the casting material into the porous ice layer was observed to be approximately 0.8 cm in most cases, but may have been as large as 2.5 cm in part of one cast. These figures suggest a thickness of approximately 1 cm for the lowest, extremely porous part of the transition layer. The total thickness of the transition layer is variously estimated to be between 1 and 20 cm.

There have been a few observations of the acoustic properties of the transition layer and its effect on reflection. Bogorodskii et al. [1976] report very high frequency (800 kHz) measurements showing a compressional wave speed less than that in seawater in a newly grown ice layer approximately 1 cm thick overlying seawater. In thicker ice

layers, the compressional wave speed approaches twice that in seawater. However, because these measurements were made on newly grown ice layers rather than in thin ice layers comprising a thicker ice sheet, there may be some question as to the applicability of results in the latter case.

Stanton et al. [1986] report reflection coefficient measurements at 100–800 kHz for an artificial sea grown in a pond. They found that the presence of a dendritic transition layer (under conditions of rapid ice growth) decreased the reflection coefficient at 188 kHz by a factor of three over a case when no transition layer was present. The reported thickness of the transition layer is comparable to the acoustic wavelengths at 10–100 kHz. This suggests that an acoustic effect will also be observed at these lower frequencies. Modeling by Posey et al. [1985], Yew and Weng [1987], and Chin-Bing [1985], among others, supports this idea. This work will be reviewed in greater detail in Chapter 5.

Acoustic transition layer effects are likely to be important in the backscattering problem because of their effect on reflection and/or scattering from blocks of ice in keels and on forward reflection and/or scattering from relatively flat ice. In the case of ice blocks in keels, the effect may occur if ice growth on the keels also leads to formation of transition layers [see Chin-Bing, 1985]. In the case of relatively flat ice, the potential role of transition layers in preventing shear mode conversion could substantially alter behavior of the ice–water reflection coefficient [Posey et al., 1985]. Finally, the results of Stanton et al. [1986] suggest that the operation of upward-looking sonars, such as those used for studies of ice draft, may also be influenced by transition layer effects through their modification of the ice reflection coefficient. These are the bases for my designation of transition layer effects as the third element of the backscattering problem.

In summary, the approach in the remainder of this report is to treat the problem of high frequency underice backscattering as a composite of at least three fundamentally different physical effects or elements. The approach to better understanding the composite phenomenon is to develop a better understanding of and physical models for the component processes. The effects of the problem elements can then be combined, perhaps using simulation, to test our understanding of the composite problem. The first three proposed problem elements are scattering from localized regions in ice keels, forward reflection and/or scattering from relatively flat ice, and ice–water transition layer effects on ice acoustic properties.

Finally, note that the approach in this report differs fundamentally from previous theoretical approaches to underice backscattering. For example, Greene and Stokes [1985], Middleton [1985], and McDaniel [1987] develop two-scale roughness models for the underice surface and compute backscattering cross sections assuming that scattering from the rough ice–water interface is the dominant effect for both ice keels and undeformed ice. Ellison [1980], on the other hand, assumes that backscattering from ice keels is due to reflection from the faces of an ensemble of ice blocks formed in the deformation process. No other physical effects are considered. By contrast, the approach in this report considers potential contributions to backscattering by several physically distinct mechanisms, separately considering possible contributions from two physically very distinct types of ice. The nature of reflection and scattering from different ice types is not

assumed a priori, but rather inferred, to the degree possible, from observations. Further measurement programs can then be defined to confirm or eliminate hypothetical physical explanations of the observations. The sequence of investigations is guided iteratively by cycles of observation and theoretical development, rather than set by a particular theory of backscattering which, a priori, determines the important questions to ask and eliminates other possibilities from consideration. While the present approach is clearly more limited in its ability to provide immediate results, I think it will provide a more direct path through the morass of potential issues to a physical understanding of underice backscattering.

Chapter 3: DIRECT BACKSCATTERING FROM ICE KEELS

Section 3.1: Introduction

The discussion of direct backscattering from ice keels in Chapter 2 ended with the evidence in the data that returns frequently originate from spatially localized areas. In this chapter, I will examine further evidence as to the nature of the scattering producing the returns and suggest an approach for further investigation.

The next section reviews two recent experiments and their results which bear on the nature of the backscattering process in keels. In both experiments, long range backscattering was measured in a way similar to previous experiments, but in these cases the behavior of backscattering with varying acoustic frequency was also observed. One of the experiments included backscattering measurements at short range and produced especially interesting results. Section 3.3 then presents an assessment of the state of current knowledge and some recommendations for further experimental investigation. The proposed focus of experiments should produce data that are immediately useful in simulations of underice backscattering, as well as in better understanding the nature of scattering in keels.

Section 3.2: Background

Garrison et al. [1986a and 1987] report measurements at 20 and 30 kHz made during October and early November 1984 in the Beaufort Sea. Short range observations of a single, newly formed keel at 20 kHz are reported primarily in the first reference, with additional observations at differing times and transducer depths reported in the second. Long range observations of many keels at both 20 and 30 kHz are reported in the second reference.

In the series of long range measurements [Garrison et al., 1987], the transducers were suspended at approximately 60 m depth. The range of ice observed varied between 545 and 1404 m. Conditions in the water column produced strong upward ray-bending for these ranges and transducer depths. The pulse length in most measurements was 0.4 ms, though in a few cases lengths of 1 and 2 ms were used. Vertical and horizontal split-beam phases were recorded and later used to locate scatterer positions.

One particular keel (denoted keel K) containing many scatterers with large target strengths was selected for more detailed study. Garrison et al. [1987] observed agreement between azimuthal scatterer locations derived from transducer pattern matching and those derived from horizontal split-beam phase measurements (see Section 2.2) to within 3° (30 m at 600 m range) in 33 out of 34 scatterers in keel K at 20 kHz. In 27 cases, the two estimates of azimuthal location agreed to within 1.5°. Note, however, that the comparison described here was carried out only for strong scatterers.

Qualitatively, very little correlation was observed between the apparent positions of strong scatterers at 20 kHz and those at 30 kHz. This was true both for keel K and more

generally for all keels and scatterers observed. It should be noted, however, that possibly two hours elapsed between the sets of measurements at different frequencies. Returns at 20 kHz were shown to be repeatable over periods of up to 15 minutes. The question of whether this result would hold over periods of hours, even at a single frequency, was not addressed. Thus the significance of the observed lack of correlation remained unclear. Looking at the aggregates of targets observed at the two frequencies, target strength distributions at 30 kHz were somewhat higher than those at 20 kHz, i.e., there were somewhat greater numbers of scatterers of a given target strength at the higher frequency.

The short range measurements reported by Garrison et al. [1986a] were observations of a ridge that developed near the APL ice camp during early October 1984. Monostatic observations of the new keel at 20 kHz and range 90–130 m were made. Initially, a line array at 60 m depth was used to examine the keel. These measurements are reported by Garrison et al. [1987]. Eight days later, a more extensive set of measurements was made using a piston transducer at 12 m depth. The latter measurements are reported by Garrison et al. [1986a]. The positions of scatterers observed in the two cases do not correlate well. It is unknown whether this was partially or completely due to changes in the keel during the intervening time, to the differing incidence angles due to differing transducer depths, or both.

Scatterer positions in the new keel were estimated during the second, more extensive set of measurements using both transducer pattern matching and split-beam phase data. Of 19 distinct scatterers observed, 15 traced out a good replica of the transducer beam pattern as they were scanned, providing a first estimate of their azimuthal position. For these 15 scatterers, the standard deviation of split-beam azimuthal position estimates indicates a position accuracy of 0.75 m.

Plots of scatterer positions show a marked clustering along the keel with characteristic cluster diameters on the order of 15 m (see Figure 3.1, reproduced from Garrison et al., 1986a). Clusters this size and smaller would appear as a single localized scatterer in the long range measurements reviewed above. Closely spaced adjacent clusters could easily produce the overlapping beam pattern signature frequently observed in azimuthal scans. The azimuthal scan signature of clusters larger than about 15 m could be broad and flat if the cluster is composed of numerous small elemental scatterers, or very erratic if the cluster consists of only a few large scatterers. Furthermore, the frequency response of clusters would be chaotic and decorrelate over very short frequency shifts, just as reported by Garrison et al. [1987] and in a later report that will be reviewed momentarily. Thus clusters of scatterers represent a promising hypothesis as to the nature of backscattering from keels. Unfortunately, there were no simultaneous long and short range observations of the same keel during the course of this experiment with which to test this hypothesis.

Garrison et al. [1989] report further long range backscattering observations with more detail concerning the frequency dependence of scattering between 20 and 50 kHz and with more attention given to calibration issues. A study of the effects of pulse

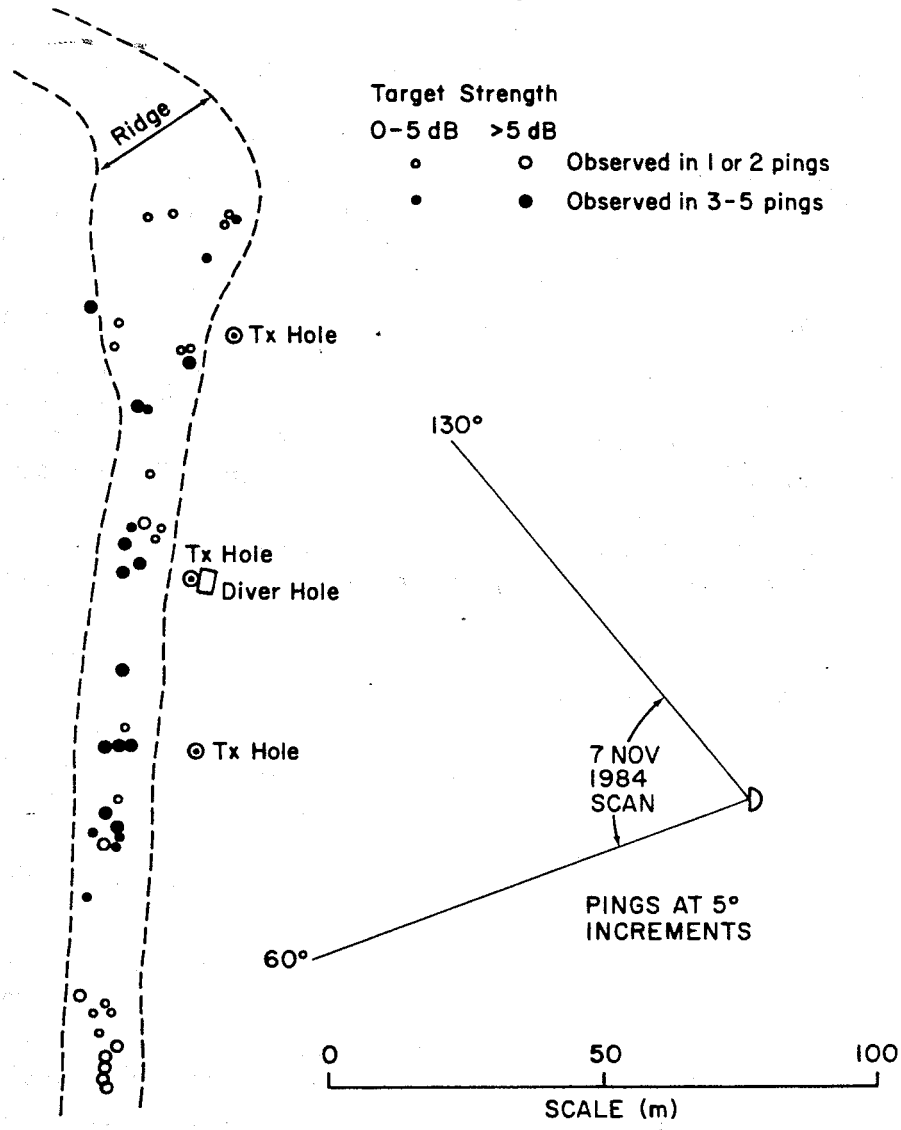

Figure 3.1. The location of the keel reflectors observed in a 20 kHz scan from 120 m away.

lengths was made for pulse lengths in the range 0.3 to 50 ms. The experiment was conducted at an ice camp in the Beaufort Sea in March 1986. The ice camp was situated on multiyear ice next to a frozen lead approximately 2 m thick.

Newly formed keels were observed to have a much higher density of scatterers than older keels. Divers examined areas under the ice near the apparent origin of large acoustic returns, but the resulting associations of underice morphology with acoustic features were not conclusive. Of 31 detailed observations of strong scatterers reported in this experiment, only 10 scatterers produced good replicas of the transducer beam pattern as they were scanned. This is a considerably smaller fraction than that found in previous experiments.

Pulses were transmitted at a series of frequencies at 5 kHz intervals, beginning at 20 kHz and continuing to 50 kHz. This series was immediately followed by another series at 2 kHz intervals, beginning again at 20 kHz and continuing to 28 kHz. The two 20 kHz pulses were transmitted 28 s apart, allowing for a short time-scale check. Several of the largest returns show up at all frequencies, though the detailed form of the return as a function of time or range varies considerably even over 2 kHz intervals. Numerous returns appear to fade and then reoccur as frequency shifts by 4–6 kHz (see Figure 3.2, reproduced from Garrison et al. [1989]). The cross-correlation between echos at different frequencies from the same regions of ice drops within 2–4 kHz to between 0.7 and 0.9, sometimes seeming to rise again for differences in frequencies near 20 kHz (see Figure 3.3, also reproduced from Garrison et al. [1989]). However, correlation of the two 20 kHz returns (25 s apart) is near but less than one, indicating some source of decorrelation probably unrelated to the ice. The horizontal arrival angle estimate from split-beam phase measurements also varied with frequency by 1–2° (page 43 of Garrison et al. [1989]).

In interpreting these observations, one should note that the pulse shapes actually transmitted varied substantially as functions of frequency (see the authors' appendix on calibrations using freon-filled spheres). It is also possible that the returns observed at the ranges used were actually combinations of those arriving directly from keel scatterers and those arriving via a forward reflection or scattering event on relatively flat ice between the transducer and the keel. Thus the observed frequency behavior may not characterize the behavior of the keel scatterers themselves. The observed variation of estimated horizontal arrival angle could conceivably be equipment-related. However, taken together, I think that these observations tend to support the hypothesis that scatterers in keels consist of collections of more elemental, spatially localized, interfering scatterers. Numerical simulations reported by Garrison et al. [1989] and the fact that estimates of azimuthal position based on beam patterns do not differ wildly from split-beam phase estimates indicate that the azimuthal separation of elemental scatterers subtends an angle small compared with the beamwidths of the transducers at ranges of hundreds to a thousand meters.

Section 3.3: Assessment and Proposed Measurements

Inferences from the studies reviewed above and in Chapter 2 can be summarized as follows. Newly formed ice keels show a much higher spatial density of scattering centers than do older, presumably more consolidated, keels. A substantial fraction of backscattering events observed at ranges of hundreds to thousands of meters evidently arise from spatially localized regions of ice having a characteristic size on the order of 15 m. A substantial number of the remaining events seem to arise from pairs of such localized regions appearing simultaneously within the acoustic beam, and the remainder simply show a broad azimuthal pattern. The number of events belonging to each class has varied substantially between experiments at different times in different locations, and thus remains poorly determined. The frequency dependence of events observed at long

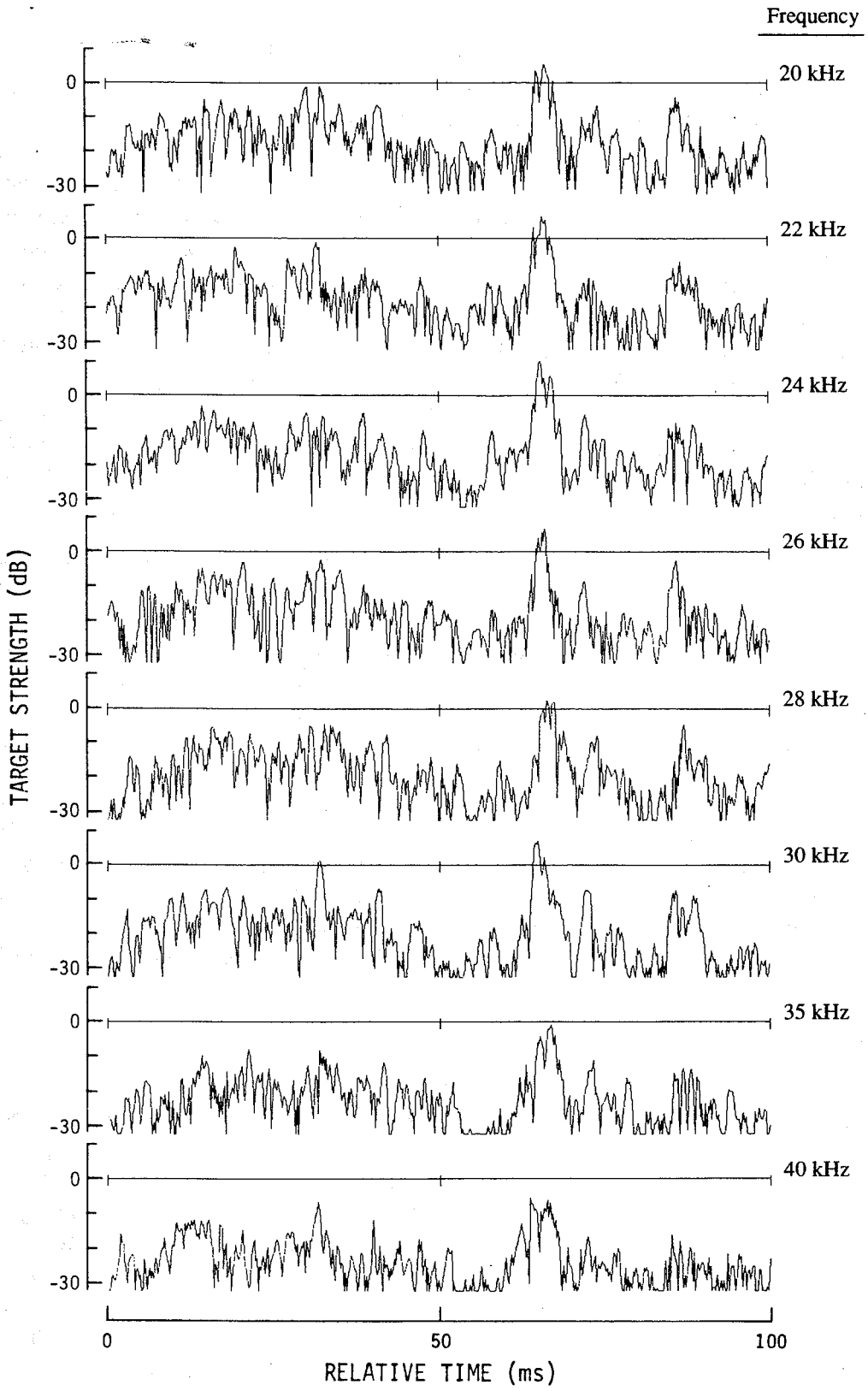

Figure 3.2. Frequency-varying reverberation for underice areas containing keels.

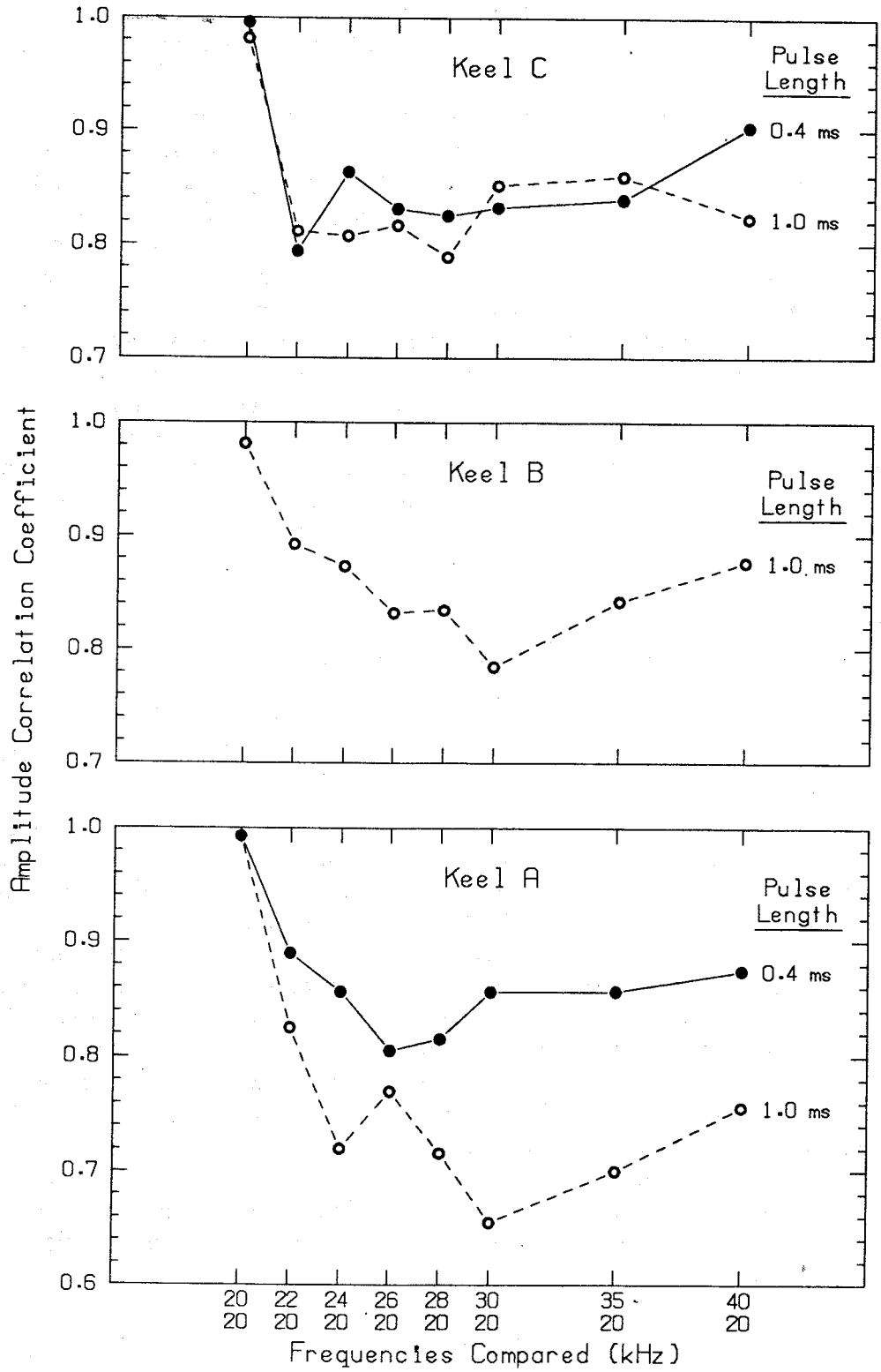

Figure 3.3. The correlation between 10 ms intervals of reverberation at different frequencies for Keels C, B, and A.

ranges is chaotic even for frequency shifts of a few kilohertz, though part or all of this may be due to interference between direct and forward-bounce paths involving relatively flat ice between the transducer and the keel.

The sole set of observations at short ranges, i.e., at approximately 100 m range, strongly suggests that scattering centers in keels often occur in clusters with characteristic size 15 m, at least in newly formed keels. This in turn suggests that backscattering events observed at long range are in fact coherent superpositions of interfering elemental scatterers. This would at least qualitatively explain the chaotic frequency dependence observed at long ranges. Variations in the physical sizes and spacing of clusters could be expected to produce instances of events appearing to originate from closely spaced regions and of events with broad azimuthal patterns, as are in fact observed. The nature of elemental scatterers remains completely obscure. Such scatterers might in fact be just blocks of ice oriented to produce backward reflection (as is assumed, for instance, by Ellison [1980]), but could just as well be blocks of ice fortuitously arranged to produce a corner reflector, properly shaped water voids between ice blocks, or perhaps other configurations. A reasonable guess is that elemental scatterers arise from a variety of ice structures. However, so far as I have been able to uncover, no substantial evidence for any particular view exists. Furthermore, there are many unresolved issues such as what is the size scale on which clustering occurs, does this scale depend on the ridge being formed predominantly by shearing or by compression or does it depend on the thickness of the ice before ridging. What controls the number and target strength distribution of elemental scatterers within a cluster is likewise obscure. It seems possible that clustering takes place on a range of spatial scales; multiscale behavior is very common among other random natural processes. However, virtually no data exist on what scaling laws, if any, apply to such clustering.

From a fundamental physical standpoint, I would recommend that further study of direct backscattering from keels focus mainly on clustering for the following reasons. First, whatever the characteristics of elemental scatterers, the characteristics of clustering are vital to understanding the nature of backscattering. In fact, characteristics of backscattering may be largely controlled by cluster characteristics (e.g., the number of scatterers per cluster and size of the cluster) rather than by properties of the elemental scatterers (see, for example, Jao [1984]). Second, the characteristics of clustering, once known, may provide some clues about, or limit possible models of, elemental scatterers. For example, the minimum spacing between elemental scatterers will limit the physical size of any configuration of ice hypothesized to produce an elemental scatterer. Finally, it may turn out that such a wide variety of ice configurations can serve as elemental scatterers, or that such a wide variety of any particular form occurs that no model of elemental scatterers based on first principles is possible or desirable. This would leave data on cluster characteristics as the only information useful in understanding and predicting the acoustic environment.

The first thing to establish, then, is that the clusters observed at short range by Garrison et al. [1986a] are typical and that they are indeed associated with the localized scattering centers observed at long range. Simultaneous short range and long range

observations are essential. I would recommend picking a strong, apparently well-isolated scatterer from a long range survey for short range acoustic inspection while long range observations are continued or resumed. Establishing a firm correspondence between acoustic objects in these two sets of observations is likely to be easier than when using long range acoustic observations and divers, because once the short range sonar is in place, a relatively large area can be quickly mapped out, and because the comparison of observations is between sets of acoustic data rather than between acoustic and visual data. The short range sonar must be directional with a beamwidth similar to that of sonars presently in use in order to locate elemental scatterers within clusters. Multi-frequency observations at short range are highly desirable, in order to compare the frequency response of elemental scatterers with that of the cluster observed at long range.

If isolated clusters can be linked to isolated long range scatterers, then the next step would be to see whether pairs of clusters with short separations can produce long range observations resembling overlapping beam patterns of the long range transducer. Finally, one would want to show that very large clusters exist and that they indeed produce the strong, azimuthally broad patterns sometimes observed.

The next major step would be to study the length scale or scales of clustering, the spatial density and target strength distribution of elemental scatterers within clusters, and so on. Unfortunately, almost no quantitative guidance on characterizing the statistics of these quantities is available because one has almost no a priori idea what the statistics might be. From a scientific standpoint, as well as that of prediction, it would be fascinating to know to what extent these characteristics depend on the age of the keel and, for new keels, the conditions of formation (i.e., the relative amount of deformation due to shear versus compression, the thickness of the ice ridged, etc.). This could eventually provide a direct link between regional ice climatology and large scale ice motion data and the acoustic environment.

The experimental approach I have just recommended obviously requires development of a self-contained, sled-mobile, albeit relatively low power, sonar, as well as an (ideally quick and easy) means of deploying the transducer for such a sonar through the ice. Given the variety of small platforms that presently carry self-contained sonars, this task is certainly technically feasible. The question of whether the expense and level of effort required are justifiable depends on other than scientific considerations. A brief discussion of the importance of backscattering from keels in a few underice applications is given in Chapter 6. However, questions of justification on other than scientific grounds are for the most part beyond the scope of this report.

Chapter 4: FORWARD REFLECTION AND SCATTERING FROM RELATIVELY FLAT ICE

Section 4.1: Introduction

The aim of this chapter is to develop a strategy for better understanding acoustic forward reflection and scattering from "relatively flat" ice. This type of ice is easily defined for newly grown ice, such as that often found in frozen leads; in this case, it is simply ice that has not yet been ridged. For older first-year ice, and especially multiyear ice, the definition of "flat ice" is less straightforward because presently available data suggest that the underside of sea ice is rough on many spatial scales [Rothrock and Thorndike, 1980]. In such cases, the definition of "relatively flat" ice depends largely on the specific problem of interest. Very little information on underice roughness on the small (1 cm–100 m) spatial scales of interest in high frequency acoustics exists. Thus it seems most reasonable for the present to simply set a threshold (say, approximately 1 m) for deviations of the underice surface from the local mean ice draft (averaged over an appropriately sized local area, on the order of hundreds to perhaps thousands of square meters) and to define any contiguous piece of sea ice to be "relatively flat" if it contains no deviations greater than the threshold. This operational definition (perhaps with some modification of the parameters) should serve to separate most ice having deformation features that would produce large isolated acoustic returns from ice with roughness due to weathering, differential snow cover, etc. As noted in Chapter 2, the level of direct backscattering from the latter type of ice is comparatively very low. If and when more information on the underside roughness of ice on small spatial scales becomes available, some modification of the proposed definition, perhaps involving a maximum ice surface slope, may be needed.

The reasons for studying the mechanism of forward reflection and scattering as part of the complete backscatter problem have been discussed in Chapter 2. Briefly, these are that (1) typical geometries of practical interest make it likely that such a mechanism plays a role in backscattering, (2) although it is highly variable, the observed intensity of sound forward reflected or scattered from undeformed ice is a significant fraction of the incident intensity, especially at grazing angles less than about 30°, and (3) there is some evidence that this mechanism is present in observations of ice keel scattering [Garrison et al. [1986a]. There are several possible practical implications of forward reflection and scattering as part of the backscattering process. These include elongation of the back-scattered pulse, and complicated interference between returns directly backscattered from keels (or other objects) and returns backscattered via a forward reflected or scattered path. The latter can have especially serious effects on systems that estimate the arrival direction of the reflected or scattered wavefront.

The discussion in Chapter 2 did not consider the physical nature or the detailed quantitative characterization of forward reflection and scattering. A more detailed review of the available experimental data can be combined with basic reflection and scattering theory, to partially clarify the nature of this process. Section 4.2 contains a

review of relevant published experimental work, and Section 4.3 contains a review of the relevant theory. These are in turn followed by a section (4.4) that gives hypotheses which could qualitatively explain the data, and briefly discusses the practical implications of each hypothesis. All this is preparatory for Section 4.5, which presents proposals for further experiments and analyses that should clarify the nature of the forward reflection and/or scattering mechanism and provide data for quantitative modeling of this mechanism.

Section 4.2: Relevant Observations

Consider first direct field measurements of the intensity forward reflected and/or scattered from natural sea ice. There are evidently only a few sets of such measurements in existence.

Section 4.2.1: Fletcher's Ice Island

The first of these is the set of measurements made with the Unmanned Arctic Research Submersible (UARS), a programmable, autonomous vehicle built and operated by the Applied Physics Laboratory at the University of Washington (APL-UW) in the early 1970s [Francois and Nodland, 1973; Francois, 1977]. The forward reflection/scattering experiment for which data are reported took place near Fletcher's Ice Island (T-3) in early May 1972 (at which time the island was near 84°5′N, 84°5′W). The transmitter was a 50 kHz beacon on the UARS, and the receiver was a fixed hydrophone suspended beneath the ice. The transmitter depth below the nominal ice–water interface was approximately 41 m; the receiver depth was approximately 26 m. Horizontal range varied from less than 91 m to approximately 450 m. Both transmitter and receiver beamwidths were very wide, but because the beacon transducer was on the underside of the vehicle (i.e., the side facing away from the ice) it was necessary to carefully correct the raw data for transmitter pattern directivity. This was done using vehicle position data from a passive acoustic range, and from attitude and depth data sensed and stored aboard the vehicle itself. The transmitted pulse was a square CW pulse of 1.3 ms duration, which would indicate that a large area of ice situated between transmitter and receiver was ensonified. (The significance of this observation will become clearer in the next section.) The amplitude of the pulse arriving via the surface path was estimated from the first 0.2 ms of the recorded pulse. The number of samples of the forward reflected or scattered intensity was not reported.

As for environmental conditions, the air temperature at T-3 rose from approximately −40°C in April to approximately −18°C on 9 May, the day of the measurements. Clearly no melting of the ice had begun, so the underside of the ice must have been in a state characteristic of late winter, probably with the growth of congelation ice continuing. CTD data indicate that there was little or no ray bending in the water column. For the experimental runs analyzed, the nominal specular point of reflection moved along lines on the underside of multiyear ice in a "bay" of the ice island. The ice was evidently quite old, thick (approximately 5 to 7 m), and weathered.

A reflection coefficient was computed for the ice assuming range spreading of the amplitude of the form $(r_1 + r_2)^{-1}$, where r_1 and r_2 are the distances from the transmitter and receiver to the nominal specular point, respectively. The nominal grazing angles ranged from approximately 10° to 40°. The measured reflection coefficient fluctuates by approximately ±5 dB about 0 dB when plotted as a function of nominal grazing angle or as a function of nominal specular point position. The authors' plots of the fluctuations have been smoothed using a five-point running mean. It is difficult to tell by inspection whether the fluctuation is purely random or not, but the data certainly did not show any clear trend in nominal grazing angle.

Further details concerning experimental procedures and results are given by Francois and Nodland [1973]. Temporally concurrent data on the underice surface roughness are also given there and are reviewed below.

Section 4.2.2: Beaufort and Chukchi seas

Complementary forward reflection and scattering measurements have also been made by APL-UW, and have been reported by Garrison et al. [1976a and b], and Garrison et al. [1983]. All these measurements were made using transducers suspended below the ice and by varying the depth of either transmitter or receiver in order to vary the nominal grazing angle and location of the nominal specular point. Note that with this arrangement only one or, at best, only a small number of independent samples of the forward reflected or scattered intensity in a given small range of grazing angles is obtained, unless extra holes are drilled and the experiment is repeated.

The measurements reported by Garrison et al. [1976a and b] were made in the Beaufort Sea (about 30 miles from Barrow, Alaska) in April 1974 and in the Chukchi Sea in April 1975, respectively. In each of these cases, a collection of transmitting transducers on a common mounting was used to transmit square CW pulses at several frequencies between 7.1 and 60 kHz. A single receiving transducer was raised and lowered to obtain varying nominal grazing angles and locations of the nominal specular point. A variety of horizontal ranges were used, because these measurements were actually done as an adjunct to measurements of acoustic attenuation and transmission fluctuation in the water column.

In the Beaufort Sea measurements [Garrison et al., 1976a], the frequencies used were 10, 20, 30, 40, and 60 kHz. The transmitter beam axis was horizontal, with vertical pattern widths ranging from approximately 20° at 60 kHz to 60° at 10 kHz. The transmitter azimuthal patterns were virtually isotropic, and the receiving patterns were very broad in both directions. The source depths ranged between 40 and 80 m, while the receiver depths ranged between 10 and 70 m. The horizontal transmitter/receiver separation ranged from approximately 400 to 1000 m. The nominal grazing angle ranged from approximately 5° to 20°. However, CTD data showed that the sound speed in a layer of water 20 m thick immediately below the ice was much lower than that in the water below, causing significant upward refraction. The receiver was apparently situated beneath second-year or older ice. However, because of the varying range and placement

of the transmitter, the ice type under which the nominal specular point occurred evidently varied over the course of the measurement. In fact, during the course of the experiment, a ridge formed between at least one of the transmitter locations and the receiver, introducing a noticeable shadowing effect. The data were not separated to try to isolate ice type or shadowing variations. The air temperature fluctuated between approximately −22°C and −30°C during the measurement period; the ice was apparently still in a late winter state. A 4 ms square CW pulse was used. The amplitude of the forward reflection/scattering signal was sampled approximately 1 ms from the initial rise, which was not necessarily its highest value, for the determination of the forward reflected/scattered amplitude. Further information on the typical pulse shapes is, unfortunately, not given.

Like the UARS data, these data fail to show any definite trend with nominal grazing angle, except in cases where shadowing by the newly formed keel occurred. The computed reflection gain [again using $(r_1 + r_2)^{-1}$ spreading] fluctuates chaotically on many scales between 0 and −10 dB. The computed reflection gain fluctuates more rapidly as a function of receiver depth as frequency increases. It seems reasonable to ask whether this might be an effect of refraction and scintillation in the water column, and, indeed, the reflection gain does fluctuate more quickly as a function of receiver depth at small nominal grazing angles. However, the frequency effect is clearly observed even at the largest grazing angles observed ($\approx 20°$), which would argue that it is a real effect of the reflection and/or scattering mechanism. A very weak maximum around 20–30 kHz of the reflection gain averaged over grazing angles is the only other variation of note. This feature might be an artifact, since there was some uncertainty in the 10 kHz transmitter beam pattern [see Garrison et al., 1976a, p. 55] and at 60 kHz the transmitter pattern was comparatively quite directional.

The Chukchi Sea experiment [Garrison et al., 1976b] was almost identical to the Beaufort Sea experiment in terms of procedure and equipment, except that the lowest acoustic transmission frequency was changed from 10 to 7.1 kHz, and a 1.2 ms pulse was used. Winter conditions again prevailed up to and during the experiment; the air temperature never exceeded −18°C. However, there was much less sound speed variation in the water than in the Beaufort Sea experiment; there appears to have been no significant ray bending. The ice condition and mix of ice types from which forward reflection/scattering was sampled appear to have been approximately the same as in the Beaufort Sea measurements. The results are also very similar in all respects to those from the previous measurements, both in terms of fluctuation behavior and the apparent maximum in reflection gain averaged over grazing angle at approximately 30 kHz.

Section 4.2.3: Kane Basin

An experiment in Kane Basin in April of 1979 reported by Garrison et al. [1983] is particularly useful from a fundamental point of view, not because the conditions were characteristic of conditions in the Arctic in general, but because the measurements were

of a pure type which would occur in characteristic conditions. The measurements were made under a large, uniform expanse of undeformed first-year ice. No melting had begun; again, the ice was in a condition characteristic of late winter. The ice thickness was between 1 and 2 m, and the ice was virtually undeformed over the entire experimental area [G.R. Garrison, personal communication, 1987]. The sound speed profile beneath the ice was exceptionally uniform.

Measurements were made using a fixed, suspended receiving transducer while raising and lowering a transmitter at varying ranges between 275 and 1100 m. The transducers used were the same as those used previously in the Beaufort and Chukchi seas. Forward reflection/scattering was measured at 10, 20, 30, 60, and 75 kHz, using a square CW pulse 1 ms long.

Like previous measurements, the computed reflection gain fluctuates in the neighborhood of 0 dB between approximately −5 and +10 dB, going from one extreme to the other as the transmitter depth is varied by as little as 1 m. There is no clear trend in the data with nominal grazing angle. There may be a slight linear trend toward larger reflection gains at higher frequencies, but this is uncertain given the fluctuations in the data. A comparison of fluctuations in the reflected/scattered signal versus the direct signal shows the former to be much larger, with variation on a wider variety of scales of transmitter depth, and thus nominal grazing angle. By combining the data from all transmitter depths for each frequency, it was possible to plot histograms of the computed reflection gain in decibels for each frequency. Several, though not all, of these show a marked skewness, with the longer tail of the distribution on the small reflection gain side.

Photographic records of the oscilloscope traces of forward reflected/scattered pulses are included in the data report on this experiment. These records are particularly useful from a fundamental viewpoint, and form one of only two such sets in the literature of which I am aware (the other set is described below). Typical oscillograms and derived reflection coefficients, reproduced from Garrison et al. [1983], are presented in Figures 4.1 and 4.2, respectively. The shape of the forward reflected or scattered pulses is square; they are virtually pulse replicas, except that their amplitude fluctuates as described above. Their arrival time is that expected for specular reflection, to within experimental errors. This behavior is clearly different from that observed for incoherent forward scattering from the ocean surface, for example [cf. Thorsos, 1984]. Hypotheses that could explain these observations will be developed in Section 4.3.

Section 4.2.4: Beaufort Sea

Some forward reflection/scattering measurements made in September 1980 in the Beaufort Sea are also reported by Garrison et al. [1983], but these were made under heavily deformed ice of mixed type and under highly refractive conditions. Their interpretation is thus greatly complicated, and I will not consider them further here.

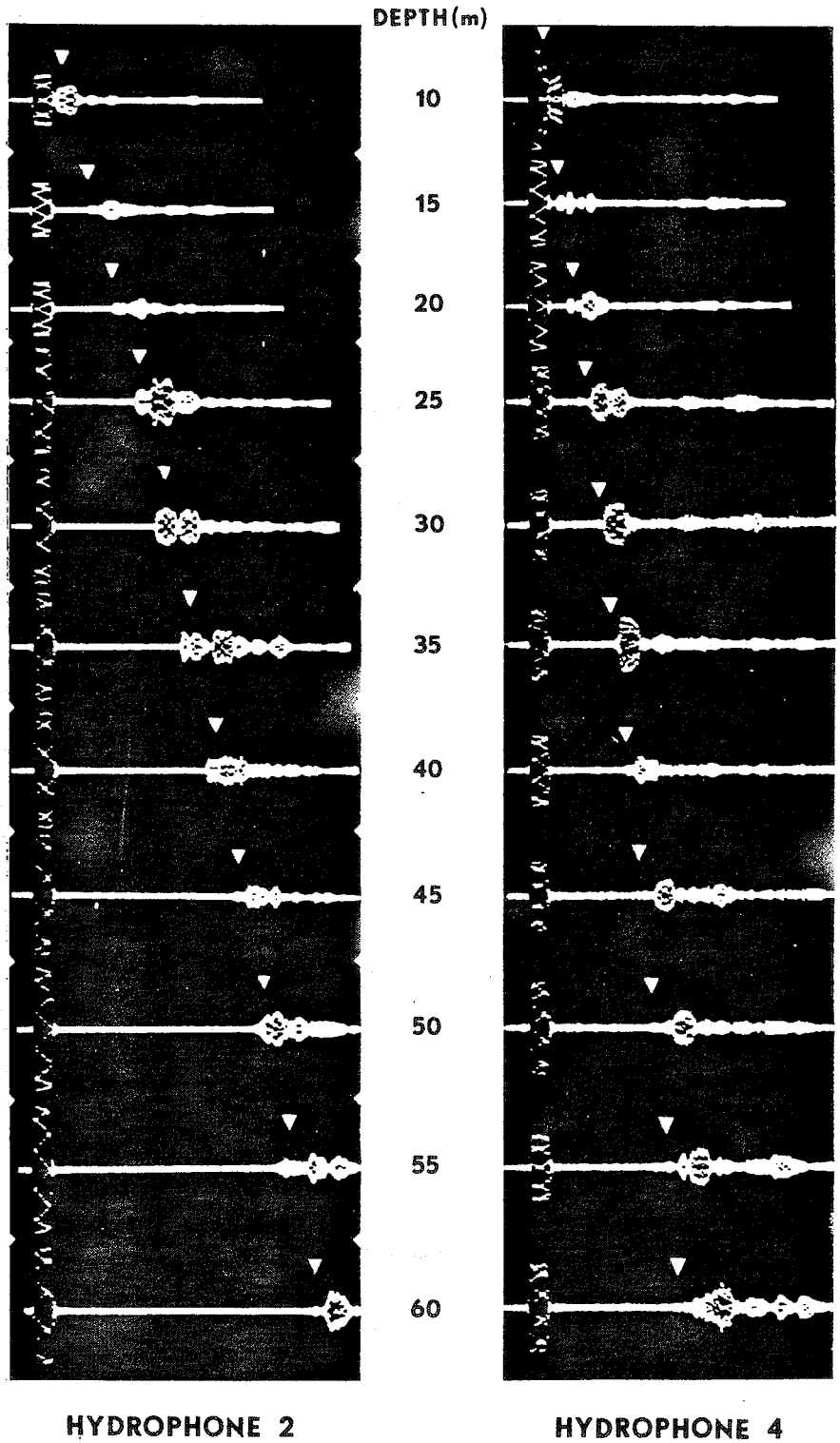

Figure 4.1. Underice surface reflections (20 kHz) at every 5 m of transmitter depth at two hydrophones. The triangle indicates the calculated time of arrival of a specular reflection.

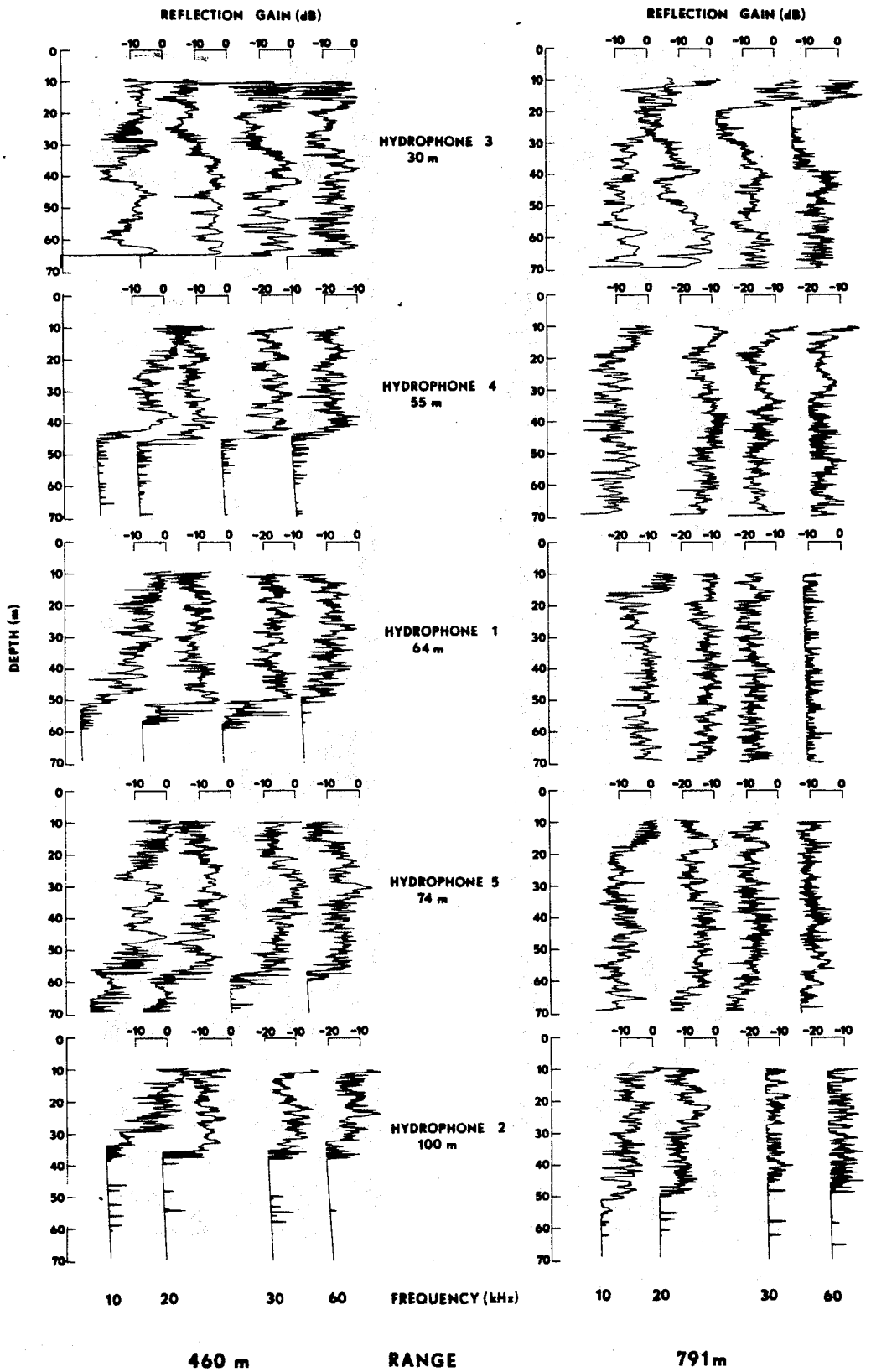

Figure 4.2. The reflection gain as the transmitting transducer was raised at two ranges.

Section 4.2.5: Ellesmere Island

Two field experiments on scales considerably smaller than the APL-UW measurements are also reported in the literature. The first is that reported by Langleben [1970]. Forward reflected or scattered intensity measurements were made under smooth, 2.36 m thick first-year ice (salinity approximately 4 ppt). The experiment took place during April and May 1969 in a fjord on Ellesmere Island, Canada; temperature profiles of the ice indicated continuing congelation ice growth at the ice–water interface. Measurements were made at 13 frequencies ranging from 18 to 435 kHz, using apparently highly directional transducers. The experimental geometry was such that the grazing angle varied from 15° to 75° while maintaining a constant acoustic path length of 8.6 m. The same patch of ice was ensonified for all measurements at each grazing angle, and the experiment was performed on just one patch of ice. A CW pulse of unspecified shape and length was used.

The results of Langleben's measurements show only an apparently random variation on the order of 2–3 dB with frequency at any given grazing angle. However, when averaged over frequency, they display a strong grazing angle dependence, with the computed coherent reflection coefficient ranging from less than 0.2 at a 75° grazing angle to greater than 0.8, on average, at a grazing angle of 15°. The increase in average reflection coefficient is approximately linear between grazing angles of 30° and 75°. It is worth noting that at 75°, the computed reflection coefficient is actually greater than one at two frequencies (1.22 at 47 kHz and 1.06 at 126 kHz). It is very interesting that this phenomenon observed in the much larger scale APL-UW measurements persists in small scale measurements.

Section 4.2.6: Canadian Archipelago

The second smaller-scale field experiment is reported by Verrall and Ganton [1977]. In this case, several sets of forward reflection/scattering measurements were made under very smooth first-year ice in the Canadian Archipelago during April and May 1971–73. Ice thickness was 1.8 m in 1971 and 1972, and 2.4 m in 1973. Though no temperature information is given, the ice was evidently still in a late winter condition (i.e., no melting appears to have begun). The range between transmitting and receiving hydrophones was 100 m except in a handful of cases where the range was 300 m. Typical hydrophone depths ranged between 5 and 50 m, leading to nominal grazing angles between 5° and 31°. Measurements were made over a range of frequencies from 200 Hz to 20 kHz using a CW pulse, the length of which is not given.

The results, plotted as a function of frequency for given grazing angles, again show an erratic frequency dependence at kilohertz frequencies, often with fairly sharp minima at which the reflection gain approaches –20 dB (i.e., a reflection loss of 20 dB is measured). Reflection gains of greater than 0 dB were also observed in this experiment a number of times, though less frequently than in the measurements reviewed above. Three results in this data set are especially notable. First, six pairs of measurements were made in which the areas of ice responsible for reflection/scattering were physically

separate though located near each other, while geometric and acoustic parameters were otherwise identical. The variations in reflectivity between members of the pairs appear no different from the variations between pairs. This indicates that some property of the ice that varies rapidly from location to location (e.g., roughness) rather than bulk ice property variations are responsible for the observed variations. Second, a photo of an oscilloscope trace is also given by the authors. Near reflectivity minima, the pulse received from the surface does evidently show some interference effect at its beginning and end, suggesting an interference phenomenon. Finally, divers measured the relief of the underice surface on a 1 m grid over an area of 8×31 m, obtaining an rms height deviation of 2 cm and a maximum deviation of approximately 10 cm.

Section 4.2.7: Transition layer

All the measurements reviewed to this point have involved sea ice in a late winter state. The variation of forward reflected or scattered intensity has been studied by Francois et al. [1981] as the ice warmed at a camp on shorefast, multiyear ice. The study took place northeast of Barrow, Alaska, from approximately 2 June through 11 July 1977. A transmitter suspended 12.5 m below the ice and three receiving hydrophones at 7.3 m depth and ranges 80, 164, and 77 m were used to measure the forward reflected or scattered intensity relative to the intensity of the pulse that arrived directly through the water. Reliable data were acquired at 20, 30, and 60 kHz. The forward reflected/scattered intensity decreased by 5–10 dB during late June and early July; at the same time water temperature under the ice rose 1°C and considerable melting of the upper ice surface began. This is consistent with observations of the variation of acoustic reflectivity of the ice–water interface at normal incidence at very high frequencies (100–800 kHz) under warming conditions [Stanton et al. 1986]. Both groups of authors suggest that their observations are connected to seasonal variation in the ice–water transition layer, the properties of which evidently depend strongly on the growth or melt rate of the ice [Maykut, 1985]. Questions regarding the transition layer and its characterization are considered further in Chapter 5.

Section 4.2.8: Interpretation

Interpretation of the data discussed above will require additional data on the roughness of the underside of flat ice, either to test hypothetical explanations of the data involving rough surface scattering or to rule out rough surface effects. To be useful for these purposes, it is necessary that the roughness measurements be of ice statistically similar to that from which reflection/scattering measurements are made. Moreover, we need roughness data with horizontal spatial resolution roughly on the order of the acoustic wavelengths of interest and vertical resolution considerably smaller than these wavelengths. (These statements will be made more precise in Section 4.3.) Submarine upward looking sonar data provide neither the necessary horizontal or vertical resolution.

Evidently, the only existing data set with properties approaching those necessary is that collected with the UARS instrument concurrently with the forward

reflection/scattering measurements described above [Francois and Nodland, 1973; Francois, 1977]. The UARS included a pulsed, upward looking sonar operating at 500 kHz. The researchers recorded the time delay between pulse transmission and arrival of the reflected signal from the underside of the ice, the vehicle tracking data, and other data necessary to reconstruct the underice profile. The minimum resolvable spatial wavelength of roughness in the underice surface was approximately 1.2 m, and the precision of individual ice draft measurements was estimated at approximately 9 cm. The overlap of sequential ensonified spots on the underice surface was approximately 56%.

There has been some limited analysis of profiles of the underside of the old ice from which the UARS forward reflection/scattering measurements were made. Results are reported by Francois and Nodland [1973] for three profiles, each approximately 300 m long. The quantitatively reported analysis is limited to a set of surface slope estimates. These are statistics of the first differences of the profile data, computed at a number of spatial lags ranging between 2 and approximately 20 sampling intervals. The mean surface slopes measured in this way are as large as 5° at the minimum spatial lag and decay quickly with increasing lag to approximately 2°. Less quantitative information can also be obtained from plots of the profiles presented by Francois and Nodland. From these it is clear that deviations of the underice surfaces from planar are sometimes as large as one meter, though the rms roughness is probably smaller than that. Thus it is clear (see next section) that at least this sample of "relatively flat" ice is in fact rough in the context of high frequency acoustics, for which the acoustic wavelengths are on the order of centimeters.

In fact, very few natural surfaces are smooth to within a few centimeters over the length scales of typical ensonified spot sizes in underwater acoustics. The small scale, in situ underice measurements reported by Verrall and Ganton [1977] that were discussed above show variations of centimeters in underice relief over horizontal scales of meters. Qualitative in situ observations for a number of ice types reported by Grishchenko [1979] are consistent with this. Video recordings of the spreading of oil under ice, made as part of experiments conducted by APL-UW, seem to show qualitatively that even the underside of new first-year ice deviates from plane by perhaps a few centimeters over horizontal distances of about a meter. However, no firm conclusions about the mechanism (or mechanisms) of underice forward reflection and/or scattering can be drawn from the observations reviewed here and in Chapter 2; the existing data are simply not sufficient to test and rule out hypotheses. Two of what I think are the most plausible hypothetical mechanisms will be discussed below. To understand one of these requires a background in the subject of reflection and scattering from gently undulating, randomly rough surfaces and, in some specialized aspects of this phenomenon which may be important, in underice scattering. Section 4.3 provides the necessary background.

Section 4.3: Forward Reflection and Scattering from Randomly Rough Surfaces

The aim of the following is to provide an understanding of the relevant physics and formulae for physical length scales and parameters in the rough surface problem. Of course, which physics and formulae are relevant depends on the applications one has in mind. For simulations of acoustic reverberation, the range behavior (i.e., spreading of reflected and scattered intensity) is relevant, as is any distortion and/or stretching of acoustic pulses. The sizes of relatively flat underice regions that participate in reflection and scattering may also be important in simulation and certainly are important in the design of experiments for characterization. The number of independent samples needed to estimate the statistics of scattered radiation to within a given precision is clearly also important in experimental design. Thus, in this section, I will pay special attention to these topics.

What follows is a succession of cases beginning with the relatively simple one of perfectly coherent reflection, progressing to partially coherent reflection and scattering from a randomly rough surface, and concluding with two cases of completely incoherent scattering. One of the latter cases seems to have arisen only rarely in studies of scattering from other geophysical media, but may be particularly relevant to the flat ice acoustics problem. However, the discussion here will be limited to cases in which the surface height variations have finite, small slopes, are gently undulating on the length scale of the acoustic wavelength, and have a Gaussian probability distribution. These conditions are consistent with, in fact even suggested by, what is presently known about the underside of relatively flat ice. I will also assume that incident and scattered grazing angles of interest are greater than about twice the average surface slope angles. The stated assumptions will allow the use of the Kirchhoff approximation to compute scattered fields. In this approximation, the unknown fields on the rough surface at a given point are replaced by what their values would be if a plane interface existed at that point tangent to the actual surface, separating the two materials actually separated by the rough surface. This approximation considerably simplifies the scattering problem and aids in developing intuition about the scattering process. Recent work by Thorsos [1988] provides useful insight about the limitations of the Kirchhoff approximation and quantitative guidelines for those instances in which it can be expected to be accurate, particularly at low grazing angles. Note, however, that the qualitative features of rough surface scattering described here are typically observed even in cases where the Kirchhoff approximation does not apply.

Consider the situation shown in Figure 4.3. An acoustic source, which for now may or may not be directional, is situated below a surface at position $\mathbf{r}_t = (0,0,d_t)$. A receiver, which also may or may not be directional, is situated at $\mathbf{r}_r = (r,0,d_r)$. In the case of a planar surface, the surface is taken to coincide with the x-y plane, and the mean surface is identical to the surface itself. If the surface is rough, the mean surface, defined in some suitable way depending on the nature of the roughness, is taken to coincide with the x-y plane. A nominal specular point can be defined even for a rough surface as that point on the mean surface which would be the specular point if the surface was flat and coincided

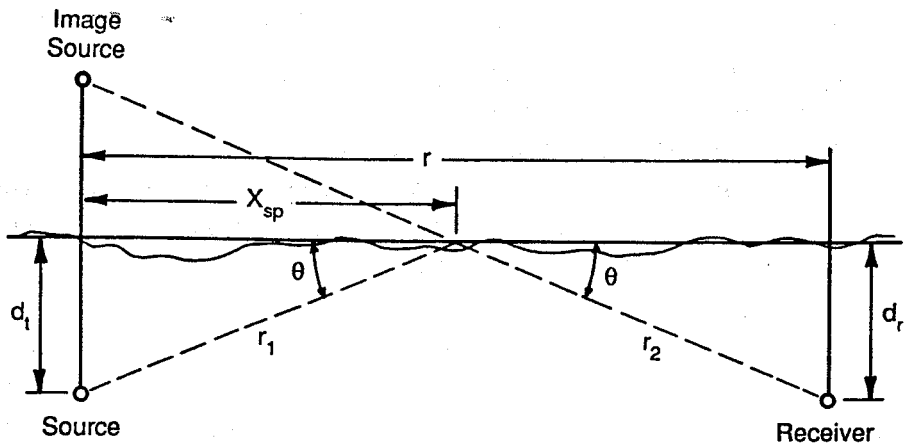

Figure 4.3. Acoustic source and nominally specular reflection.

with its mean. Then the nominal grazing angle is just the angle the specular ray would make with horizontal under the same conditions. The nominal specular point position and grazing angle are simply

$$\mathbf{r}_{sp} = (x_{sp},0,0) \quad , \quad x_{sp} = r\left[1 - \frac{d_r}{d_t + d_r}\right] , \tag{4.1}$$

and

$$\theta = \tan^{-1}\frac{d_t}{x_{sp}} = \tan^{-1}\frac{d_r}{r - x_{sp}} \quad . \tag{4.2}$$

First, we must define a way of specifying the roughness of a surface. In practice, the roughness of a surface for purposes of reflection and scattering is measured by the Rayleigh roughness parameter [see, for example, Kerr et al., 1951]

$$\chi = 2k\,h\,\sin\theta \tag{4.3}$$

where $k = 2\pi/\lambda$ is the radiation wavenumber corresponding to the acoustic center frequency (in the case of pulsed measurements), θ is the grazing angle of rays (i.e., wavefront normals) from the source at the specular point, and h is a typical variation of the surface from its mean plane in the $\hat{z}$ direction (taken to be the standard deviation of surface height for a randomly rough surface with a Gaussian distribution of surface heights). Although the parameter χ is usually heuristically derived, it does arise naturally as a measure of surface roughness when using the Kirchhoff approximation and has been widely found to be useful in practical studies, including, for example, sea surface scattering [Thorsos, 1984].

Section 4.3.1: Reflection from an acoustically flat surface

An acoustically flat surface is defined by the characteristic that essentially all the radiation from the source incident on the surface is reflected specularly. Whatever roughness is present on the surface is so small in comparison with the radiation wavelength that it has negligible effect. Ulaby et al. [1982] argue for a criterion for flatness equivalent to restricting the Rayleigh roughness criterion at normal incidence to less than 0.4, which corresponds to restricting rms surface roughness to less than approximately 3% of the radiation wavelength.

The phase of the field reflected from an acoustically flat surface possesses a constant, well-defined relationship to the ensonifying field, as does its amplitude. Thus in the absence of measurement noise, one sample of the field is sufficient to characterize the reflection for any given frequency and grazing angle. To the receiver, the reflected radiation looks as if it had come from a source positioned at the image point of the true source, provided one can ignore surface wave effects (Figure 4.3). The so-called coherent amplitude spreading loss is simply $(r_1 + r_2)^{-1}$, where r_1 and r_2 are the distances from the source and receiver to the specular point, respectively.

The reflected field is actually generated, however, by monopole and dipole source densities which are induced on the surface by the ensonifying radiation. The difference in phase of induced sources at different points is just the difference in the phase of the ensonifying radiation at those points. Thus, the contributions of two distinct points to the reflected field at the receiver differ in phase by k times the sum of the differences in path length from the source to the two points and from the two points to the receiver. In cases where the source or receiver or both are highly directional, all contributions to the received reflected field may be nearly in phase. More generally, there will be interference between contributions from different parts of the ensonified interface. The loci of points on the interface from which contributions add in phase are (generally nonconcentric) ellipses with semimajor axes along the line connecting the projections of the source and receiver positions in the x-y plane. The Fresnel zones for this problem are annuli bounded by pairs of ellipses for which the reflected field contributions differ in phase by π radians. Contributions from adjacent Fresnel zones excluding the first, largest zone (in which the phase of contributions varies from 0 to π) are successively out of phase with each other, and therefore tend to approximately cancel. This is particularly easy to see for very simple geometries and sources (see, for example, Hecht and Zajac, 1974). However, in the general case, when source and receiver directionalities are broad enough to ensonify and observe, but differently weight, contributions from several Fresnel zones, it is less clear that the predominant contribution to the reflected field can be ascribed to one or a small number of Fresnel zones. An analysis by Beckmann [Beckmann and Spizzichino, 1963] indicates that the significant contributions still come essentially from the first Fresnel zone. (Although Beckmann argued for the possible importance of zones immediately above and between the two transducers, it is clear from his development that there is strong cancellation between neighboring contributions in those regions, negating their importance.) Thus, the reflected field is primarily generated by induced

surface sources within an elliptical region (the first Fresnel zone) which overlaps, though in general is not centered on, the specular point. The dimensions and center coordinates of the Fresnel zone ellipses are given by Kerr et al. [1951]. Note, however, that there is a misprint in the equation for the center coordinates of the first Fresnel zone. For completeness, the corrected equations are given in Appendix 4A.

Thus, the length of the semimajor axis of the first Fresnel zone defines the size of the active acoustic region on the interface for the reflection problem, unless the source and/or receiver are so directional as to further limit the size of this region. Irregularities in the acoustic properties of the ice and/or surface height on spatial scales comparable to or smaller than this size will cause scattering, while those on larger scales simply lead to a regional variation of the reflection coefficient. To get an appreciation for a typical size scale, use the following parameters similar to those in the experiments discussed previously

$$d_t = 35 \text{ m} \ , \ d_r = 20 \text{ m} \ , \ R = 400 \text{ m} \ , \ \lambda = 5 \text{ cm}$$

and the relations in Appendix 4A. The length of the first Fresnel zone is approximately 31 m; its width is approximately 4 m. In general, the Fresnel zone ellipses are narrow ellipses for grazing angles appreciably less than 90°, with width approximately one tenth their length or less. This ratio decreases rapidly with decreasing grazing angle.

Finally, although travel time along the specular reflection path is a minimum over all paths, for sound in the ocean this minimum is surprisingly broad. For example, for the geometry just considered, contributions from everywhere within the first Fresnel zone arrive at the receiver within less than 0.05 ms. Thus, there is no pulse distortion for coherent reflection except for very short intervals near the beginning and end of the pulse.

Section 4.3.2: Scattering in the case of small to moderate roughness

Now consider a randomly rough surface with small to moderate roughness, $0.4 \lesssim \chi \lesssim 2$. In this case, the radiation redirected away from the surface consists of two parts. The first is a coherent, specularly scattered part, similar to the field reflected from a flat surface, though with reduced amplitude. In addition, radiation is incoherently scattered into a range of directions, usually including the specular direction. The latter radiation has no consistent phase relationship to the illuminating radiation from realization to realization of the rough surface. The amplitude, phase, intensity, etc. of radiation scattered in any given direction are random variables related to the random surface roughness. In the following, I will first separately discuss the coherent and incoherent scattered fields, and then discuss the total scattered field as the sum of these two parts. Again, the details of this discussion depend on the Kirchhoff approximation and Gaussian surface height statistics, but scattering in cases where these approximations do not apply generally shows qualitative features similar to those presented here.

The coherent scattered field is a phase coherent average (over realizations of the surface) of the complex scattered field. Thus, it is the part of the scattered field which

retains a consistent phase relationship to the illuminating field. For a given source location or angle of incidence, it behaves like a field reflected from the mean surface, in that it looks to an observer below the surface as if it had originated from an image of the actual source reflected in the plane of the mean surface. Thus, like a reflected field, its amplitude falls off with range like $(r_1+r_2)^{-1}$. However, its amplitude is reduced from that which would be reflected by a plane surface, because some energy is lost to incoherent scattering. According to the Kirchhoff approximation, the amplitude of the coherent scattered field when a plane wave is incident, sometimes called the coherent reflection coefficient, is given by

$$R(\theta) = R_0(\theta) \exp\left[-\frac{\chi^2}{2}\right] , \tag{4.4}$$

where θ is the grazing angle of the incident wave, $R_0(\theta)$ is the reflection coefficient for a plane interface between the same two media as are actually separated by the rough surface at grazing angle θ, and χ is the Rayleigh roughness parameter given by equation 4.3. Note that the amplitude of the coherent scattered field generally increases with decreasing grazing angle and frequency, but that separate frequency and grazing angle dependencies in R_0 may complicate the dependence. The spatial scale of the active surface region responsible for the coherent field is again the size of the first Fresnel zone, and, analogous to a reflected pulse, there is virtually no pulse distortion of the coherently scattered part of a pulse. In contrast to reflection, though, estimation of the coherent scattered field requires an averaging process. In order to discuss this process and its sampling statistics, it is first necessary to discuss the incoherent part of the scattered field.

The incoherently scattered field consists, in general, of waves scattered in both specular and nonspecular directions. It is typically characterized by statistical moments of the field scattered in particular directions or observed at a given point. Common examples include the mean scattered intensity at a point and the covariance of the complex field at two points. Contributions to the incoherent field have no consistent phase relationship among themselves, so there is no average cancellation of contributions to decrease the effective active area, such as occurs in reflection. Thus, the active surface region for incoherent scattering is, in principle, the entire directly and indirectly ensonified surface region. However, in specific cases the extent of the active surface region can be limited to an area smaller than the ensonified zone because of the particular physical scattering mechanism involved. (It is difficult to give a concrete example of this phenomenon in the case of moderate roughness, but in the very rough surface case to be discussed momentarily, a classic example will be given.) Nonetheless, the active surface region for incoherent scattering is typically larger than for coherent scattering, even for moderate roughness [Gulin and Malyshev, 1963]. This can lead to significant elongation of the scattered pulse in comparison to that transmitted, in cases where the active region is large enough that an appreciable travel-time difference from source to receiver (compared with the transmitted pulse length) exists for signals scattered from different parts of the active region. In order to discuss the statistics of the incoherent field, it is necessary to consider two physically different cases.

The relevant length scale is that of the random fluctuations of the induced surface source densities. By far the simpler case is that in which this length scale is much smaller than the dimensions of the ensonified region. Note that the dimensions of the ensonified area may be limited by source and receiver beamwidth, by pulse length, or by both. The stated condition holds, for example, when the surface roughness correlation length is much smaller than the dimensions of the ensonified area. For a very rough surface to which the Kirchhoff approximation can be applied, even this restriction can be eased somewhat [Winebrenner 1985, Appendix A]. In any case, when the condition is satisfied, the incoherent field at a given point or scattered in a given direction is the sum of many independent contributions from the ensonified area, and the mean incoherent intensity can be thought of as the incoherent sum of contributions from different parts of the ensonified region. Thus, the far-field region (i.e., the Fraunhofer zone) of the ensonified patch is considerably closer to the patch itself than it would be if the contributions were coherent [details are given by Winebrenner, 1985]. (Note, however, that for any single realization of the rough surface and incoherent field, contributions from different parts of the ensonified area may indeed interfere; this is the source of speckle [see, for example, Dainty, 1976]. It is only in the mean that intensity contributions can be added incoherently.) Also, the far-field intensity contribution from each elemental surface region falls off with range as $(r_1' r_2')^{-2}$, where r_1' and r_2' are the ranges from the source and receiver to the contributing surface region, respectively. This is because the intensity of radiation from the source falls off as $r_2'^{-2}$, and the reradiated intensity from individual contributing regions in turn falls off as $r_1'^{-2}$.

The incoherent scattered field in this case is a complex Gaussian random variable, provided that no small number ($\lesssim 5$) of contributions dominates the total return, and that the variance of the number of contributions is small compared with its mean [Kerr and Goldstein, 1951; Jakeman and Pusey, 1976]. This result holds even at small grazing angles [Long, 1975; Moore, 1970; Skolnick, 1970; Jakeman and Pusey, 1976]. The in-phase and quadrature components of a complex Gaussian signal are zero-mean, independent, real Gaussian random variables with identical variances, say, σ^2. The magnitude (i.e., the envelope) of the complex signal is a Rayleigh distributed random variable, and the magnitude squared is exponentially distributed. Since the magnitude squared is proportional to the intensity, denote it by I. The mean value of I is then

$$\langle I \rangle = 2\sigma^2 \quad . \tag{4.5}$$

Furthermore, since the variance of an exponentially distributed random variable is equal to the square of its mean,

$$\mathrm{var}\, I = \langle I \rangle^2 \quad . \tag{4.6}$$

A single sample of the intensity of the incoherent field will range over a broad, asymmetric interval about its mean. It will with probability 0.10 lie more than approximately 13 dB below or 5 dB above its mean [for an excellent discussion of this part of the problem, see Ulaby et al., 1982, pp. 476–491]. It will be useful to introduce a quantity m^2, defined by

$$m^2 = \frac{\mathrm{var}\, I}{\langle I \rangle^2} \quad . \tag{4.7}$$

This quantity is known as the scintillation index in the theory of scattering in random media [Ishimaru, 1978], and I will use the same term for it here. Intuitively, the scintillation index is a measure of the variability of intensity. In the present case of Gaussian field statistics and complete incoherence, the scintillation index is theoretically equal to one.

In order to accurately estimate the mean incoherent intensity, a number of independent samples of intensity (in the same scattering direction, or with the same geometry relative to the mean surface) must be averaged. The sample mean of N independent, identically distributed samples $\{ I_i \}$ of an exponential random variable with mean $<I>$, given by

$$\bar{I} = \frac{1}{N} \sum_{i=1}^{N} I_i \quad , \tag{4.8}$$

is a χ-square random variable with $2N$ degrees of freedom, with mean $<I>$ and variance

$$\mathrm{var}\,\bar{I} = \frac{<I>^2}{N} \quad . \tag{4.9}$$

Thus, the fractional standard error of the estimate is given by

$$\frac{\sqrt{\mathrm{var}\,\bar{I}}}{<I>} = \frac{1}{\sqrt{N}} \quad . \tag{4.10}$$

If, for example, an estimate accurate only to 3 dB is required (fractional standard error 0.5), four independent samples will suffice. The number of samples needed grows quickly, though, as smaller errors are demanded. For an estimate accurate to 1 dB, 25 independent samples are required.

The sampling statistics of the scintillation index estimated from a finite number of intensity samples are clearly also of interest. For the case of exponentially distributed intensity samples, these statistics do not appear in the literature. S.O. McConnell and D.B. Percival of APL-UW have, however, estimated confidence limits to be about one for the sample scintillation index in this case, assuming independent samples of intensity. Their results are given as a function of sample size in Table 4.1.

Table 4.1: Scintillation index confidence limits.

Number of Independent Samples	90% Interval (5%–95%)	98% Interval (1%–99%)
10	0.31 – 1.65	0.21 – 2.33
20	0.45 – 1.59	0.35 – 2.13
50	0.62 – 1.45	0.53 – 1.79
100	0.71 – 1.32	0.64 – 1.55
200	0.79 – 1.24	0.72 – 1.38
500	0.86 – 1.15	0.81 – 1.27

It is clear from these results that estimating the scintillation index requires many more independent samples than are required merely to estimate mean intensity.

Discussion of how independent samples of I can be obtained in practice is deferred to Section 4.5.

Now return to the problem of scattering near the specular direction, where the scattered signal contains both coherent and incoherent parts. Under the same conditions that ensure that the scattered field is a sum of many contributions, the complex field even near specular must be a complex Gaussian random variable. However in this case, the (real) Gaussian random variables representing the in-phase and quadrature parts of the complex signal have nonzero means corresponding to the in-phase and quadrature components, respectively, of the coherent field. The amplitude of the field is no longer Rayleigh distributed, but rather has a distribution known as the Rice-Nakagami distribution [Rice, 1954; see also Kerr and Goldstein, 1951]. The sampling statistics for the coherent intensity can be derived as follows. Let the complex field near specular be

$$Z = X + i\,Y \quad , \tag{4.11}$$

and define ζ by

$$\zeta = Z - \langle Z \rangle \quad . \tag{4.12}$$

Then ζ is the incoherent "noise" in measurements of Z, and is by definition a zero-mean complex Gaussian random variable. To estimate $|\langle Z \rangle|^2$, we must coherently average, say, N independent samples $\{Z_i\}$ of Z,

$$\bar{Z} = \frac{1}{N}\sum_{i=1}^{N} Z_i \tag{4.13}$$

$$= \langle Z \rangle + \frac{1}{N}\sum_{i=1}^{N} \zeta_i \quad .$$

The mean of the estimate $\bar{Z}$ is clearly $\langle Z \rangle$. The independence of the samples means that the samples ζ_i of ζ are independent. The variance of this estimate is

$$\langle [\bar{Z} - \langle \bar{Z} \rangle][\bar{Z}^* - \langle \bar{Z}^* \rangle] \rangle = \frac{1}{N^2} \left\langle \sum_{i=1}^{N}\sum_{j=1}^{N} \zeta_i \zeta_j^* \right\rangle = \frac{\langle |\zeta|^2 \rangle}{N} \quad . \tag{4.14}$$

To measure the coherent intensity to within a given fractional standard error E, it is necessary to choose N such that

$$\frac{\langle |\zeta|^2 \rangle}{N} = E^2 \langle |Z|^2 \rangle \quad . \tag{4.15}$$

In cases where the coherent intensity is greater than the mean incoherent intensity, fewer samples are required to estimate the coherent intensity to within a given precision than are required to estimate the mean incoherent intensity to within the same precision. In the opposite case more, in some cases many more, samples are needed. In contrast to the case of Gaussian statistics and complete incoherence, the scintillation index in this case is theoretically strictly less than one.

$$m^2 = \frac{\mathrm{var}\, Z}{<|Z|^2>} \qquad (4.16)$$

$$= \frac{<|\zeta|^2>}{|<Z>|^2 + <|\zeta|^2>} < 1 \quad .$$

Intuitively, this is because the case in which there is some coherence is less disordered than the completely incoherent case. I have been unable to find any investigation of sampling statistics for the scintillation index when the envelope possesses a Rice-Nakagami distribution. Rice [1954] explores various other problems involving the Rice-Nakagami distribution in detail.

Before leaving this topic, note that when a coherent signal is present and a pulse is used to ensonify the surface, the first part of the near-specular scattered signal (in time) will be nearly a pulse replica. If the active region for the incoherent field is large enough that signals arriving from its different parts are appreciably delayed in comparison with the pulse length, then there will also be a latter part of the signal consisting of an incoherent tail. This has been observed by Gulin and Malyshev [1963] and by S.O. McConnell of APL-UW [personal communication, 1987] in connection with sea surface scattering. The overall spreading losses of such a signal are somewhat complicated, since the two components spread according to different laws. The situation is simplified, though, in the case where the source and receiver beamwidths are wide enough to capture virtually all the scattered intensity. In this case, the spreading loss for the total intensity (coherent plus incoherent) is simply $(r_1 + r_2)^{-2}$. Thorsos [1984] discusses this result and provides further references.

Some readers may also be interested in the variances of amplitude and phase fluctuations for the scattered field near specular where the conditions given above hold. A theoretical study in the limit of very small roughness is given by Gulin [1962], and experimental studies in a wider range of regimes are reported by Gulin and Malyshev [1963] and Melton and Horton [1970]. Also, the case of (slightly) non-Gaussian surface roughness statistics has been treated by McDonald and Spindel [1971]. However, all these studies were made for the special boundary conditions corresponding to acoustic scattering from the sea surface.

It is necessary to reconsider the properties of the incoherent field in cases where (1) the characteristic length scale of fluctuations in the induced surface source densities are comparable to the dimensions of the ensonified area, (2) where a few contributions dominate, or (3) where the variance of the number of contributions is comparable to its mean [Jakeman, 1980; Jao, 1984]. These are cases where the central limit theorem does not hold, and the statistics of the scattered fields are non-Gaussian. Unfortunately, few generally applicable, quantitative statements can presently be made about scattered field properties in such cases. Log-normal [Long, 1975], Weibull [Skolnick, 1970], generalized gamma [Ewart and Percival, 1986], and K-distributions [Jakeman and Pusey, 1976; Jakeman, 1980; Jao, 1984] have been used to model the field envelope distribution. The latter seem to show particular promise, and also admit a physical interpretation [Jao, 1984]. Qualitatively, non-Gaussian field statistics tend to produce "heavy-tailed" intensity distributions, and the scintillation index tends to be greater than one. Estimates to

within a given precision tend to require more independent samples than are required for the same precision in the Gaussian case. General, quantitative results on sampling statistics in this case are evidently not available, but Ewart and Percival [1986] discuss parameter estimation from samples for the generalized gamma distribution, which empirically describes a wide range of non-Gaussian cases. Spreading may also be affected in the non-Gaussian case, since the entire active region may act as a single scatterer or small number of scatterers. Here again, it is difficult to give a concrete example of this situation in the case of moderate roughness, but an example with a simple physical interpretation will be given in the next section.

Section 4.3.3: Scattering in the case of large roughness

In cases where $\chi \geq 2$, the coherently scattered component of radiation is negligible in comparison with the incoherent component in all scattering directions, including the specular direction. I will refer to this case as that of large roughness.

Consider scattering in the high frequency limit from a surface for which the Kirchhoff approximation is valid. That is, consider the case in which the surface varies in elevation only on horizontal scales much longer than the radiation wavelength, and in which the variation in surface elevation is large in comparison with the wavelength ($\chi \geq 2$). A simple physical interpretation of scattering in this case has been given by Kodis [1966], who shows that the main contributions to the scattered field in a given direction come from points on the surface at which surface slope is such that a *locally* specular reflection of rays from the source to the receiver occurs (see Figure 4.4). The magnitude of the contribution from each specular point depends on the principal radii of curvature of the surface at that point. Each contribution is also weighted by the plane wave reflection coefficient for a plane surface separating the media actually separated by the rough surface, evaluated at the grazing angle of the locally specular reflection. In

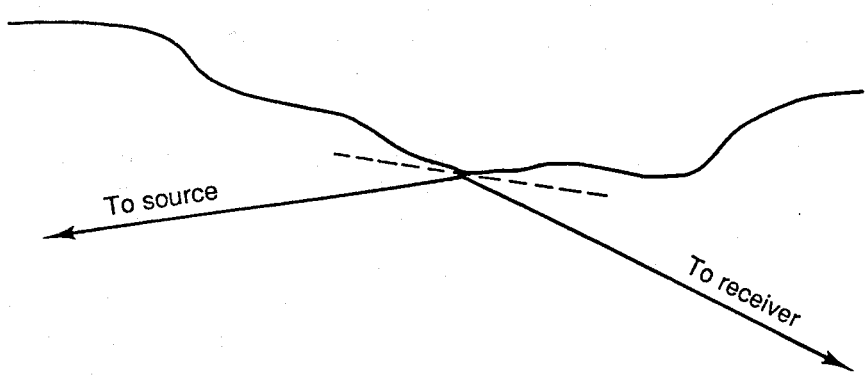

Figure 4.4. Locally *specular reflection.*

practice, however, this weighting is usually approximated as being the same for all specular points and equal to the value of the reflection coefficient at the nominal grazing angle [Ishimaru, 1978; Hagfors, 1967; Stogryn, 1967]. Because the physical picture of specular point scattering involves rays (which are intuitively appropriate in the high frequency limit), this type of scattering is also often called geometric optics in the radar literature and geometric acoustics in the acoustics literature.

In the mean, the intensities of contributions from distinct specular points add incoherently, but for any given realization of the rough surface, there is generally interference between contributions. Thus, the mean scattering strength of the rough surface is frequency independent (aside from frequency dependence introduced by the reflection coefficient), and involves only the statistical geometry of the surface. However, for any single realization, the intensity scattered in a given direction may vary chaotically with frequency over a broad range because of the variation with frequency of acoustic path length differences between specular points.

Within this scattering regime, the effective active surface region for radiation scattered in a given direction is clearly that surface region which is ensonified *and* in which surface slopes necessary for locally specular reflection occur with appreciable probability. For any particular scattering direction, this region can be much more limited than the entire ensonified region. Note, however, that contributions from the entire ensonified region may have to be considered if one is simultaneously considering the fields scattered in all directions.

In the case of forward scattering, the active region is the ensonified portion of a highly elongated elliptical region on the surface between the source and receiver, with the semimajor axis of the ellipse lying along the line connecting the horizontal positions of the transducers. The approximate dimensions of the ellipse can be deduced in the following heuristic way. Let the line in the plane of the mean surface which connects the horizontal positions of the source and receiver be defined as one coordinate axis, say the x-axis, with the positive x-direction in the direction from the source to the receiver, as shown in Figure 4.5. Define a y-axis perpendicular to the x-axis with the positive y-direction out of the figure's plane. Place the origin of the coordinate system at the location of the nominal specular point (note this origin is shifted from that used in Figure 4.3).

At the surface point whose horizontal location coincides with that of the nominal specular point, only a point with zero slope in the x- and y-directions will produce a locally specular reflection from source to receiver. This horizontal location approximately marks the center of the active region. Moving away from this point in either direction along the x-axis, points with nonzero slope in the y-direction will reflect rays away from the forward scatter direction. Let θ_i be the angle, measured from horizontal, from the surface point to the source, and let θ_s be the analogous angle from the surface point to the receiver (see Figure 4.5). Note that both θ_i and θ_s are positive. The necessary slope angle in the x-direction (with a positive angle implying a positive slope, and vice versa) is then $\frac{1}{2}(\theta_s - \theta_i)$. A slope angle of only half the difference is required

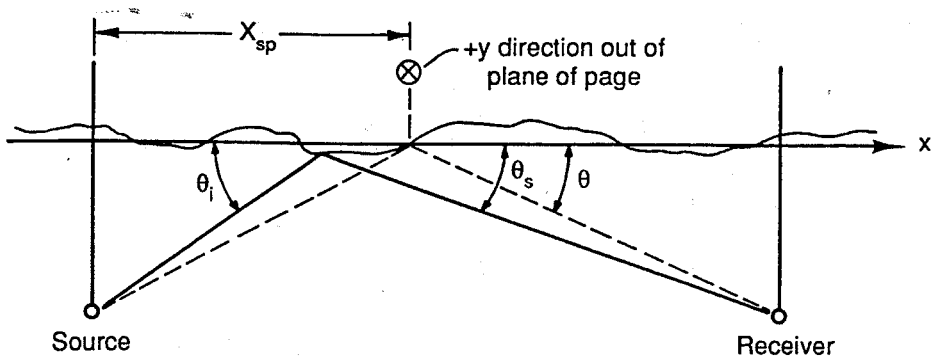

Figure 4.5. Angles for computation of the active region boundaries.

because tilting the surface by an angle α causes an angular displacement 2α of the specularly reflected ray [Hecht and Zajac, 1974, Section 5.4]. Moving farther along the x-axis, the magnitude of the necessary slope increases. At some point, the surface roughness statistics will make a slope of the necessary magnitude very unlikely, and the approximate edge of the active region will be reached.

On the other hand, moving away from the horizontal location of the nominal specular point along the y-axis, points with nonzero slope in the x-direction will reflect rays away from the receiver. Referring to Figure 4.6, let ϕ_i and ϕ_s be defined as the azimuthal angles shown, with positive angles measured in the counterclockwise sense from the x-axis. In this case, θ_i and θ_s are generalized slightly to be defined as shown, but are still measured from the horizontal and are both positive. For points along the y-axis, $\theta_i = \theta_s$, and for small displacements along this axis (relative to the source–receiver separation), both are approximately equal to the nominal grazing angle θ (because the coordinate origin coincides with the nominal specular point). The slope angle γ in the y-direction needed for reflection to the receiver can be derived directly from the geometrical relations given by Kodis [1966], and is given by

$$\gamma = -\tan^{-1}\left[\frac{(\sin\phi_i - \sin\phi_s)}{2\tan\theta_i}\right] \tag{4.17}$$

$$\approx -\tan^{-1}\left[\frac{(\sin\phi_i - \sin\phi_s)}{2\tan\theta}\right] .$$

Moving along the y-axis in either direction, the slopes necessary for locally specular reflection increase, and at some point they again become so large as to be very unlikely given the surface roughness statistics. As before, this point marks the approximate boundary of the active region.

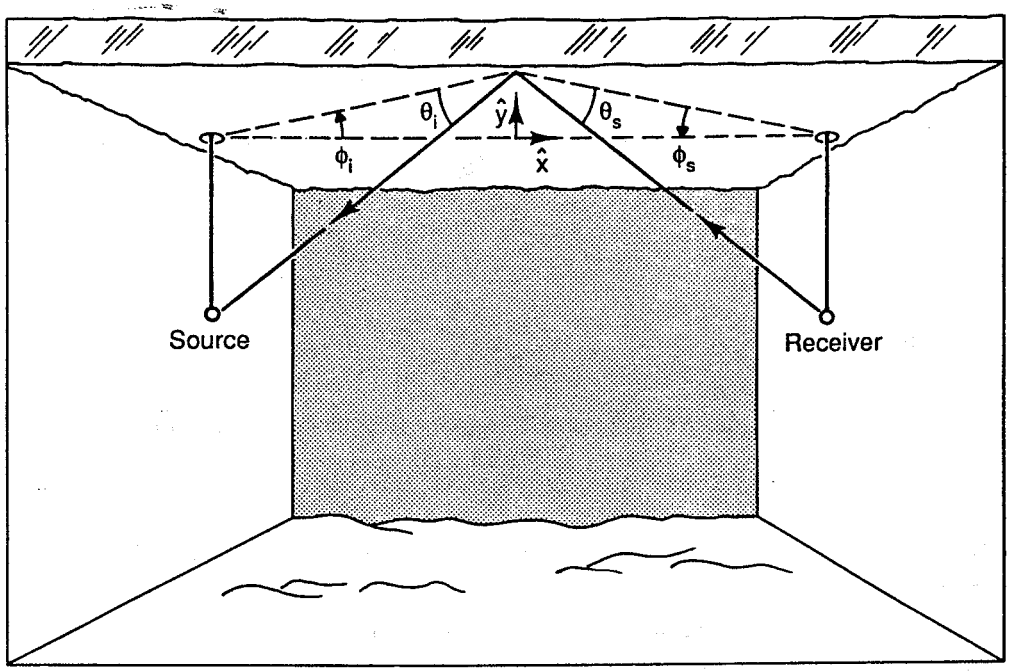

Figure 4.6. Out-of-plane scattering.

The ellipse with semimajor and semiminor axes so defined is much longer in the x-direction than in the y-direction for surfaces with isotropic slope statistics. Thus, even if the source and/or receiver beamwidths are azimuthally broad, only a narrow sliver of the surface lying along the line between the transducers has an appreciable probability of contributing to the forward scattered signal. As an example, consider again the case in which the source and receiver are at equal depths of 35 m and are separated horizontally by 400 m. The active region is centered at the nominal specular point, $\sin\phi_i = -\sin\phi_s$, the nominal grazing angle $\theta = 9.9°$, and

$$| \tan\gamma \tan\theta | \approx | \sin\phi_i | \quad . \tag{4.18}$$

For an underice surface with spatially isotropic slope statistics and a maximum slope of 5°, the length of the active surface region along the line between the horizontal transducer positions is approximately 170 m; the width of the active region midway between the transducers is only approximately 6 m. These dimensions can be compared with the dimensions of the first Fresnel zone for this geometry (31 m long by 4 m wide) which were computed in Section 4.3.1. The difference in travel times between the specular path and the longest path from the source to receiver via the active region is, assuming a sound speed of 1500 m/s, approximately 0.85 ms. Thus, appreciable pulse distortion would typically be expected in this case.

In the relatively simple case where the scattered field is Gaussian, the sampling statistics given in Section 4.3.2 for the incoherent field apply, and the scintillation index

is 1. It can be shown for this case that the bistatic scattering cross section is proportional to the surface slope probability density function, evaluated at the slopes which give rise to the appropriate locally specular reflection. This result holds even in cases where the surface height statistics are non-Gaussian [Barrick, 1968b]. The intensity impulse response for electromagnetic backscatter at normal incidence has been investigated for this case in connection with satellite altimetry [for a review, see Barrick and Lipa, 1985]. The intensity impulse response for acoustic scattering from a pressure release surface has been treated theoretically by McDonald and Spindel [1971] for directions near specular, and has been measured experimentally for general bistatic scattering by Zornig et al. [1977].

The scattered field statistics may fail to be Gaussian either if there are, on average, a few ($\lesssim 5$) dominant specular points or if the number of specular points has a variance that is comparable to its mean. There is inherently more variability in the scattered field in these cases. Intuitively, fluctuations in the brightness, number, location, and relative phase of contributions from a few dominant specular points clearly affect the resultant scattered field more strongly than do similar fluctuations when there are many infinitesimally contributing specular points. If the variance in the number of specular points is comparable to the mean, the probability that some realizations of the rough surface produce only a few specular points is appreciable; these cases lead to increased variability in the scattered field. The second possibility leading to non-Gaussian field statistics is often associated with bunching of scatterers [Jakeman, 1980; Jao, 1984]. Intuition aside, the comments on the case of non-Gaussian field statistics made at the end of Section 4.3.2 still hold. In particular, a greater number of independent scattered field samples are likely to be necessary to estimate field moments to a given precision than are needed to obtain the same precision with Gaussian field statistics, and the scintillation index tends to be greater than 1. Even for this relatively simple, intuitive scattering mechanism, sampling statistics and the scintillation index have not yet been computed. However, there is a basis for further quantitative theoretical investigation in the special case of surfaces with Gaussian surface height distributions. In a series of papers, M.S. Longuet-Higgins has developed theoretical expressions for the distributions of slope and curvature, for the mean number of specular points per unit area, and for the distribution of curvature at specular points, assuming Gaussian surface height statistics, but at least in principle, with no restrictions on the spectrum of surface roughness [Longuet-Higgins, 1958, 1959, 1960a, b, c, and d]. More restricted and less rigorous, though simpler results have also been derived by Barrick [1968a] and Yordanov and Michalev [1988]. As of this writing, it appears to me feasible to compute the intensity distribution of individual specular point contributions (at least numerically), as well as specular point spatial statistics, in the special case just described. These computations would allow the derivation of scattered field statistics based directly on surface roughness statistics. Note that these statistics would depend on the incident and scattered grazing angles, but not on acoustic frequency. To my knowledge, this would be the first such derivation in rough surface scattering theory. Provided that these results were experimentally confirmed, they would obviously be of great value in simulation, as well as in experimental design.

Section 4.4: Hypotheses about Reflection and Scattering Mechanisms

With the previous section for background, we can return now to the particular problem of high-frequency acoustics under ice in light of the observations discussed in Section 4.2. This section considers several scattering mechanisms which are consistent with the qualitative characteristics of the reported observations, discusses the observational support (or lack thereof) of each potential explanation of the data, and very briefly discusses practical implications of certain hypothetical scattering mechanisms.

Upon initial consideration, it would seem that scattering from inhomogeneities within the ice might play a significant role, especially at high frequencies. It is well known from studies of ice growth and morphology that the salinity of arctic sea ice is highly inhomogeneous on centimeter to meter length scales. In the case of first-year ice, the inhomogeneity is inherent in the brine drainage structure, which has a tree-like form with the "trunks" in the lower part of the ice [Bennington, 1967; Lake and Lewis, 1970; Eide and Martin, 1975; Wakatsuchi and Kawamura, 1987]. In the case of multiyear ice, horizontal and vertical salinity fluctuations are observed which are apparently related to differential weathering [Cox and Weeks, 1974]. The elastic properties of sea ice are known to vary with brine volume [Schwarz and Weeks, 1977; Maykut, 1985]. Thus, it is entirely reasonable to suggest that the observed inhomogeneities in sea ice could cause significant acoustic volume scattering, especially when the acoustic wavelength is comparable to the size of the inhomogeneities, as it is in the present case. Interference between scattering centers might then qualitatively account for the chaotic fluctuations in "reflection gain" which are observed as the experimental geometry and acoustic frequency vary.

In order for significant volume scattering to occur at a given frequency and grazing angle, there must first be significant transmission of acoustic energy into the ice. However, all theoretical computations of the reflection loss for a flat interface between seawater and perfectly homogeneous sea ice indicate that there is little penetration at high frequencies and at grazing angles less than approximately 25°. The computed reflection losses for these grazing angles are typically less than 3 dB [Jezek, 1985; McCammon and McDaniel, 1985; Posey et al., 1985]. When the ice–water interface is modeled as an abrupt transition, transmission becomes significant near 30° grazing angle because of conversion to shear modes within the ice. When the gradual nature of the ice–water transition (and the ability of the material within it to support shear) is modeled, the conversion and associated transmission are, according to Posey et al. [1985] greatly diminished. (Note, however, that the results of Yamamoto and Badiey [1986] seem to be somewhat at variance with this conclusion, so the degree of transmission at larger grazing angles to be expected on theoretical grounds is uncertain.) Even if underice surface roughness were to enhance transmission at low grazing angles, the large surface reflectivity would tend to cause surface scattering effects to dominate volume scattering effects. Furthermore, the computed reflection losses are approximately equal to the mean observed reflection loss (see Section 4.2). Thus, it appears unlikely that a significant fraction of the total acoustic energy to be scattered is available for volume scattering.

The shape of forward reflected/scattered pulses reported by Garrison et al. [1983] also tends to argue against volume scattering, at least as a dominant mechanism. In the experiment reported by these authors, the transducer beam patterns were wide (see Section 4.2), causing a large volume of ice to be ensonified. Volume scattering is usually characterized by a very broad (bistatic) angular scattering pattern. Given the geometry of this experiment, one should expect the active scattering region to be quite large and there should be considerable pulse stretching. However, this is exactly the opposite of what was observed. This is the result of only one experiment and certainly requires further verification. However, if this result is more widely substantiated, then any volume scattering mechanism operating in the present case must be unusual in comparison with those observed in scattering from other geophysical media [cf. Ulaby et al., 1982, Chap. 11].

While the above arguments do not completely rule out the importance of volume scattering, they do point out significant difficulties that any argument for volume scattering must overcome. These difficulties are even more significant because they do not occur with the two hypothetical mechanisms discussed below.

Indeed, the first argument above against volume scattering suggests that surface reflection and/or scattering may be responsible for the acoustic observations. In the following, two hypothetical surface scattering mechanisms are discussed. The first is simply rough surface scattering; the second is more speculative and theoretically less well explored. For reasons to be discussed, the second mechanism probably acts together with rough surface scattering, if it contributes at all.

Given the observations of the underice surface discussed in Section 4.2, it is obvious that the possibility of rough surface scattering from the underside of the ice must be considered. From the UARS observations, divers' reports, and videotapes of underice surfaces [F. Olsen, personal communication, 1987], and from the Canadian data reported by Verrall and Ganton [1977] and the qualitative data reported by Grishchenko [1979], the following qualitative picture of the underside of relatively flat ice emerges. Both new and old ice display very gentle undulations in the ice draft, with vertical amplitudes typically in centimeters, and with horizontal lengths from tens of centimeters to meters to perhaps tens of meters. The undulations are of larger amplitude on the underside of old (multiyear) ice; newly frozen leads can be very flat, although at least one videotape seems to qualitatively show gentle roughness with amplitudes of one to a few centimeters, even under very new ice. The gentleness of the undulations means that the slopes of the underice surface are small; even comparatively rough multiyear flat ice shows a maximum slope of only approximately 5°, according to the UARS data.

The Rayleigh roughness parameter χ is plotted in Figure 4.7 for several values of the grazing angle, as a function of the rms surface height deviation normalized by the acoustic wavelength. For a typical acoustic wavelength of 5 cm, the underice surface described above is at least moderately rough at all grazing angles of interest. At grazing angles greater than 10°, underice surfaces may well be very rough, according to the definition of the last section. Scattering models for surfaces with small roughness are evidently not appropriate at high frequencies. (A model for scattering from a slightly

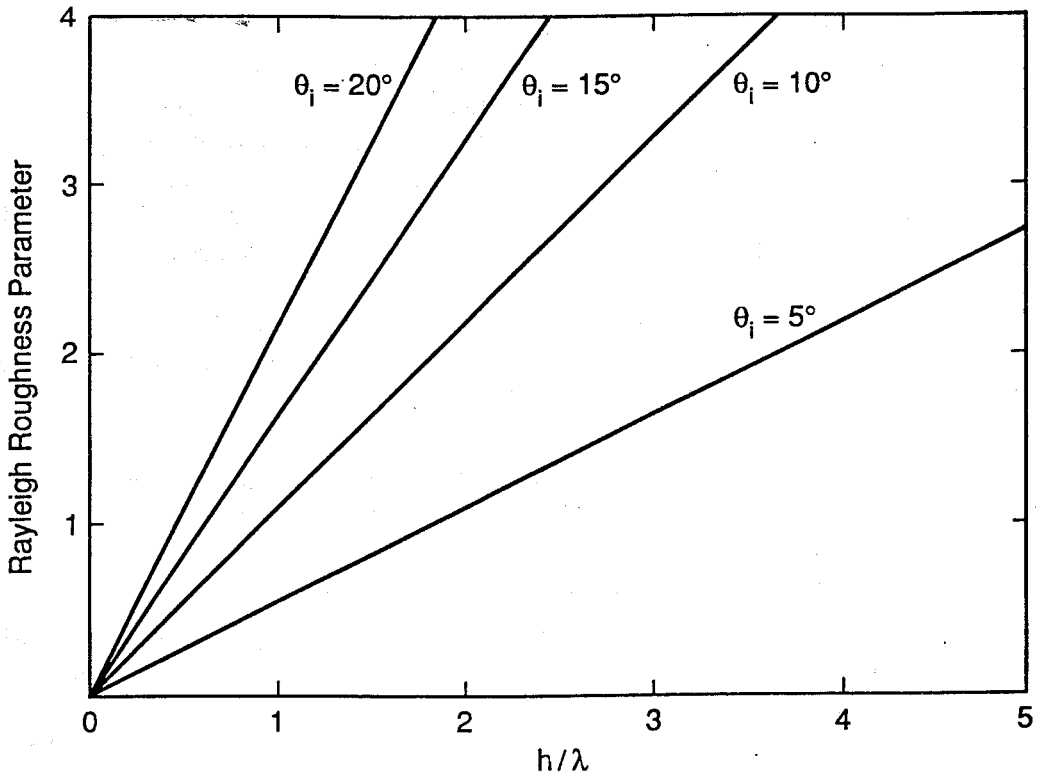

Figure 4.7. Rayleigh roughness parameter vs rms surface height for several incidence angles.

rough surface bounding an elastic medium has been given in the Soviet literature by Lapin [1964, 1966, 1968, 1969, 1970]. This work is reviewed by Pierce and Hickox [1983]. The angular distribution of the scattered field obtained from this model, although interesting, is inconsistent with the data discussed in this chapter. McDaniel [1988] has also given a model for only the incoherent part of the field scattered from a slightly rough surface bounding an elastic solid. Since forward reflection and scattering from a slightly rough surface depends strongly on the coherent and incoherent fields, this model is inappropriate in the present problem because of its limitations on both roughness and field coherence.) In view of the gentle undulations and small slopes of the underice roughness, the Kirchhoff approximation does appear to be appropriate, at least for grazing angles larger than twice the rms surface slope.

The observed magnitude of the fluctuations in forward reflected or scattered intensity suggests substantial, perhaps complete incoherence of the forward bounce signal. This is consistent with what little is known about the rms underice surface roughness.

The observations reported by Garrison et al. [1983] and by Verrall and Ganton [1977] show a nearly complete lack of pulse distortion (except perhaps just at the beginning and end of pulses) and a signal arrival time essentially identical to that expected for

reflection. Taken together, these observations indicate that the active surface scattering region is relatively small (on the order of the size of the first Fresnel zone) and that it is situated around the nominal specular point. A small active region would be consistent with small underice surface slopes (though this inference should be considered somewhat tentative pending further supporting observations).

The data show no clear trend in the mean level of scattered intensity with frequency from 20 to 80 kHz, which is what one would expect from a specular point scattering mechanism, provided that the reflection coefficient near the nominal grazing angle is also frequency independent over this range. On the other hand, the scattered intensity fluctuates more rapidly with changing source–receiver geometry as the acoustic frequency increases. This also is to be expected from the specular point scattering mechanism. For any given realization of the rough surface, contributions from distinct specular points interfere, causing fluctuations as acoustic path lengths from source and receiver to each of the specular points change. The changes in acoustic path length for a given change in geometry increase with frequency.

Even a highly simplified specular point model can be used to demonstrate how the observed intensity fluctuations can be reasonably explained. Consider the situation shown in Figure 4.8, where the spatial dimensions correspond to a case reported by Garrison et al. [1983]. The range is 551 m, the receiving transducer depth is 39 m, and

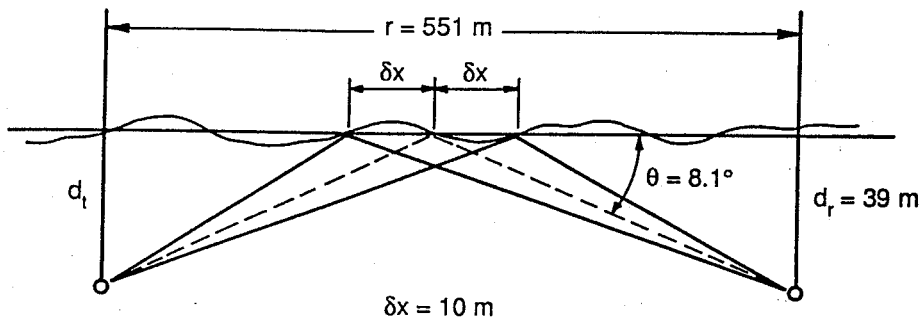

Figure 4.8. Interference between two specular points.

the source depth varies in this example by a few meters about 39 m. The nominal grazing angle is approximately 8.1°. Suppose that there are two specular points which reflect field contributions of equal amplitude into the forward scattering direction. For convenience, suppose that they are both situated vertically at the level of the mean surface and equidistant horizontally from the nominal specular point, along a line connecting the horizontal source and receiver positions. Let the separation of either specular point from the nominal specular point be δx. In this example, take δx = 10 m. Now suppose further that the position of the specular points and the relative amplitude of their contributions is constant as the source is raised or lowered by small amounts relative to its initial depth. Neglect any changes in spreading losses as this occurs. These suppositions certainly oversimplify the situation somewhat, but the resulting model still serves to demonstrate that the observed fluctuations are consistent with specular point scattering.

For an acoustic wavelength of 5 cm, a straightforward calculation shows that raising or lowering the source from 39 m by only 2 m causes contributions from the two specular points at the receiver to change in relative phase by π radians. The travel time difference between paths passing through the two specular points, however, is a maximum of only 16 μs for this amount of source displacement. Thus, as the source is raised or lowered by very modest amounts, it is easily possible for the interference between specular point contributions to go from constructive to destructive, with pulse distortion remaining nil during the entire process. Specular points farther apart will produce interference fringes with even less source displacement, while those closer together will produce larger scale fluctuations. The phase coherent interference between specular points is capable of producing apparent reflection gain, which is a feature of the observations.

Intuitively, a somewhat periodic-looking interference pattern may even result from modest changes in geometry, if there are only a few contributing specular points in the active region. In fact, the gentle undulations of the underice surface seem likely to produce only a low spatial density of specular points.

Thus, a Kirchhoff approximation surface scattering model, especially a specular point scattering model, is strongly suggested by observations to date. However, the measurements previously reviewed are insufficient in at least two ways to quantitatively test such a model. First, the experimental geometries used provide only between one and three samples of the forward reflected or scattered field that are likely to be independent, for reasonable ranges of frequency and/or grazing angle. (This will be further discussed in the next section.) In view of the apparently considerable incoherence present, larger numbers of samples are clearly necessary for computation of field statistics, the scintillation index, and so on. Second, underice surface roughness data for (statistically the same) ice under which forward bounce measurements were made is also lacking. Thus we lack the inputs for the scattering models needed to test whether they agree with the data. I discuss ways of eliminating this situation in the next section.

Before leaving the surface scattering hypothesis, though, consider two practical implications that surface scattering would have in the present context. Both of these result from the possibility of interference between signals directly reflected from an ice keel or a target and those which travel a path including forward reflection or scattering from relatively flat ice. First, a keel reflector or target, together with its image in the surface or the contributions from surface specular points, forms a complex target with interfering scattering centers. The interference changes with system geometry and frequency. In the case of forward scattering (rather than reflection), these changes in interference would be chaotic and would vary from realization to realization of the rough surface (i.e., from location to location). Such interference can strongly affect systems which use spatial phase difference information to estimate the arrival angle of incoming wavefronts. A resulting phenomenon known as glint error can lead to bearing estimation errors for the complex target so large that the estimated target position actually lies several target diameters from the true target position. This phenomenon has been studied extensively in the radar literature. Good entry points into this literature include Ostrovityanov and Basalov [1985], Wright [1984], Barton [1974], Sims and Graf [1971], and

Dunn et al. [1959]. Skolnick [1980] provides an especially good introductory discussion. A good entry into the apparently more limited acoustic literature is given by Henderson [1987].

A second potentially important implication of surface reflection and scattering is that spreading losses from a target or reflector near a surface may change dramatically with range. Long [1975] discusses the transition of range dependence of target or reflector return with increasing range from R^{-4} to R^{-8}, as a function of frequency and surface roughness. A complete discussion of either of these possible implications lies beyond the scope of the present work, but a rather full account is given in the reference.

Lastly, consider a second hypothetical surface scattering mechanism based on random variations in ice distinct from draft variations. The natural morphological variations discussed above in connection with volume scattering might also alter the density, thickness, and other elastic properties of the ice–water transition layer in a spatially random way. Other factors such as differential snow cover may also produce such a variation, by modulating heat flow between seawater and the atmosphere and/or shortwave transmission and heating. The length scale over which variations might occur seems open to broad speculation, and I have found no data bearing on this question. I will refer to any surface characterized by spatial variation of its acoustic parameters as a mottled surface.

Theoretically, it has been shown that even an acoustically flat mottled surface scatters radiation. Heuristically, the amplitudes and relative phases of source densities induced on the surface by the ensonifying radiation are distorted from what they would be on a surface with homogeneous properties. The contributions from these source densities to the acoustic field away from the surface interfere in a random way, and radiation is thus randomly scattered from incident direction into various directions. Again, for any single realization, one would expect the interference to be frequency dependent, and this could qualitatively explain the chaotic frequency dependence of observations. In general, variation with frequency in moments of the scattered field would also be expected. Indeed, Watson and Keller [1983] have theoretically found such behavior in the case of fluctuations that are small in comparison with the mean values of the acoustic properties at the interface. Scattering in this case is qualitatively similar to scattering from a slightly rough interface bounding homogeneous material. However, scattering from mottled surfaces in more general cases is evidently largely unexplored, both theoretically and experimentally.

It seems highly plausible that this type of scattering could play a role in underice forward scattering. Yet one cannot at present develop a more specific, convincing argument for likelihood of the importance of this mechanism from theory or scattered field observations. The lack of data showing that acoustic property fluctuations of the underice surface exist makes it difficult to argue convincingly for the importance of this mechanism. Furthermore, the amount of ice characterization data necessary to test such a model may be very large. (An experiment proposed in the next chapter, however, should shed some light on acoustic property fluctuations.) Finally, as has been previously discussed, the available evidence indicates that even relatively flat underice surfaces are probably moderately to very rough at high frequencies. Thus it appears likely

that even if a mottled surface mechanism does contribute to forward scattering physics, it is very likely to do so in conjunction with the more familiar rough surface scattering mechanism.

To summarize, of the preceding three hypothetical mechanisms that might explain existing observations, volume scattering seems to have the least support. The mottled surface hypothesis presently has little substance or support, and in any case probably does not act alone. On the other hand, the behavior of forward reflection and scattering from a randomly rough ice–water interface is highly consistent with existing observations. In fact, the observations suggest this as the primary mechanism responsible. Furthermore, this mechanism is relatively well understood theoretically and, as is discussed in the next section, is probably the least difficult to test further experimentally. I have been unable to produce other plausible candidate scattering mechanisms. Thus, the next section takes as its premises that forward reflection and scattering is likely to be due to one or more of the mechanisms discussed here, and that further measurement and analysis should aim toward clarification of their relative importance and quantitative characterization. Even so, I would encourage the reader to develop alternative scattering mechanism hypotheses for this part of the underice acoustics problem.

Section 4.5: Proposed Measurements and Analysis

As in Chapter 3, the measurements I propose here would provide direct empirical characterization needed for simulation, as well as provide the data necessary for experimental tests of scattering models.

The approach here follows directly from the discussion of the previous section. Forward reflection and scattering from a rough ice–water interface appears at present to be the most likely mechanism responsible for the observations to date and is one of the less difficult mechanisms to test quantitatively. It seems sensible, therefore, to begin by trying either to confirm the dominance of rough surface effects and quantify them, or to show that rough surface effects cannot, or cannot alone, explain the observations. This approach should also produce a body of data that is useful for investigating other scattering mechanisms.

In order to test the rough surface scattering hypothesis, two independent sets of measurements are required. First, an appropriate number of independent samples of the scattered intensity (or whatever other field moment is of interest) are required, for each incident and scattered grazing angle and for each frequency of interest. The appropriate number of samples depends on the nature of the scattering process (e.g., the degree of coherence and scattered field statistics) and, to a lesser degree, on the angular and frequency resolution desired in estimates for the field moments. The measurement statistics characterize the nature of the scattering process, while estimates of the field moments can be compared with theoretical ensemble averages. The second set of measurements are those which characterize the rough surface. The results of these measurements provide input for theoretical models for the field moments.

Consider first the problem of characterizing the scattered field. Further measurements and analyses are needed to clarify certain remaining basic issues concerning the

nature of the forward reflection and scattering process. These issues include the degree of coherence in the process, the physical nature of whatever incoherent scattering is taking place (e.g., specular point or other types of scattering), the size of the active surface region as a function of experiment geometry, and the statistics of the scattered field for typical ensonified region sizes. The results of Garrison et al. [1983] can be used to place a (relatively small) upper bound on the active region for that particular experiment, but it has not been verified that the active region is always small under relatively flat ice. The number of independent samples of reflected or scattered intensity is very small (1–3) for each grazing angle and frequency of interest in each of the experiments previously reviewed. It is not possible to examine intensity statistics except by combining data from relatively large ranges of grazing angle and/or frequency. Such a combination would obscure potentially significant angular variations in these statistics, such as might be expected for specular point scattering (see Section 4.3.3). The small number of independent samples also makes it impossible to estimate the mean intensity, as a function of grazing angle, given the substantial incoherence that is qualitatively observed. (This remains true of the present data sets even when the potential benefits of averaging over nominal incidence angles are considered. A discussion of this follows momentarily.)

Perhaps the most striking observation as to the nature of forward reflection and/or scattering would be direct observation of discrete specular points. Evidently, no such observations have ever been made. A bit of analysis convincingly shows why not. Trial computations with various forward scattering geometries and active region sizes (based on the UARS estimates of underice slopes) indicate that larger grazing angles ($\gtrsim 30°$) and ranges increase the time separation between signals arriving from specular points at the near and far edges of the active region. However, the temporal resolution necessary for direct specular point observation is always on the order of microseconds. Such resolution appears difficult to achieve in acoustics at kilohertz frequencies using standard wide-bandwidth techniques. (It is possible that multidimensional matched filtering, such as that discussed by Bell and Ewart [1986], could provide the temporal resolution needed for direct specular point observation, provided that each specular point returns a good replica of the transmitted pulse. The high signal to noise ratio available in forward scattering experiments favors this approach. However, I will leave the investigation of this advanced technique for future work.) The spatial resolution requirements for direct specular point observation also seem impractical.

Given, then, that presently existing observations are inadequate and that direct observation of the nature of the scattering is difficult or impossible, the best experimental strategy appears to be proper statistical characterization of the forward reflected/scattered field. The fundamental requirement for such characterization is a suitable number of effectively independent samples of the acoustic field within each interval of nominal grazing angle and frequency of interest. Strictly speaking, the requirement for independent samples of the field means that the surface roughness of the active surface region for each sample must be independent of the roughness in the active region for every other sample. Thus strictly, the forward reflection/scattering experiment must be performed at different locations under statistically homogeneous ice, once for each independent sample to be collected for a given grazing angle and frequency.

For estimating the mean intensity it is sometimes possible to obtain a few effectively independent samples within an acceptably small range of grazing angles or frequencies by averaging over fluctuations within those ranges. For example, consider a data trace such as one of those presented by Garrison et al. [1983]. The received intensity fluctuates widely within even small ranges of nominal grazing angles. Consider a section of the trace within which the change in grazing angle is less than or equal to the desired angular resolution for measurements of the mean intensity. The desired angular resolution should be small enough that the mean intensity can be expected to vary by less than an acceptable amount over such a small angular range. Think of this section of the trace simply as a function of grazing angle, and consider its one-sided bandwidth W in cycles/degree, which might be estimated from several such sections. Averaging over grazing angle can be thought of as integrating the data trace over a range from θ to $\theta + \delta\theta$ and normalizing. The variance of the angle-averaged intensity (from realization to realization) is reduced in comparison with the variance of intensity measured at a single angle by a factor of approximately $2 \mid \delta\theta \mid W$, independent of the distribution of the values of the data [Ulaby et al., 1982; Henderson, 1987; for excellent fundamental discussions, see Slepian, 1976, 1983]. Thus the effective number of independent samples resulting from such averaging is $N = 2 \mid \delta\theta \mid W$. Similarly, one can consider an experiment in which the geometry is fixed but the center frequency is swept, and the resulting observed function of intensity versus frequency is averaged over ranges of frequency commensurate with the desired frequency resolution. The desired resolution should be small enough that the mean scattered intensity can be expected to vary little over such a frequency range. Both techniques are widely used in radar scatterometry [Ulaby et al., 1982]. The physical principle behind these techniques is that one is averaging over effectively independent realizations of the interference between scattering centers, since this interference changes with experimental geometry and frequency.

With the preceding in mind as to the acquisition of independent samples, we can consider at least two possible types of experiments to statistically characterize forward reflection and scattering. The first type of experiment would be carried out using transducers suspended through holes drilled in the ice. This is similar to the previous practice of investigators at APL-UW, except that more holes would be necessary to gather more independent samples of intensity. Consider the possible experimental arrangement sketched in Figure 4.9. A receiver and data collection installation are placed at the center of a circular array of holes, where they can remain fixed. A mobile transmitter is lowered through each of the holes on the periphery of the circle, and a set of measurements of forward reflected/scattered intensity can be made for a variety of frequencies and nominal grazing angles. Split-beam cross-correlation measurements at the receiver, which can be used to characterize the angular widths of the scattered pressure field, would also be relatively easy to make.

The active region for each measurement extends along the radius of the circle between the transducers. Its width is determined by the nature of the forward reflection or scattering process, but is always small compared with its length. The minimum angular displacement between holes around the circle is determined by the requirement that the individual active regions contain independent surface roughness. In the absence of

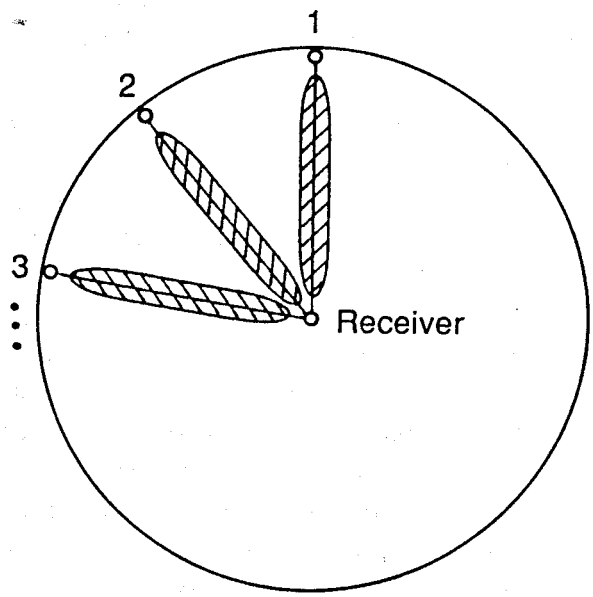

Figure 4.9. Possible experimental arrangement for a forward reflection/scattering experiment using transmitting hydrophones suspended through holes in the ice. Shaded areas schematically denote active regions.

quantitative information on underice surface roughness, it seems reasonable to begin experiments merely requiring that estimated active regions consist of physically disjoint surface regions. Note that since the nature of the surface reflection and scattering process limits the active surface region, the beam patterns of the transducers are not very important so long as they ensonify the entire estimated active region. Note also that there is an interplay between the estimated active region width, the magnitude of the radius of the circle (i.e., the range), and the number of transmitter locations that can be fitted about the circle. Other things being equal, it appears that relatively short ranges are to be preferred, since any scintillation and/or ray bending in the water column will be minimized, and since this should make the logistics of any moving of transmitters from hole to hole less difficult. Finally, note that if there is substantial directional anisotropy in the underice roughness, samples from differing angular sectors of the circle may have to be treated separately, reducing the number of independent samples available for each theoretical test of a given configuration.

It is not difficult to find an acceptable compromise between range and the number of possible transmission holes. As an example, consider a case in which the range is set to 200 m. Conservatively (over)estimate the likely rms surface slopes to be 7°, and set transmitter and receiver depths at 20 m. The nominal grazing angle in this case is 11°. Assume isotropic roughness of the underice surface. Using the results of Section 4.3.3, the width of the active region for completely incoherent scattering midway between source and receiver is approximately 3 m, and the active region subtends an azimuthal

angle at the source or receiver of approximately 3°. Thus even if transmission holes were conservatively placed every 6° around the circumference of the circle, there would be room for 60 holes.

This brings us to the fundamental issue, namely that of how many transmission holes are likely to be needed for acceptable characterization of the reflected/scattered intensity. As noted above, a strict application of scattering theory would require one transmission hole with an independent (estimated) active region for each set of measurements at various grazing angles and frequencies. For example, 25 holes would be needed to estimate the mean intensity with a relative standard error of 1 dB for incoherent Gaussian field statistics. Fewer samples would suffice if some coherence is present, and potentially many more would be necessary in the case of non-Gaussian field statistics (see Sections 4.3.2 and 4.3.3). As noted above, directional anisotropy of underice surface roughness would also increase the number of holes needed to obtain a given number of independent samples for each scattering geometry. If the scintillation index is to be estimated, Table 4.1 indicates that 100 or more samples may be needed to obtain useful accuracy. An experiment based completely on transducers suspended from holes is not robust (in terms of the effort and time necessary) with respect to changes in assumptions on field statistics. The difficulties would also increase with the thickness of the ice for which underice scattering is to be investigated.

It appears that averaging over small ranges of grazing angles in the way described here can partially lessen the need for many transmission holes. Appendix 4C presents a preliminary examination of a subset of the forward reflection/scattering data from Kane Basin reported by Garrison et al. [1983]. The (one-sided) bandwidth of short segments of these data (2° in nominal grazing angle) varies from approximately 2.5 cycles/degree at 10 kHz to 3 cycles/degree at 75 kHz. If this initial estimate can be substantiated and shown to hold more widely, then the number of transmission holes needed to estimate the mean intensity to any given precision is thus similarly reduced by a factor of 10–12, provided the scattered field statistics are Gaussian. However, estimates of parameters such as the scintillation index and parameters of the intensity distribution may still require many truly independent field or intensity samples. One might try to increase the number of samples over the number of holes by selecting as many equally spaced points on the data trace in angle or frequency bins as there are independent samples, and then considering these points to be approximately independent for estimating statistical parameters other than the mean intensity. Such a procedure has evidently not been justified, though it is commonly done in a number of applications [D.B. Percival, personal communication, 1988]. Without justification, there is a risk of serious error in using such a procedure. Thus, angle and/or frequency averaging can only partially lessen the problem of drilling many holes in experiments to characterize the reflected/scattered field.

Use of an autonomous or semiautonomous underwater vehicle to carry a transmitter would allow considerably more flexibility and robustness in a field characterization experiment because it would then be relatively easy to collect many independent field samples under relatively flat ice of any thickness. This advantage would come at the cost of much more development work on equipment and experimental technique.

One possible experimental arrangement is displayed in Figure 4.10. A programmable vehicle with a side-mounted transducer could be set to trace out a square spiral around a stationary suspended receiver connected to the primary reception and data recording electronics. On each straight leg of the spiral, the vehicle transmits pulses, producing forward reflection and scattering data from independent active regions under the ice for as long as the receiver is within the transmit beam. As the depth and/or range of the vehicle varies, the nominal grazing angle changes. The square spiral shape allows the depth and attitude of the vehicle to be stabilized while data are being acquired, so that the nominal grazing angle can later be obtained and any necessary beam pattern corrections can be made. Here again, split-beam cross correlation measurements at the receiver could be made relatively easily.

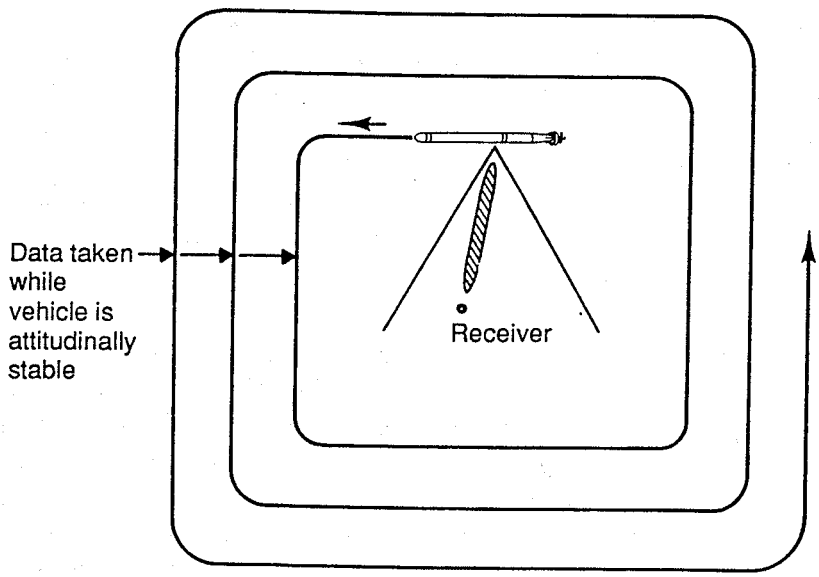

Figure 4.10. Possible run pattern for underice roughness measurement.

Depth and three-axis attitude data would evidently need to be sampled and stored aboard the vehicle for later use in the data reduction. A transmitter beam pattern as wide as possible in azimuth (i.e., in the direction along the length of the vehicle) is desirable, since this will produce the greatest amount of data along each leg of the spiral. The limitations on beamwidth may be the transmit power available aboard the vehicle and the signal to noise ratio needed for the experiment. Synchronized receiver and transmitter clocks and a vertical beamwidth large enough to allow a direct (as opposed to surface bounce) pulse to be received would allow for a simple computation of source range even in the absence of other vehicle tracking.

For example, the range of the vehicle might vary from 100 to 400 m, with transmitter and receiver depths of 20 m. At a vehicle speed of 4 knots, a range of 200 m (nominal grazing angle of 11°), a pulse repetition rate (at a particular frequency) of 0.1/s, and an azimuthal beamwidth of 50°, eight independent samples of the reflected or scattered field or intensity could be obtained on each leg of the spiral, for a total of 32 samples. This estimated number of independent samples per leg is based on the same conservative assumptions about underice surface slopes as the example used in discussing the hole-based experiment. Smaller surface slopes would allow more independent samples per leg. The time needed to acquire the measurements, excluding deployment and recovery time, is small. The time necessary for these latter operations probably controls the overall temporal efficiency of the scheme. Transducer engineering considerations may limit the experiment to a single acoustic frequency or small range of frequencies, at least initially.

Regardless of the experimental scheme used to characterize the forward reflected/scattered field, possible effects of ice conditions (temperature, growth, or ablation rate on the underside, etc.) and ice type (new, first-year, multiyear ice, etc.) on field and intensity statistics should be investigated. As noted in Section 4.2 and Chapter 2, the literature indicates important variations in acoustic properties of sea ice with ice conditions. It is likely that roughness varies with ice type even for undeformed ice, and it is plausible that there is even a seasonal variation of underice surface roughness. This argues for the most versatile, flexible experimental scheme possible within practical constraints.

As noted at the beginning of this section, characterization of the acoustic field and intensity is only part of the difficulty in quantitative testing of surface scattering models. Independent surface roughness characterization is also necessary. The three most important statistical measures of surface roughness in surface scattering theory, and in particular in Kirchhoff approximation based models, are the univariate surface height probability density function (pdf), the univariate surface slope pdf, and the surface roughness power spectrum or correlation function over a particular range of spatial scales.

The height pdf enters the computation of both the coherent reflection loss and the backscatter cross section (see Section 4.3.2). This pdf is nearly always assumed to be Gaussian, but the angular variation of the coherent reflection loss in particular is strongly affected by the form of this pdf [Clay and Medwin, 1970; McDonald and Spindel, 1971; Clay et al., 1973]. Thus independent measurements of surface height at distinct points should be used to check the gaussianity of surface heights. In the high frequency limit, the slope pdf determines the angular behavior of the scattering cross section (see Section 4.3.3). The slope pdf is also usually assumed to be Gaussian. However, a non-Gaussian slope pdf produces significantly different backscatter from a Gaussian pdf (Barrick [1965] and Yordanov and Michalev [1988]). The slope pdf should therefore also be checked for gaussianity. However, the roughness data needed for these pdf checks are not likely to be the most stringent requirements for testing the surface scattering model. The surface roughness power spectrum must be estimated precisely over a range of spatial scales, and the data needed for this estimation should be sufficient for the other purposes as well.

The surface roughness power spectrum strongly influences the angular behavior of scattering cross sections. The largest important spatial scale of roughness in the scattering problem is, in part, determined by the ensonified area in the problem. Surface height variations on much larger horizontal scales than the dimensions of the ensonified area effectively introduce only a large scale geometric tilt and/or distortion of the ensonified spot and should be modeled separately from smaller scale surface roughness. Note, however, that the size of the ensonified area may vary widely even for a given application. Alternatively, the size of the pieces of the scattering medium (the floe sizes in the present problem) may set the limit on the largest spatial scale of importance. Finally, the surface roughness spectrum may contain negligible energy on spatial scales larger than some value. We do not know whether the underside roughness of sea ice has a maximum spatial scale smaller than the floe size (though this seems likely). Thus, it is presently desirable to characterize the surface roughness spectrum on spatial scales as long as possible without exceeding floe boundaries.

The precise value of the shortest important spatial scale, corresponding to the largest spatial wavenumber, depends on the surface scattering theory appropriate to the problem. Typically, though, the largest wavenumber of significance is very roughly the radiation wavenumber. For a forward scattering model based on the Kirchhoff approximation, Appendix 4B shows that this is a good approximate rule. In order to obtain a reliable estimate of the surface roughness spectrum at this spatial scale, it is necessary to sample the surface height on a finer spatial scale to prevent aliasing [Blackman and Tukey, 1959]. Thus, sampling is desirable at a spacing of $\lambda/2$, where λ is the radiation wavelength. In high frequency acoustics, such sampling would require measurement spacings of a centimeter or less. Such fine spacing may be impractical. However, spectral information even at longer spatial scales is useful for modeling the rough surface, particularly if the shortest spatial scale that can be measured is within one or two octaves of the desired scale and the spectrum can be extrapolated with some confidence. Alternatively, some sort of fixed experiment might provide fine spatial resolution of roughness heights over an area of perhaps a few square meters. Candidate techniques might include stereo photography or an acoustic profiler operating a meter or less below the ice. Ideally, this latter experiment would produce spectral estimates in a range of wavenumbers overlapping the highest spatial wavenumbers in the spectral estimate from the vehicle-based experiment, allowing the two estimates to be matched up into a single spectral estimate extending to the fine spatial scales. In any case, the requirement for the shortest spatial scale for which the spectrum is to be estimated in this problem is simply that it be as short as is practically feasible.

How accurate the surface height measurements should be is determined by the magnitude of the smallest significant surface height deviations, and this magnitude is determined by the radiation wavelength. As noted in Section 4.3.1, rms surface roughness deviations of less than approximately 3% of the radiation wavelength produce so little scattering that in most cases, it can be neglected. Ideally then, it is desirable to acquire roughness measurements with this accuracy. At 30 kHz, this would require an accuracy of approximately 1.5 mm, or approximately a 1 μs (one part in 6000) accuracy in the time of flight measurement on the shorter horizontal scales where surface relief is small.

(On longer horizontal scales with larger relief, it appears that an accuracy of a few percent of the relief is sufficient.) Assuming that measurement noise is independent of the surface roughness, the spectrum of the sum of the surface roughness measurement plus noise is just the sum of the individual spectra at each point in spatial wavelength space. Measurement error introduces a "noise floor" into the estimated roughness spectrum. If millimeter accuracy is not practically feasible, it may be possible to estimate and subtract the measurement noise spectrum to improve the roughness estimate [Jones, 1981]. In any case, as when measuring small spatial scales, measurements with an accuracy even close to that desired will prove more useful in modeling than no data at all.

Up to this point, I have not addressed the question of the spatial pattern on which roughness measurements should be made. Regular or random sampling on a full two-dimensional grid of the area discussed above would produce an impractical quantity of data for analysis. Collection of roughness measurements along lines under the ice would be much more manageable. However, there is a distinct possibility of directional anisotropy in underice roughness statistics, due, for instance, to anisotropic snow cover (sastrugi, etc.), rafting early in ice growth, and so on. Thus roughness measurements taken along lines in several different directions would be valuable.

There is also good reason to expect variations in underside roughness for different ice types. Spatially varying snow cover, seasonal flushing and so on are likely to cause spatially varying ablation and ice growth which depend on thickness, and thus on ice type. Seasonal variation of underside roughness may also occur. The presence or absence of these variations should be documented for possible incorporation into models and simulations.

I have not been able to think of a method of making the measurements just described under ice without using an underwater vehicle. Investigation of the isotropy and of the unknown largest spatial scale of underice roughness would seem to virtually require a method based on a vehicle that can roam underice for distances on the order of a hundred meters. An upward looking sonar measuring only time of flight would appear to be a practical way of measuring ice draft as a function of position along a line under the ice. From draft, the necessary surface roughness statistics could be obtained, provided the depth of the vehicle is known to within the accuracy described above, i.e., about 1 mm, over short distances. Again, as a practical matter, accuracy of 1 mm in depth measurements is required only over short horizontal distances of several meters, since underice surface height variations on longer spatial wavelengths will typically have amplitudes larger than a few millimeters. The smallest spatial scale feasible in the roughness measurements is determined by the smallest feasible acoustic spot size on the underice surface, which is in turn determined by the depth at which the vehicle must operate, the size of the sonar transducer, sonar frequency, and by the sonar pulse repetition frequency. Vehicle speed and ping rate then partially determine the requirements for data storage aboard the vehicle, and this determines how much of the underice surface can be measured in a single run.

As an example, consider an upward looking sonar with a 1° beamwidth operating 3 m below the ice. To operate so close to the ice, operation would have to be restricted to a well defined area of relatively flat ice which had been acoustically surveyed. Also, the attitude of the vehicle in pitch and role would have to be held constant to within approximately 1° during the time data are recorded. The acoustic spot size on the underice surface would be approximately 2.6 cm. Suppose the vehicle speed is 4 knots (very nearly 2 m/s), and the pulse repetition frequency is set such that successive ensonified spots on the ice overlap by 50%. Then the pulse repetition frequency would be 154 per second. Since only time of flight data and depth data apparently need to be recorded, it is unclear, at least to me, how much data storage would actually be needed. Note though, that in four minutes of measurement time, 480 m of ice could be surveyed. A triangular run pattern which would allow investigation of possible anisotropy in underice roughness is shown in Figure 4.11.

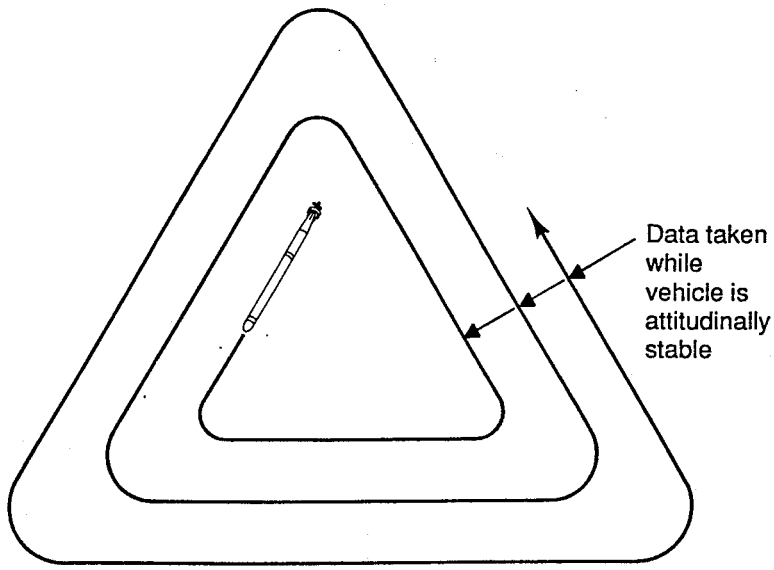

Figure 4.11. Possible run pattern for underice roughness to look for directional anisotropy.

Finally, note that with apparently minor reconfiguration, perhaps only in software, the vehicle just described could also operate at a greater depth and perform wider surveys of ridged and flat ice, yielding potentially useful larger scale draft data.

In summary, the two sets of measurements described in this section would allow several distinct experimental tests of the specular point scattering hypothesis for forward scattering from relatively flat ice. Whether the hypothesis is confirmed, partially confirmed, or ruled out, the data gathered in the effort would prove useful as empirical characterization for simulation and provide insight for further theoretical and experimental investigation.

APPENDIX 4A

Kerr et al. [1951] outline a straightforward method for finding the parameters of Fresnel zone ellipses. The essence of their approach is to find an equation for the coordinates of those points on the reflecting surface for which the difference δ in physical path length from the direct path between transducers is constant.

Figure 4A.1 shows the coordinate system used in this particular problem and defines the relevant variables. This figure essentially follows Figure 5.12 of Kerr et al. [1951]. With the method described by these authors, one finds that the desired equation relating coordinates of surface points is that of an ellipse. It is clear from Figure 4A.1 that the center of the ellipse lies on the x-axis. From the computation, one finds the x-coordinate of its center to be

$$x_o = \frac{r}{2}\left\{1 - \frac{\left[\frac{z_2^2 - z_1^2}{r^2}\right]}{\left[\frac{\delta}{r} + \sqrt{1 + \left[\frac{z_2 - z_1}{r}\right]^2}\right]^2 - 1}\right\} . \tag{4A.1}$$

Note that this equation differs substantially from equation 25 of Kerr et al. [1951], while differing only slightly in appearance. Kerr's erroneous equation is repeated in the discussion by Beckmann and Spizzichino [1963].

The correct equations, respectively, for the width $2B$ (in the y-direction) and length $2A$ (in the x-direction) of the ellipse corresponding to path length difference δ, also given by Kerr et al. [1951], are

$$2B = r\left\{\left[\frac{\delta^2}{r^2} + \frac{2\delta \sec\theta}{r}\right]\left[1 - \frac{\left[\frac{z_1 + z_2}{r}\right]^2}{\left[\sec\theta + \frac{\delta}{r}\right]^2 - 1}\right]\right\}^{1/2} \tag{4A.2}$$

and

$$2A = 2B\left\{1 + \frac{1}{\left[\sec\theta + \frac{\delta}{r}\right]^2 - 1}\right\}^{1/2} . \tag{4A.3}$$

The corresponding equations for these quantities given by Beckmann and Spizzichino [1963] evidently contain at least one error.

These equations simplify considerably when the range r is much larger than both δ and the distances from the transducers to the reflecting surface. Useful approximations for this case are given by Kerr et al. [1951].

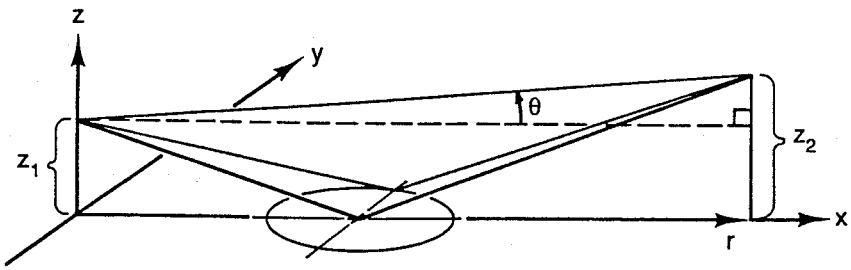

Figure 4A.1. Coordinate system for calculation of Fresnel zone boundaries.

APPENDIX 4B

The point of this appendix is to show that the Kirchhoff approximation for the forward scattered intensity is insensitive to the exact form of the surface height correlation function at spatial lags much smaller than the radiation wavelength. This will justify the claim made in Section 4.5 that the surface roughness correlation function needs to be measured at spatial lags only down to a modest fraction of the radiation wavelength in order to test the Kirchhoff approximation scattering model. I will assume in this appendix that the reader has some familiarity with rough surface scattering and with the Kirchoff approximation. A good introduction with all the background necessary for this appendix is given in Chapter 21 of Ishimaru [1978]. A problem similar to that addressed here is discussed in the case of backscattering by Jackson et al. [1986].

Because in the Kirchhoff approximation the coherently scattered intensity depends only on the variance of surface height, I will consider just the case in which the forward scattering is completely incoherent. In other words, I will assume that the surface is very rough, and thus has a Rayleigh roughness parameter > 2. The incoherent scattered field can be considered to be composed of the incoherent sum of intensity contributions from (usually) relatively small, disjoint surface regions. The size of these regions is determined by the correlation length of a random variable involving the field induced on the rough surface. The computation of this correlation length and the sensitivity of the Kirchhoff approximation result to surface roughness components with long correlation length are related to the computation described below. The essentials of this topic have been developed in Appendix A of Winebrenner [1985], where a quantitative example using the Kirchhoff approximation is given. However, a discussion of this part of the problem lies outside the scope of this appendix; the results developed here will be limited to the sensitivity of the Kirchhoff result to short correlation length components of surface roughness.

The Kirchhoff approximation for the specularly scattered intensity, assuming complete incoherence, is proportional to the following integral over the mean plane of the surface (written here in polar coordinates) [Ishimaru, 1978]

$$I = \int_0^{2\pi} d\phi \int_0^{\infty} dr\, r \exp\left\{-2k^2 \sin^2\theta_i \left[2h^2 - 2h^2 C(r,\phi)\right]\right\} \qquad (4B.1)$$

where $k = 2\pi / \lambda$ is the radiation wavenumber, θ_i is the grazing angle of incidence (and observation), h is the standard deviation of surface height variation, and C is the normalized correlation function of the surface height variation. This integral contains all the dependence of the Kirchhoff result on the two-point surface roughness statistics. For simplicity, assume that the surface roughness statistics are spatially isotropic. Then C is independent of ϕ, and the integral over ϕ trivially yields a factor of 2π.

Now consider the behavior of the integrand of I in equation 4B.1 with respect to spatial lag r. The assumption of complete incoherence of the forward scattered intensity is equivalent to the assumption that kh is large compared with 1. In other words, we have assumed that we are in a high frequency limit. The integrand is nonnegative definite. By definition, the correlation function C must be 1 (which is its maximum) at zero spatial lag, and must asymptotically approach zero for large lag. For large kh, the exponential in the integrand quickly becomes small as the correlation function decreases with increasing lag. Thus in this limit, the major contribution to I occurs at "short" spatial lags r. On the other hand, for "very short" lags, the exponential factor is nearly constant at 1 while the factor r causes a linear decrease in the integrand with decreasing lag. There is evidently some range of lags $r > 0$ responsible for most of the contribution to I.

As noted in Chapter 4, qualitative observations of the underside of relatively flat ice indicate gently undulating roughness on horizontal scales comparable to radiation wavelengths of interest. This suggests that we approximate the short lag behavior of C by a form appropriate to a random surface for which each realization possesses a derivative in the usual sense at every point. (Strictly speaking, this is the only kind of rough surface to which the Kirchhoff approximation can apply. It is possible, though, for the surface correlation function to behave over some range of lags like a correlation function appropriate to a nondifferentiable surface, while the mean square slope and curvatures of the surface remain acceptable for application of the Kirchhoff approximation [Jackson et al., 1986].) The appropriate form for the approximation is:

$$C(r) \approx 1 - \frac{r^2}{L^2} \quad . \qquad (4B.2)$$

Substituting in equation 4B.1 (and performing the integration over ϕ mentioned above), we obtain

$$I = 2\pi \int_0^{\infty} dr\, r \exp\left[-2k^2 \sin^2\theta_i\, \beta^2 r^2\right] \qquad (4B.3)$$

where $\beta = \sqrt{2}\, h / L$ can be interpreted physically as the rms slope of the rough surface, at least on short length scales. This integral can be computed analytically, and the result leads to the usual geometric acoustics scattering cross section [Ishimaru, 1978] which can be interpreted in terms of specular point scattering.

However, our interest here is to know the shortest spatial lag to which the surface correlation function must be characterized, and thus to find the significant range of spatial lags in comparison with the radiation wavelength. To this end, rewrite equation 4B.3 in terms of the normalized lag $\rho = r / \lambda$ to obtain

$$I = 2\pi\lambda^2 \int_0^\infty d\rho\, \rho \exp\left[-2(2\pi)^2 \sin^2\theta_i\, \beta^2 \rho^2\right] \qquad (4B.4)$$

The integrand of equation 4B.4 is plotted in Figure 4B.1 for values of the rms surface slope corresponding to 3°, 5°, and 7°. Clearly, as the rms surface slope decreases, the center of the range of significant spatial lags moves toward larger lags, and the range itself broadens.

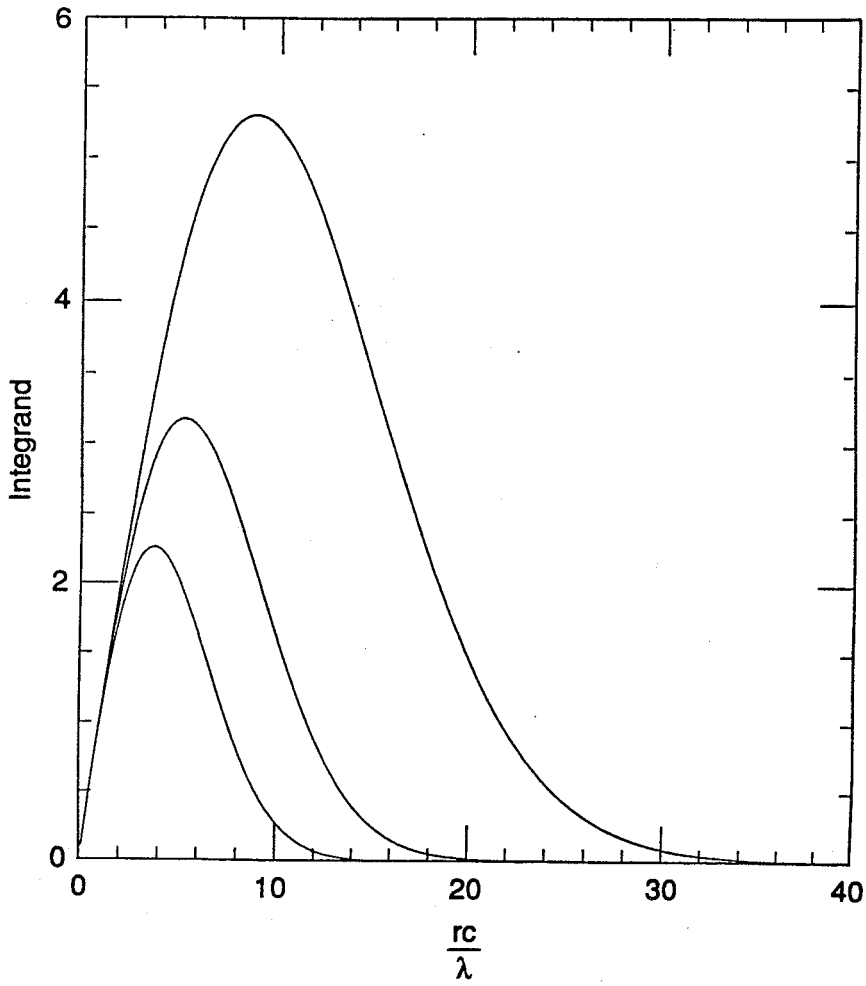

Figure 4B.1. Graph of the integrand in equation 4B.4 for three values of rms slope.

Suppose that we characterize the surface roughness correlation down to some spatial lag r_c, and that at larger lags the measured correlation function fits the form of equation 4B.2 well. If at spatial lags shorter than r_c the correlation function departs from the form of equation 4B.2, then the forward scattered intensity predicted using equation 4B.3 will differ from the prediction based on the Kirchhoff approximation and the actual surface statistics. Figure 4B.1 suggests, though, that the difference can be made quite small if r_c can be made small enough. This relationship can be quantified as follows.

Since the actual surface correlation function must approach 1 as r, or equivalently ρ, approaches zero, the exponential term in equation 4B.1 must be less than but approaching 1 for all $r<r_c$. If the actual surface correlation function approaches 1 more rapidly than $1-r^2/L^2$ at short lags, then equation 4B.3 will underestimate the true value of I, though by not more than an amount

$$E_1 = 2\pi\lambda^2 \int_0^{r_c/\lambda} d\rho\,\rho \left[1-\exp\left[-2(2\pi)^2\sin^2\theta_i\,\beta^2\rho^2\right]\right] \quad . \tag{4B.5}$$

On the other hand, if the actual surface correlation function approaches 1 more slowly than $1-r^2/L^2$, equation 4B.3 will overestimate the true value of I, though in this case by less than

$$E_2 = 2\pi\lambda^2 \int_0^{r_c/\lambda} d\rho\,\rho \quad . \tag{4B.6}$$

This latter error estimate is very crude, but allows for a wide variety in correlation function behavior at short lags, including oscillatory behavior. It is also clearly the larger of the two error estimates. The error in the estimated forward scattered intensity as a fraction of the total predicted using equation 4B.3 is then bounded above by

$$E_f = \frac{\int_0^{r_c/\lambda} d\rho\,\rho}{\int_0^{\infty} d\rho\,\rho\exp\left[-2(2\pi)^2\sin^2\theta_i\,\beta^2\rho^2\right]} \quad , \tag{4B.7}$$

or, computing the indicated integrals,

$$E_f = 2(2\pi)^2\sin^2\theta_i\,\beta^2\left[\frac{r_c}{\lambda}\right]^2 \quad . \tag{4B.8}$$

Figure 4B.2 shows plots of E_f as a function of r_c/λ for a grazing angle of 10° and for several values of β, the rms surface slope. It is clear that choosing r_c equal to half the radiation wavelength, or even equal to the radiation wavelength, leads in most cases to small upper bounds on the possible error in forward scattered intensity.

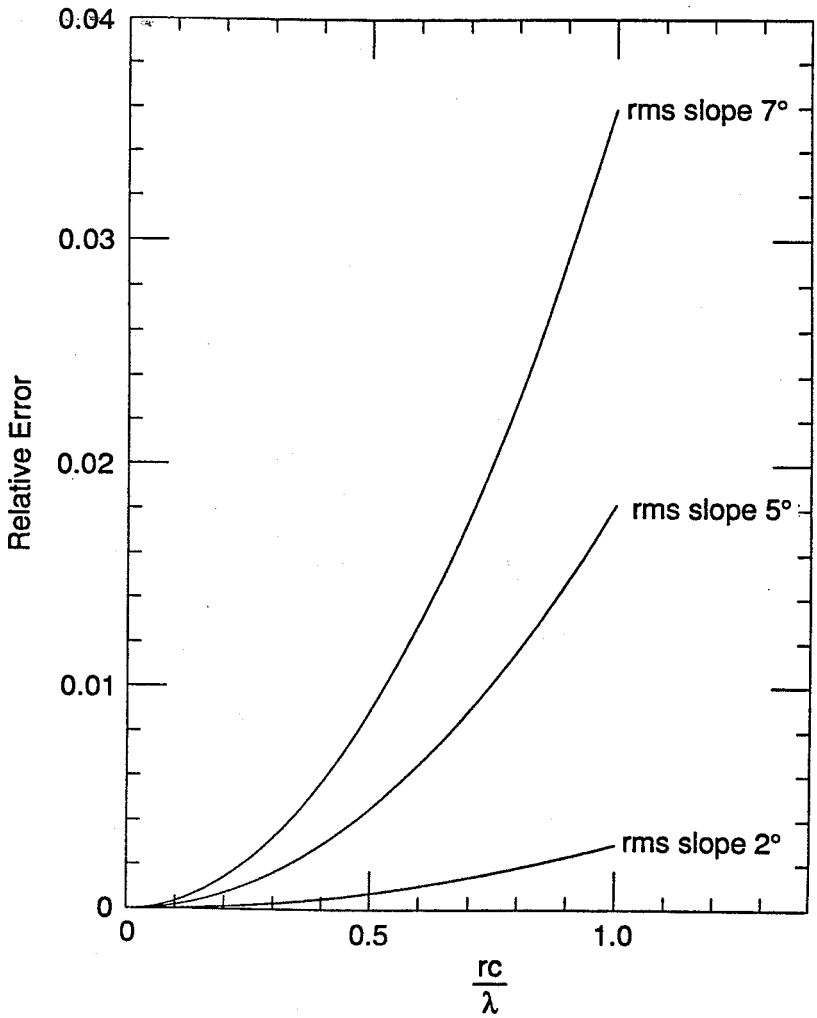

Figure 4B.2. Upper bound on the relative error in scattered intensity due to lack of information at short spatial lags.

APPENDIX 4C

by Warren L. J. Fox and Dale P. Winebrenner

The data for this study were taken from measurements in the Kane Basin in April 1979 [Garrison et al., 1983]. The experiment consisted of lowering a transmitter emitting pulses at five frequencies (10, 20, 30, 60, and 75 kHz), which were received by an array of five hydrophones. The data were digitized, and amplitudes of the direct and reflected pulses at each depth mark were stored on magnetic tape. We selected a suitable set of data (record #128) and performed the following analysis.

The depth marks were first converted to marks of nominal grazing angle. Since these angle marks were not evenly spaced, a cubic spline interpolation was used to map the original data onto a grid of uniform angle spacings. The average angle between data points (0.036°) was used as the new spacing. The data covered grazing angles of approximately 8.2 to 20.1°, but zero amplitudes were recorded for all angles beyond approximately 18.2°. From this, the data were separated into angle bins of approximately 2° (8.2 to 10.2, 10.2 to 12.2, etc.), yielding five angle bins for five different frequencies, or 25 56-point data sets.

First we plotted linear intensity versus grazing angle. Since the bandwidth of fluctuations about the mean was the quantity of interest, we subtracted the mean from the data (separately for each data set). We then performed a spectral decomposition of each data set by means of an FFT algorithm. We used a simple rectangular window and implemented zero padding to increase plot resolution.

Plots of linear intensity and their corresponding spectra in decibels are shown for the 25 data sets in Figures 4C.1–5. We visually estimated the 3 dB bandwidths of several of the spectra. These generally increase with decreasing grazing angle at the center of the range and with increasing acoustic frequency. We estimate the one-sided 3 dB bandwidths of the data to range from approximately 2.5 cycles/degree for the larger grazing angle ranges at 10 kHz to 3 cycles/degree for the same angle ranges at 75 kHz. These are the estimates quoted in Section 4.5.

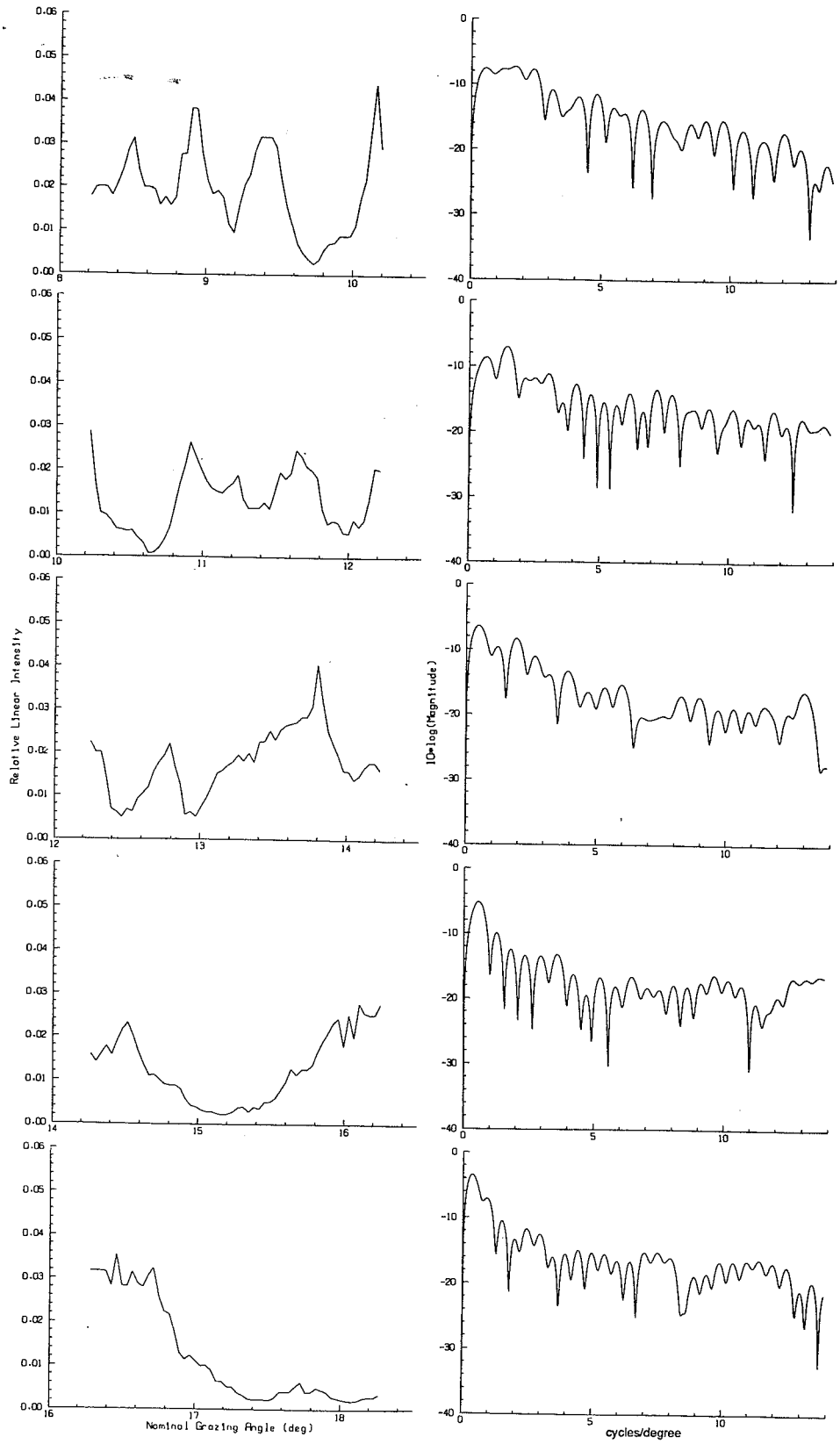

Figure 4C.1. Linear intensity and power spectra in decibels for 2° bins of forward scattering data, 10 kHz.

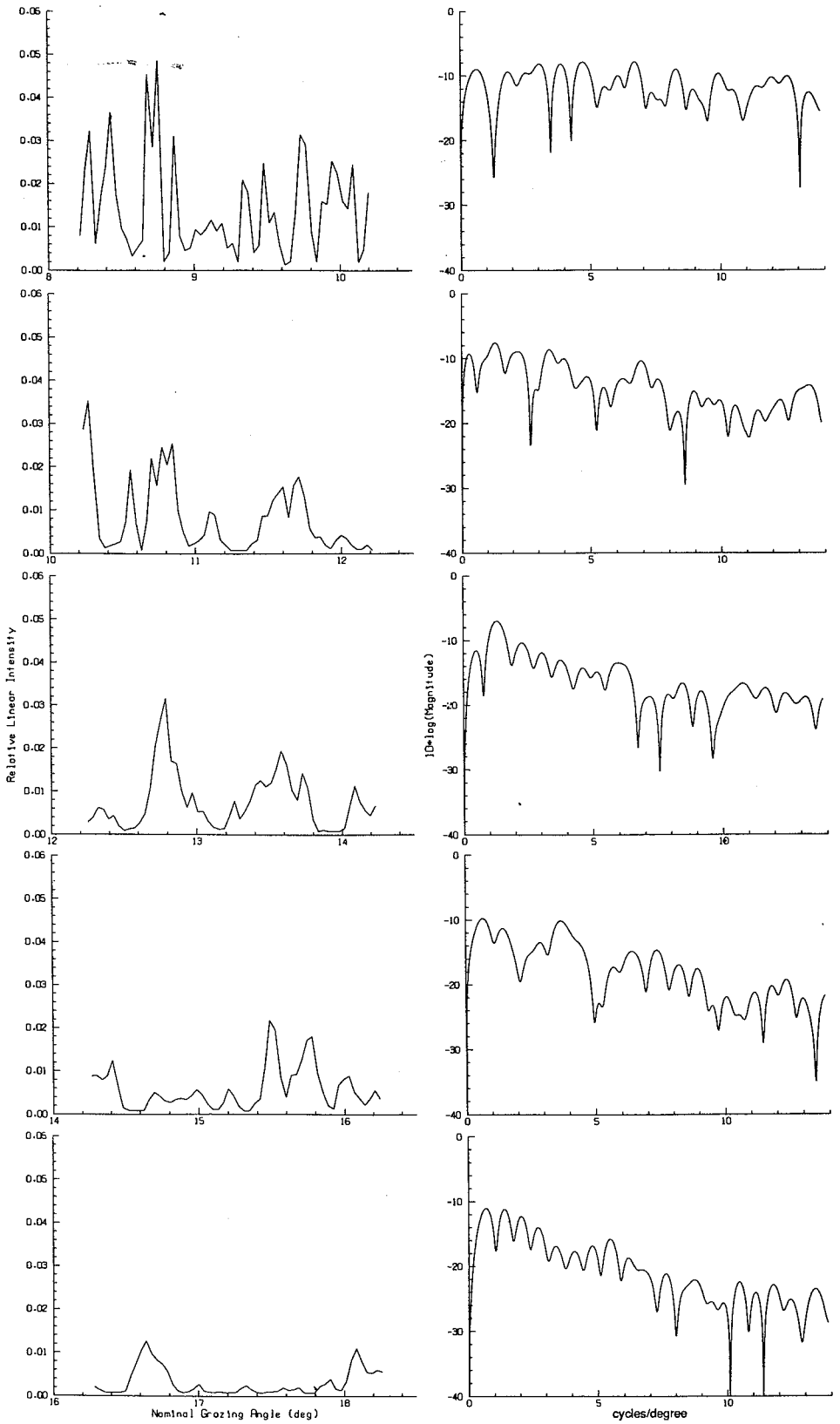

Figure 4C.2. Linear intensity and power spectra in decibels for 2° bins of forward scattering data, 20 kHz.

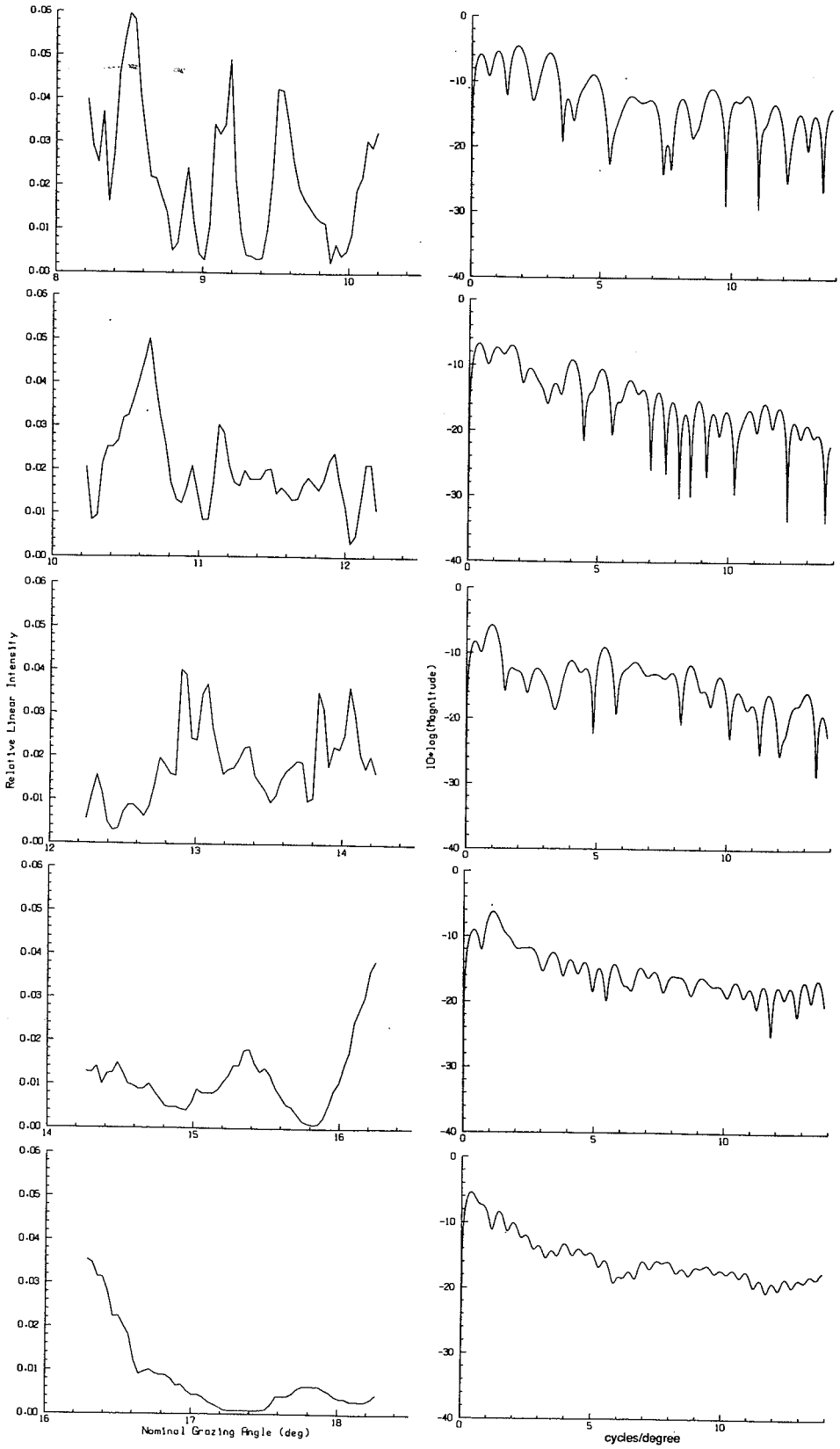

Figure 4C.3. Linear intensity and power spectra in decibels for 2° bins of forward scattering data, 30 kHz.

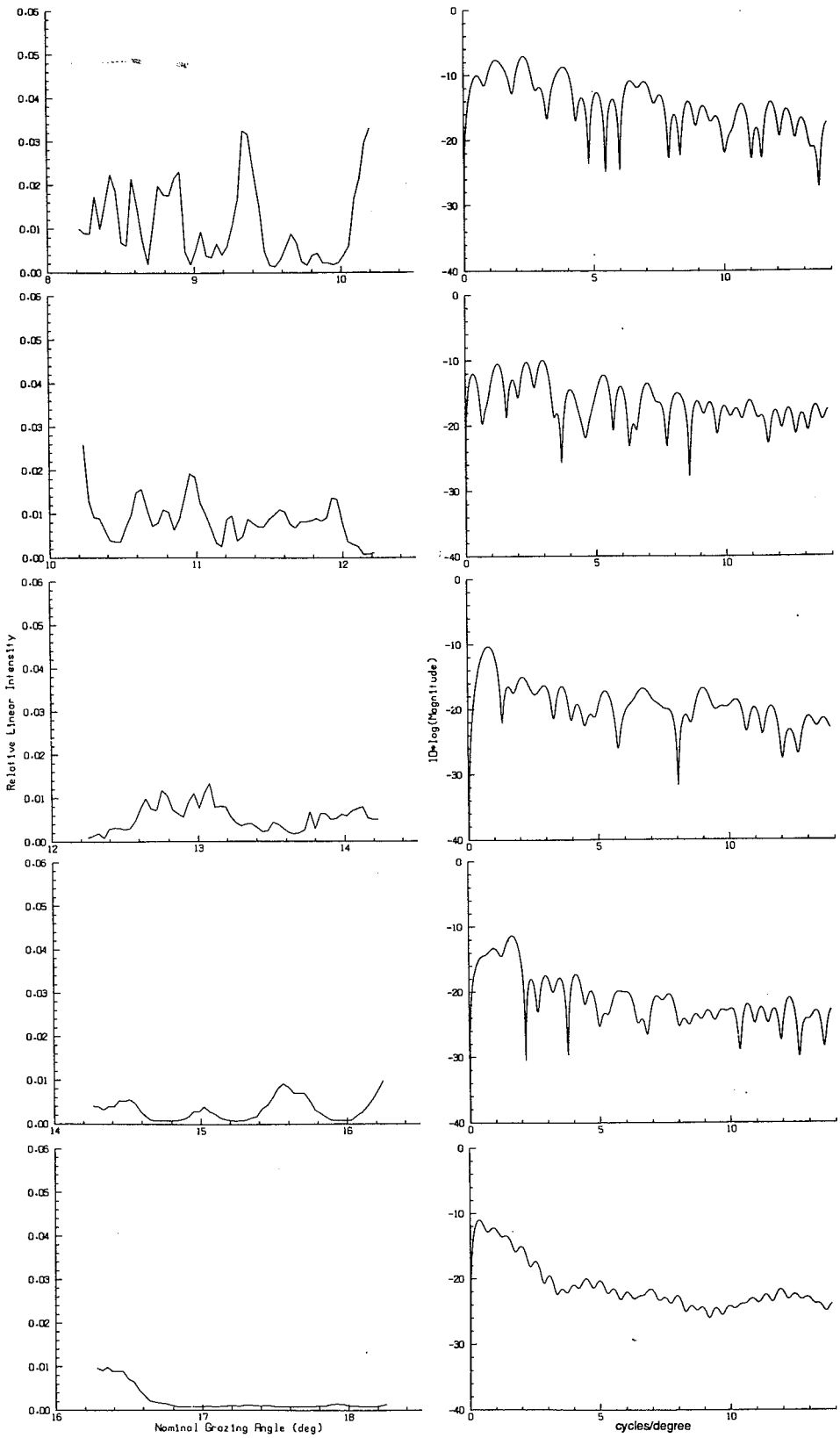

Figure 4C.4. Linear intensity and power spectra in decibels for 2° bins of forward scattering data, 60 kHz.

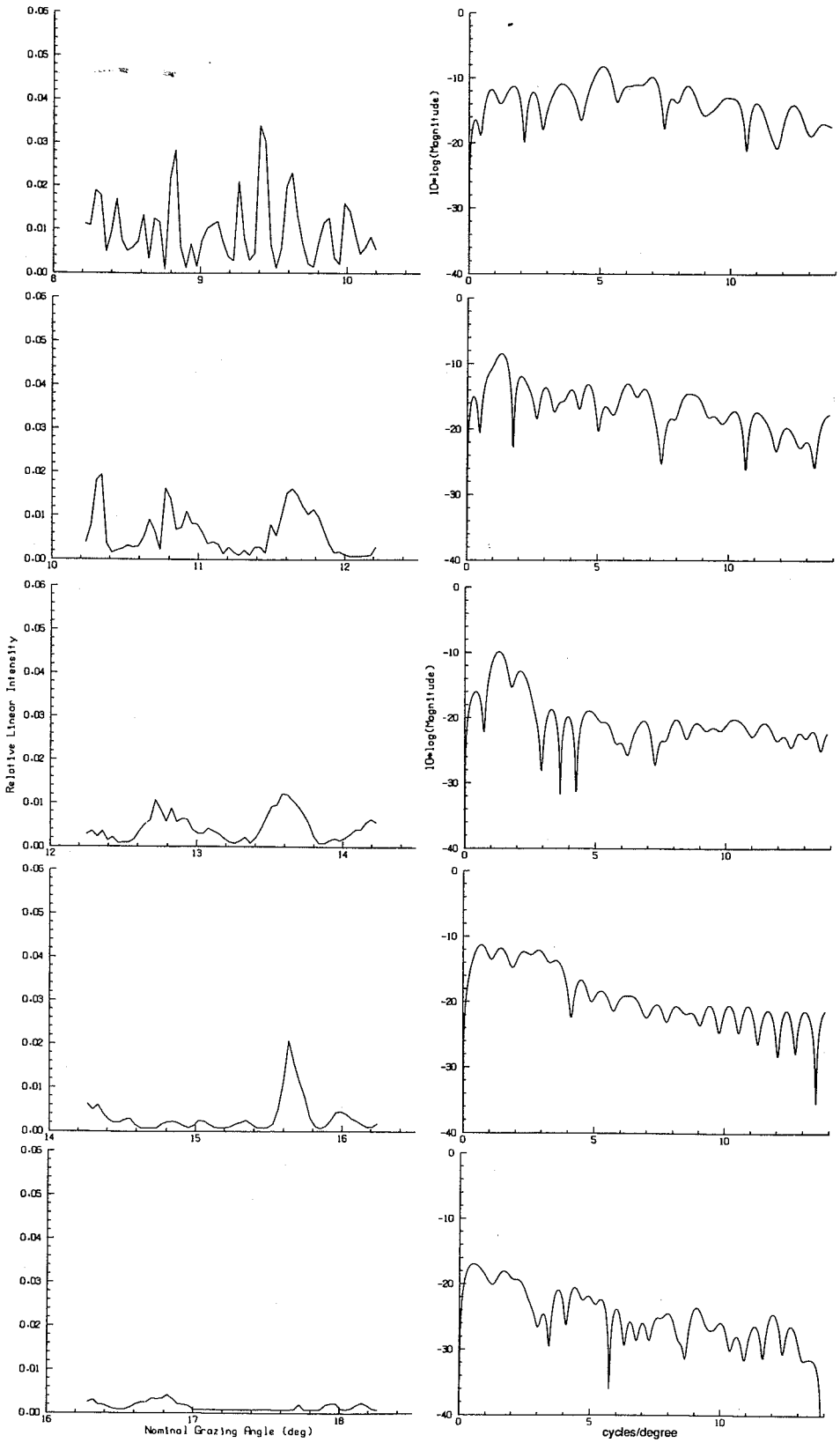

Figure 4C.5. Linear intensity and power spectra in decibels for 2° bins of forward scattering data, 75 kHz.

Chapter 5: THE SEAWATER – SEA ICE TRANSITION LAYER

Section 5.1: Introduction

Chapter 2 included a brief review of the few substantive, direct observations of the porous transition layer between sea ice and seawater. In the same chapter I also reviewed measurements of transition layer acoustic properties and effects at frequencies higher than those of interest in this report but valuable for the insights they provide.

In this chapter, I begin by reviewing some relevant though preliminary experimental results in the frequency range 20–kHz. I then discuss theoretical work on possible acoustic transition layer effects in this frequency range. These reviews are the subject of the next section.

In Section 5.3, I introduce a theoretical technique for exploring transition layer effects which has not previously been used in connection with sea ice. The technique is built on a model of the transition layer in which compressional wave (phase) speed, density, and absorption vary smoothly but otherwise arbitrarily with depth, except possibly at discrete depths where arbitrary jumps in material properties may occur. The development requires that no classical turning points occur in the smoothly varying medium. The theoretical prediction for the reflection coefficient of such a transition layer is found by numerical integration of an ordinary, first-order, nonlinear differential equation. The technique developed here is an extension of a technique given by Brekhovskikh [1980]. In its present form, its application is limited to situations where the incidence angle is near vertical. This restriction allows the neglect of coupling between compressional waves in the water and shear modes in the ice, as well as effects of anisotropy in acoustical properties of the ice. Both of these physical phenomena are likely to be important in the overall underice reflection/scattering problem. However, we will see that the insight obtained in this simplified case is useful both in its own right and in guiding further investigations using more realistic physical models.

The latter point is demonstrated in Section 5.4, which presents numerical results and a preliminary comparison with data, written in collaboration with Pierre Mourad and Kevin Williams of APL-UW. The modeling results show that some questions regarding the vertical compressional wave speed profile have experimentally testable, acoustic consequences. Thus with insight from modeling, we may be able to use acoustic data to constrain the range of possible wave speed profiles as well as better focus acoustic experiments to test hypotheses about profiles. Section 5.5 provides some guidance for theoretical extensions of the present work to a wider range of cases and some concluding remarks. Finally, Appendix 5A outlines a specialized computation for the case of a transition layer of thickness small in comparison with the radiation wavelength. This computation is used in Section 5.4 in computing the reflection coefficient of realistic ice profiles at frequencies of 20 kHz and below.

Section 5.2: Background

I have located only one data set for the frequency range of interest here in which the effects of the transition layer on reflection and scattering are separated from roughness effects. This data set results from experiments in the fall of 1984 and the springs of 1986 and 1988, and is described in three reports by Garrison et al. [1987, 1988a, 1988b]. The part of the data set taken in 1988 is the most extensive and least affected by modifications of the transition layer due to the experiment itself. Target strengths of the bottom faces of ice cylinders, cut from first-year ice cover in a lead using a thermal drill, were measured with a transducer suspended below the ice. Measurements were made at a series of horizontal transducer positions beneath the ice cylinder to locate the normal incidence return (within an uncertainty considered acceptable). The thickness of ice in the lead from which the cylinders were cut was 1.4 m. Snow cover on the lead was about 15 cm, though the snow was highly compacted in the experimental area. The temperature ranged between −35° and −20°C during the measurements. Four ice cylinders having faces with diameters of 27, 38, 58, and 84 cm were measured at acoustic frequencies of 20, 30, 40, 60, and 80 kHz. Flatness of the lower surfaces of the cylinders was verified to within approximately 2–3 mm by direct measurement. Several ice cores were taken in the vicinity of the experiment from which temperature, density, and salinity were measured as functions of depth. From the latter, approximate compressional wave speeds as functions of depth were computed. Attempts were made to vary the depth and profile of the transition layer by hauling out the cylinders and sawing off layers of ice from their lower faces. Finally, experiments were performed in which the cylinders were submerged for up to 28 hours, raising their temperatures to nearer that of seawater and thus increasing their porosity.

The measured reflection coefficients for cylinders with intact transition layers are small at all frequencies. The measurements are scattered between values of approximately 0.25 and 0.075 but tend to decrease with increasing frequency from a mean of approximately 0.20 to 0.10. However, internal checks indicate that the data are accurate only to within approximately 5 dB; thus quantitative statements are necessarily imprecise.

Attempts to saw off part of the transition layer disturbed the remaining part of the layer too much to be useful. A block that had its transition layer removed entirely and was roughly equilibrated to air temperature was found to have target strengths approximately 8 dB higher than those of natural ice, except at 60 and 80 kHz. The target strength of natural ice was actually higher than that of the cold, hard ice at 80 kHz. Clearly, a given profile of acoustic properties in the transition layer would become more gradual on the scale of the radiation wavelength with increasing frequency. Thus one would expect the effect of the transition layer, specifically any reduction in reflectivity, to increase with frequency, in contradiction to the above observations. Garrison et al. [1988a, 1988b] suggest that the observed phenomenon is due to scattering from surface

roughness on the cold ice caused by sawing. Ice cylinders raised out of the water, drained so as to entrain air in the transition layer, and then resubmerged displayed target strengths 6–8 dB higher than natural ice, again except at 60 and 80 kHz.

Finally, prolonged submergence (and presumably, increased porosity) decreased target strengths of the 84 and 58 cm cylinders. The decrease was large for the 84 cm cylinder and varied strongly and monotonically with frequency. The target strength at 20 kHz decreased approximately 2 dB over 22 hours, while that at 80 kHz decreased over 10 dB. However, observed target strengths of the 58 cm cylinder decreased by only 2 dB over 15 hours, except at 80 kHz where the decrease was approximately 9 dB. Garrison et al. [1988a, 1988b] speculate that this latter decrease may have been related to a change in surface roughness caused by melting, which was observed qualitatively on this cylinder. These authors also suggest that the difference between cylinders at other frequencies may have been related to their differing thermal masses and to the (unknown) difference in the length of time they had been submerged before time series measurements began.

These results provide useful qualitative information on the behavior and role of the transition layer. However, precise quantitative information has not yet been obtained using this methodology. Undesired disturbance of the natural ice state in addition to those changes affected for experimental purposes, possible variations in flatness of cylinder faces, and air entrainment in the transition layer continue to be problematic.

Theoretical modeling of reflection from ice with transition layers has provided some insight into potential layer effects and the layer properties likely to be important in practical problems.

Posey et al. [1985] compute the reflection coefficient for an ice model composed of discrete, planar, homogeneous ice layers in which shear and compressional mode phase speeds and attenuations are prescribed. The computations are based on the theory of McCammon and McDaniel [1985]. The discrete layer parameters were chosen to give stepwise approximations to continuous estimates of parameter profiles with ice depth and to simulate finite layers and semi-infinite half-spaces of ice. The computations densely covered the band of frequencies between 5 and 30 kHz and the full range of grazing angles from 0° to 90°.

The chief finding in this work is that the calculated reflection coefficient at grazing angles less than approximately 40° is quite sensitive to the model profile of shear wave speeds in the transition layer. A model in which shear wave speeds gradually increase with increasing distance from the ice–water interface shows little shear wave conversion from the compressional wave in the water at the smaller grazing angles. Conversion to compressional modes is prohibited by their speeds in ice, and thus the reflection coefficient remains fairly constant and near one. However, if shear wave speeds increase abruptly in the transition layer, conversion at smaller grazing angles is much more efficient, leading to a significantly smaller reflection coefficient and greater variation

with frequency than in the first case. At normal incidence, the reflection coefficient depends on only compressional wave parameters because conversion to shear modes is precluded. The normal incidence reflection coefficient appears to decrease with increasing frequency, but this is not easily quantified from the presentation of the computational results.

Chin-Bing [1985] investigated the effects on predicted backscattering from a keel due to changes in the ice–water reflection coefficient caused by the transition layer. The model used for backscattering from keels is a version of that given by Ellison [1980], modified to allow for a wider variety of block rotations. Chin-Bing found that a reflection coefficient made larger at smaller grazing angles by the transition layer strongly affects the choice of ice block thickness and parameters of the block rotation distribution used to fit, and thus "explain," a given data set.

Finally, Yew and Weng [1987] present a two-ice-layer model for the reflection coefficient in which each layer is porous and treated according to the Biot model [Biot, 1956, 1962]. (In the Biot model, the mechanical modes of fluid circulating in communicating pores, those of the solid material composing the skeletal frame of the material and their coupling, are each treated. The resulting bulk wave propagation modes are the usual shear modes and two compressional waves, one of which is highly attenuated and acts primarily as an energy sink. Note that although Yamamoto and Badiey [1986] have also used the Biot model to study reflection from sea ice, they have not modeled the transition layer or attempted to elucidate its effects.) The water–ice transition layer is modeled simply as one layer of porosity lower than that of the overlying ice.

Consider first the effects of changes in the transition layer porosity in this model at a constant frequency of 1 kHz and layer thickness 40 cm. With the porosity of the upper, overlying ice fixed at 0.1, variations of transition layer porosity in the range 0.3 to 0.5 have almost no effect at grazing angles less than approximately 30°. However, at vertical incidence, the reflection coefficient decreases approximately 3 dB with increasing porosity in the same range. In a middle range of grazing angles between approximately 25° and 55°, the variation is as large as 7–8 dB, again with lower reflection coefficients for larger porosities.

Model reflection coefficients between 1 and 4 kHz (for a fixed grazing angle of 70° and layer thickness of 40 cm) oscillate as functions of frequency. The amplitude of oscillation increases with increasing layer porosity, reaching approximately 4 dB for a transition layer porosity of 0.5. The authors do not give a physical explanation of this model behavior. Finally, for fixed porosities (0.1 and 0.5) and grazing angle (70°), the rapidity of model reflection coefficient oscillations as functions of frequency depends strongly on the thickness of the transition layer; the oscillations become more rapid with increasing layer thickness.

In fact, model reflection coefficients oscillated with changes in frequency in each of the studies by Posey et al. [1985], Chin-Bing [1985], and Yew and Weng [1987]. Also

common to each of these studies is a sea ice model consisting of discrete layers in which elastic properties are homogeneous and separated by planar interfaces. There is generally a discontinuity in elastic properties at each interface. Reflections from the interfaces are coherent and thus interfere, though the phase differences between components vary with frequency. It seems likely that interference effects are at least one significant cause of oscillations in model reflection coefficients.

However, I have as yet found no evidence that transition layers in nature are actually discretely layered structures. Intuitively, and from the few qualitative observations available, it seems more likely that material, and therefore elastic, properties in the transition layer vary gradually with depth in the ice. Interfering reflections from discrete layer interfaces in the models would then be artifacts of the models as would be the oscillatory behavior of the reflection coefficient. Of course, one might construct models with ever thinner layers hoping to approach the limit of a continuous medium within a specified accuracy. But it appears difficult to determine how a specified accuracy could be obtained and what the computational cost would be.

It is possible to avoid some of the problems of discrete layer models by treating acoustic properties in the transition layer as if they vary smoothly with depth except, perhaps, at (typically a few) discrete depths. There is a technical cost to this approach in terms of the generality of situations which it can presently be used to study. However, it seems worthwhile to develop and use such a model for comparison with layered models and to gain additional insight. The development of the model, a discussion of its strengths, and of its (present) limitations is the subject of the next section.

Section 5.3: Theory of Reflection from Vertically Stratified Media

Brekhovskikh [1980] has presented a computational model for the compressional wave reflection coefficient of a lossless fluid medium in which sound speed and density vary arbitrarily with depth except for two limitations. The first limitation is that the sound speed and density variations and their first derivatives must be continuous. The second is that the variations are such that there exist no classical turning points (i.e., points of total internal reflection) in the reflecting medium for the particular grazing angle and radiation wavelength under consideration. Brekhovskikh defines a generalized reflection coefficient, i.e., the ratio of complex amplitudes of up- and down-going waves in the medium, which varies with depth in the medium. He then derives a Riccati equation (a first-order, nonlinear, ordinary differential equation) for the generalized reflection coefficient which, using an appropriate boundary condition, can easily be numerically integrated.

The model I develop in this section is a slight generalization of Brekhovskikh's in two ways. First, I provide for the presence of modest, depth-dependent absorption in the medium and derive the resulting modified equations in the next subsection. Second, I

consider the situation where an abrupt transition in acoustic properties occurs at a given depth (i.e., a transition in which acoustic properties and/or their first derivatives are discontinuous). Applying the fundamental acoustic boundary conditions, I derive an expression for the limiting value of the generalized reflection coefficient on one side of the boundary in terms of the limiting values of the reflection coefficient on the other side and of the material acoustic properties on each side. This extension strictly applies only in the case where there is no absorption in the medium near the boundary. This is because changes in the fields near the boundary due to the physical mechanisms of absorption (e.g., viscosity) are not considered in matching the boundary conditions. It does, however, provide an approximate method to study media such as sea ice in which both smooth and any number of abrupt variations in acoustic properties may occur.

The resulting model still has a number of limitations in its present form, particularly in its application to sea ice. First, the condition prohibiting classical turning points remains. It should be possible to develop an analytical addition to the present model that allows for turning points by deriving the phase shift of the generalized reflection coefficient at such points in terms of medium properties (by definition, its magnitude is one). I leave this problem for future work. More fundamentally, the reflecting medium is modeled as a fluid with spatially isotropic sound speed and absorption. Although these quantities depend on depth, they are assumed not to depend on the propagation direction of a wave within the medium. Furthermore, a fluid supports no shear modes such as are present in an elastic medium. There is presently every reason to think that sea ice behaves as an anisotropic (perhaps porous) elastic medium. However, for vertical plane wave incidence it is necessary to consider only the vertical propagation direction, and there is no conversion into shear modes even in an elastic medium. Thus the present model can be applied to sea ice in cases that can be modeled using plane waves normally incident on horizontally homogeneous ice. Even with this limitation, we will see (Section 5.4) that the model provides insight and is useful in planning experiments to discriminate between two fundamentally differing sound speed profiles in the transition layer.

I begin by deriving the fundamental differential equation for the generalized reflection coefficient.

Section 5.3.1: Continuous Variation of Acoustic Parameters

Consider a linear, fluid, acoustic medium in which density, sound speed, and absorption (to be discussed further momentarily) do not depend on direction, but may vary with position. Suppose that the spatial variation in acoustic properties depends only on the z-coordinate, and that as $z \to \pm\infty$ the acoustic properties may be assumed constant (at different values in the two regions).

Suppose for a moment that there is no absorption in the medium. Let the density, pressure, and fluid velocity at a point in the medium be given by $\rho + \rho_1$, $p + p_1$, and

$\bar{v} + \bar{v}_1$, respectively, where ρ, p, and $\bar{v}$ are the mean values at that point and ρ_1, p_1, and $\bar{v}_1$ are the fluctuations due to the wave motion. Assume that $\bar{v} = 0$. Then to first order in the subscripted quantities (which are assumed small in comparison with unsubscripted quantities), the equation of continuity takes the form

$$\rho \nabla \cdot \bar{v}_1 + \frac{\partial \rho_1}{\partial t} = 0 \tag{5.1}$$

and Newton's Second Law leads to the equation of motion (Euler's equation)

$$\rho \frac{\partial \bar{v}_1}{\partial t} + \nabla p_1 = 0 \tag{5.2}$$

[Landau and Lifshitz, 1959; Pierce, 1981]. In a lossless medium, one typically writes the change in pressure in terms of the change of density as a proportionality:

$$p_1 = \left[\frac{\partial p}{\partial \rho} \right]_s \rho_1 \tag{5.3}$$

where the subscript s denotes a change at constant entropy. The proportionality constant is real and must be calculated from the equation of state for the material comprising the propagation medium [Landau and Lifshitz, 1959; Pierce, 1981]. According to Pierce, it is related to the adiabatic bulk modulus of elasticity, B:

$$\left[\frac{\partial p}{\partial \rho} \right]_s = \frac{B}{\rho} \tag{5.4}$$

Relation of pressure to density reduces the number of unknown field quantities in equations 5.1 and 5.2 to two. Equation 5.1 becomes

$$\frac{\partial p_1}{\partial t} + \rho c^2 \nabla \cdot \bar{v}_1 = 0 \tag{5.5}$$

where

$$c \equiv \left[\frac{\partial p}{\partial \rho} \right]_s \qquad \text{(lossless case).} \tag{5.6}$$

Finally, if we assume a harmonic time dependence $\exp(-i\omega t)$, equations 5.2 and 5.5 become, respectively,

$$-i\omega\rho \bar{v}_1 + \nabla p_1 = 0 \tag{5.7}$$

and

$$-i\omega p_1 + \rho c^2 \nabla \cdot \bar{v}_1 = 0 \ . \tag{5.8}$$

As the notation in equations 5.5 and 5.6 anticipates, c can be shown to be the phase speed of a harmonic plane wave in a lossless, homogeneous medium of density ρ in which equation 5.3 holds.

In cases where absorption occurs, the equations above may be altered in one of at least two ways. First, an additional force (e.g., viscosity) may cause dissipation in the medium. In this case, the most rigorous approach is to include the appropriate additional terms in the balance between force and the change in momentum expressed by equations 5.2 and 5.7 [Landau and Lifshitz, 1959; Pierce, 1981].

Absorption can also arise when the equation of state dictates a more complicated relationship between pressure and density than that in equation 5.3. For example, in relaxation processes equilibrium in the medium is disturbed by the acoustic wave and requires a finite amount of time to be restored. The medium removes energy from the passing wave and releases it some time later. The contribution of the medium is thus out of phase with the original wave and destructive interference takes place [Tolstoy, 1973]. The relationship between pressure and density is no longer the quasi-static relationship given by equation 5.3, but must be dynamic. Tolstoy notes that the simplest dynamic relationship is given by

$$p_1 = \left[\frac{\partial p}{\partial \rho}\right]_{sEQ} \rho_1 + r\frac{\partial \rho_1}{\partial t} \quad . \tag{5.9}$$

Thus if at time $t = 0$ we applied a constant pressure p_{1o}, the density would increase with time according to

$$\rho_1 = p_{1o}\left[\left[\frac{\partial p}{\partial \rho}\right]_{sEQ}\right]^{-1}[1-\exp(-t/\tau)] \tag{5.10}$$

where

$$\tau \equiv \frac{r}{\left[\frac{\partial p}{\partial \rho}\right]_{sEQ}} \tag{5.11}$$

is the so-called relaxation time. The subscript *sEQ* on the partial derivative in equations 5.9–11 signifies that it is the asymptotic value of the adiabatic change of density with pressure for times much longer than the relaxation time.

In the time harmonic case, equation 5.9 becomes

$$p_1 = \left[c_0^2 - i\omega r\right]\rho_1 \tag{5.12}$$

where I have (following Landau and Lifshitz [1959]) introduced the notation for the sound speed "at zero frequency":

$$c_0 \equiv \left[\left[\frac{\partial p}{\partial \rho}\right]_{sEQ}\right]^{1/2} \quad . \tag{5.13}$$

The proportionality constant between pressure and density becomes complex; the relaxation process introduces a phase lag in the response of the medium to pressure. As Landau and Lifshitz note, equations 5.6 and 5.7 remain formally applicable, the only change being that c^2 becomes complex:

$$c^2 \equiv c_0^2 - i\omega r \quad . \tag{5.14}$$

The complex wavenumber of a plane wave is then given by

$$k = \frac{\omega}{c} = \frac{\omega}{c_0}[1 - i\omega\tau]^{-\frac{1}{2}} \tag{5.15}$$

where I have used equations 5.11 and 5.13 for the relationship between relaxation time τ, r, and c_0. The square root must be taken such that the imaginary part of k is positive. Finally, when the relaxation time is much smaller than the period of the acoustic wave, i.e., when $\omega\tau \ll 1$, we have

$$k \simeq \frac{\omega}{c_0}\left[1 + \frac{i\omega\tau}{2}\right] \quad . \tag{5.16}$$

In the development below, I model acoustic absorption by simply allowing c (or equivalently the adiabatic bulk modulus of elasticity in equation 5.4) to be complex and arbitrarily frequency dependent. In the special case of a complex frequency-independent bulk modulus, this model reduces to that of a relaxation process with relaxation time τ. The frequency dependencies of sound speed and attenuation are then determined by the equations above. A frequency-dependent bulk modulus may result from a combination of relaxation processes with differing relaxation times or from some other physical mechanism. Although causality imposes a Kramers-Koenig relationship between the real and imaginary parts of c [Jackson, 1975], I will not explicitly take this into account in the following.

This approach is obviously phenomenological. However, I believe for several reasons that it is the most useful way to proceed at the present. First, the approach used here allows us to study the effect of acoustic parameters on reflection without specifying the (presently unknown) microphysics responsible for absorption in the transition layer. It thus allows us to discern and focus future theoretical study on the acoustic parameters most important for reflection. Furthermore, relaxation mechanisms are extremely common in wave propagation problems in a wide variety of media [Tolstoy, 1973]. Thus it seems that a relaxation-like mechanism should be the first choice among trial mechanisms. Finally, it is often possible to approximately model absorption due to processes other than relaxation as relaxation mechanisms, provided that the absorption is not too strong. Tolstoy gives an example in which losses due to viscosity are treated in this way. In short, the approach I use here allows for considerable flexibility and is likely to produce useful initial results.

We are now in a position to define the generalized reflection coefficient and to derive its governing differential equation. Consider a locally approximately planar wavefront in the region near $z = -\infty$ with its propagation direction (i.e., the normal to the wavefront) in the x-z plane. Suppose the angle between the propagation direction and the z-axis (i.e., the angle of *incidence*) is θ_i. Assume a harmonic time dependence $\exp(-i\omega t)$. Further assume that absorption is negligible in this spatial region. Then near $z = -\infty$ the x-dependence of the quantities which characterize the wave is given by $\exp(i K_x x)$, where $K_x = k_i \sin\theta_i$ and k_i is the (real) wavenumber in this region.

Because the acoustic properties vary only with z, the x-dependence of the wave field must be identical everywhere (this is just a manifestation of Snell's Law). Thus we may replace $(\partial)/(\partial x)$ by iK_x in the governing equations everywhere in space. We may also set $(\partial)/(\partial y) = 0$ thanks to the choice of coordinate axes. Then from equation 5.7 we can obtain two scalar equations:

$$v_{1x} = \frac{K_x}{\rho\omega} p_1 \tag{5.17}$$

and

$$\frac{\partial p_1}{\partial z} = i\omega\rho v_{1z} \quad . \tag{5.18}$$

For brevity, I have not shown explicitly the z-dependence of the acoustic parameters ρ and c or the frequency dependence of c in the notation here. From equations 5.8 and 5.17 we obtain

$$\frac{\partial v_{1z}}{\partial z} = \frac{i\kappa^2}{\rho\omega} p_1 \quad , \tag{5.19}$$

where

$$\kappa = \left[\frac{\omega^2}{c^2} - K_x^2 \right]^{1/2} \quad . \tag{5.20}$$

It proves worthwhile to seek solutions of the following forms to these equations:

$$p_1(x,z,t) = [P(z) + R(z)] \exp(iK_x x - i\omega t) \tag{5.21}$$

and

$$v_{1z}(x,z,t) = \frac{\kappa}{\rho\omega} [P(z) - R(z)] \exp(iK_x x - i\omega t) \quad . \tag{5.22}$$

P and R represent complex up- and down-going wave amplitudes; they are complex because they include the dependence of the wave phase on z. This *ansatz* is motivated by the observation that in a region of constant ρ and c we would have from equations 5.18 and 5.19

$$\frac{\partial P}{\partial z} = i\kappa P \quad \text{and} \quad \frac{\partial R}{\partial z} = -i\kappa R \quad .$$

These equations are trivially satisfied for up- and down-going plane waves, respectively, with vertical propagation constant κ.

Substituting 5.21 and 5.22 into 5.18 and 5.19 and solving for $\partial P / \partial z$ and $\partial R / \partial z$, we obtain

$$\frac{\partial P}{\partial z} = i\kappa P - \gamma(P - R) \tag{5.23}$$

where

$$\gamma \equiv \frac{1}{2} \frac{\frac{\partial}{\partial z}\left[\frac{\kappa}{\rho}\right]}{\frac{\kappa}{\rho}} \tag{5.24}$$

and

$$\frac{\partial R}{\partial z} = -i\kappa R + \gamma(P - R) \quad . \tag{5.25}$$

In solving for these equations, it is necessary to divide by κ. Thus the magnitude of κ must be bounded away from zero. Equivalently, there may be no classical turning points in the medium to which the method given here is applied.

Multiplying 5.23 by R and 5.25 by P and then subtracting the latter from the former, we obtain

$$R\frac{\partial P}{\partial z} - P\frac{\partial R}{\partial z} = 2i\kappa PR - \gamma(P^2 - R^2) \quad . \tag{5.26}$$

The next step is to divide equation 5.26 by P^2. Thus we must require that P^2 never be equal to zero. I interpret this also to mean that the remainder of the formalism cannot be applied above any classical turning point in the medium (however, see Section 25.8 of Brekhovskikh [1980] for some subtleties regarding this interpretation). Next, we define the generalized reflection coefficient V by

$$V = \frac{R}{P} \quad .$$

Note that V is a ratio of complex amplitudes. Then observing that

$$\frac{R\frac{\partial P}{\partial z} - P\frac{\partial R}{\partial z}}{P^2} = \frac{\partial}{\partial z}\frac{R}{P} \quad , \tag{5.27}$$

we obtain from equations 5.26 and 5.27 a Riccati equation for V:

$$\frac{\partial V(z)}{\partial z} = -2i\kappa(z)V(z) + \gamma[1 - V^2(z)] \quad . \tag{5.28}$$

Note that V, κ, and γ are in general also complex functions of frequency ω.

Section 5.3.2: Abrupt Changes at a Given Level

It is clearly desirable to avoid infinite values and discontinuities in the coefficients of V in the numerical solution of equation 5.28. These occur at levels $z = z_o$, i.e., interfaces in the medium, where the complex sound speed, the density, or their z-derivatives are discontinuous. At such points, an analytical expression can be obtained for V just to one side of the interface in terms of V just to the other side of the interface and the limiting values of ρ and c on both sides. The expression follows directly from applying the acoustic boundary conditions at the interface.

Consider a situation in which there is a discontinuity in acoustic parameters ρ and c at a horizontal, planar interface. We can without loss of generality set the z-coordinate of the interface to zero. The limiting values of the P, R, and V and of acoustic parameters on either side of the interface are then

$$P_2 \equiv \lim_{z\to 0^+} P(z) \qquad P_1 \equiv \lim_{z\to 0^-} P(z) \quad , \tag{5.29}$$

$$R_2 \equiv \lim_{z\to 0^+} R(z) \qquad R_1 \equiv \lim_{z\to 0^-} R(z) \quad , \tag{5.30}$$

$$V_2 \equiv \lim_{z\to 0^+} V(z) = \frac{R_2}{P_2} \qquad V_1 \equiv \lim_{z\to 0^-} V(z) = \frac{R_2}{P_2} \quad , \tag{5.31}$$

$$\rho_2 \equiv \lim_{z\to 0^+} \rho(z) \qquad \rho_1 \equiv \lim_{z\to 0^-} \rho(z) \quad , \tag{5.32}$$

and

$$\kappa_2 \equiv \lim_{z\to 0^+} \kappa(z) \qquad \kappa_1 \equiv \lim_{z\to 0^-} \kappa(z) \quad . \tag{5.33}$$

The first acoustic boundary condition is continuity of pressure. Using equation 5.21, we obtain

$$P_2 + R_2 = P_1 + R_1 \quad . \tag{5.34}$$

The second boundary condition is continuity of the component of fluid velocity normal to the interface, i.e., v_{1z}. From equation 5.22,

$$\frac{\kappa_2}{\rho_2\,\omega}\,[P_2 - R_2] = \frac{\kappa_1}{\rho_1\,\omega}\,[P_1 - R_1] \quad . \tag{5.35}$$

Note that in using these equations, I have ignored the possibility that the physical mechanism producing absorption may also produce new acoustic modes which become important at interfaces. For example, the presence of viscosity in a fluid makes possible transverse acoustic modes. These modes are typically unimportant except at interfaces, where they become significant in satisfying the boundary conditions [Pierce, 1981].

Thus while the following equations should be accurate to a good approximation when absorption is moderate, modification may be needed when the mechanisms of absorption in the transition layer are better understood. The development here continues the somewhat phenomenological approach to absorption begun earlier.

From equation 5.34, then, we obtain

$$1 + V_2 = \frac{P_1}{P_2}(1 + V_1) \quad , \tag{5.36}$$

while equation 5.35 yields

$$\frac{\kappa_2 \rho_1}{\kappa_1 \rho_2} \frac{(1-V_2)}{(1-V_1)} = \frac{P_1}{P_2} \quad . \tag{5.37}$$

Combining these two equations, we obtain

$$V_1 = \frac{1 - \frac{\kappa_2 \rho_1}{\kappa_1 \rho_2} \frac{(1-V_2)}{(1+V_2)}}{1 + \frac{\kappa_2 \rho_1}{\kappa_1 \rho_2} \frac{(1-V_2)}{(1+V_2)}} \quad , \tag{5.38}$$

which is the desired result.

Section 5.4: Numerical Experiments

The purpose of this section is to demonstrate the theory developed above, to show that different plausible compressional wave speed profiles produce acoustically distinguishable behavior in the reflection coefficient, and to show the usefulness of modeling in experimental design.

Figure 5.1 shows a sound speed profile computed from measured ice properties (temperature and salinity) via empirical relationships. These two profiles were taken from adjacent ice cores that were separated by a few meters [Francois et al., 1989]. Note how the sound speed starts at a relatively small value in the ice at the ice–water interface and then increases rapidly to its bulk value, which stays constant through the rest of the ice. Unfortunately, error bars on these data would show only that the trend to lower values in sound speed from a bulk value is firmly established because of brine drainage from the ice cores near the ice–water interface. Even the sign of the derivative of the sound speed profile at the ice–water interface is questionable based on the present data. However, the unknown shape of the sound speed profile near the ice–water interface represents an interesting preliminary problem that we can begin to probe with the theory presented above. Different sound speed profiles near the interface produce different frequency-dependent reflection coefficients. Moreover, one can draw general conclusions about their relationship.

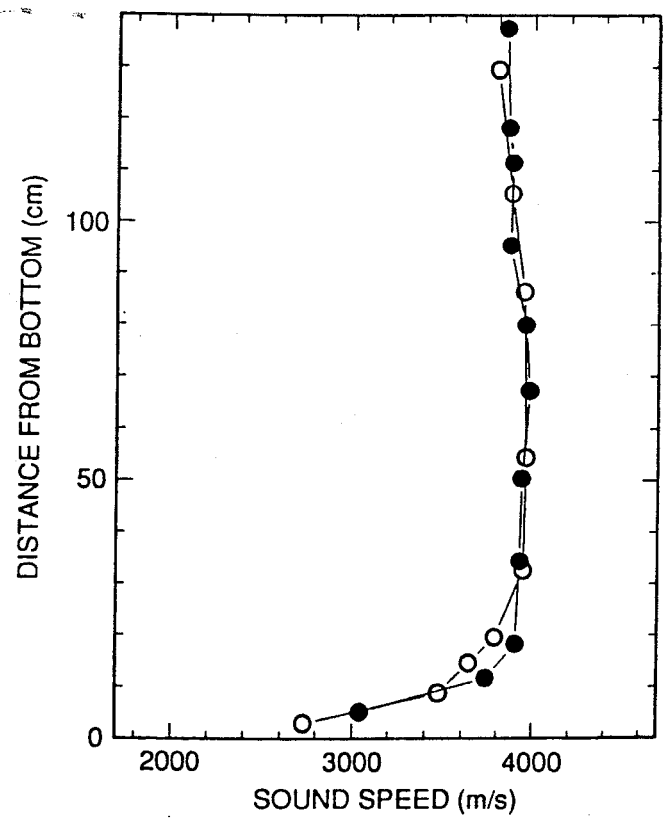

Figure 5.1. Sound speed profile computed from measured ice properties.

Two plausible sound speed profile shapes are shown in Figures 5.2 and 5.3. Both have been constructed to match the observed bulk values of the sound speed profile, with some liberty taken so that the associated reflection coefficients (Figures 5.4 and 5.5) best match observations. Note that $c(z)$ in Figure 5.2 is discontinuous at the interface, while dc/dz is not. In Figure 5.3, both are discontinuous. The analytical form for the profile in Figure 5.2 is

$$c(z) = \begin{cases} c_o\,, & z \le 0 \\ \tfrac{1}{2}\left[(c_a + c_1) - (c_1 - c_a)\cos\dfrac{\pi z}{L}\right], & 0 < z < L \\ c_1\,, & z \ge L \end{cases} \qquad (5.39)$$

when c_o = 1437 m/s, c_a = 1700 m/s, c_1 = 3800 m/s, and L = 5 cm. The profile in Figure 5.3 is given by

$$c(z) = \begin{cases} 2(c_a - \frac{c_1}{2}) + (c_1 - c_a)\,[1 + \tanh(\delta_o z)] \;, & z > 0 \\ c_o \;, & z < 0 \end{cases} \qquad (5.40)$$

when c_o, c_1, and c_a are equal to those above and δ_o = 100,000.

In computing vertical incidence reflection coefficients, we have assumed that absorption, R, in the transition layer is negligible even though absorption may in fact be significant. It is necessary, however, to construct a baseline case from which to acquire some intuition about the problem. We have also assumed that the density ρ is equal to 1 in seawater, in the transition layer, and in the overlying ice. Since actual density variations are approximately only 10%, and since model sensitivity to density seems to be of the same order as its sensitivity to sound speed, the effects of actual density variations are likely to be minor.

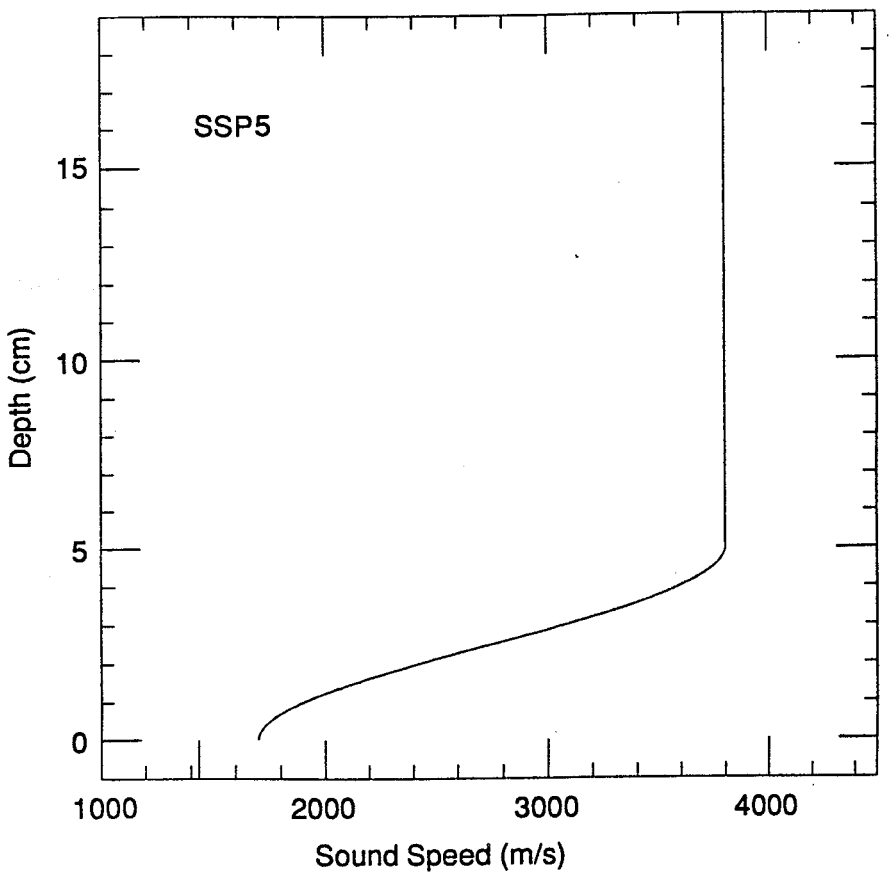

Figure 5.2. Cosine-based sound speed profile for reflection coefficient computation.

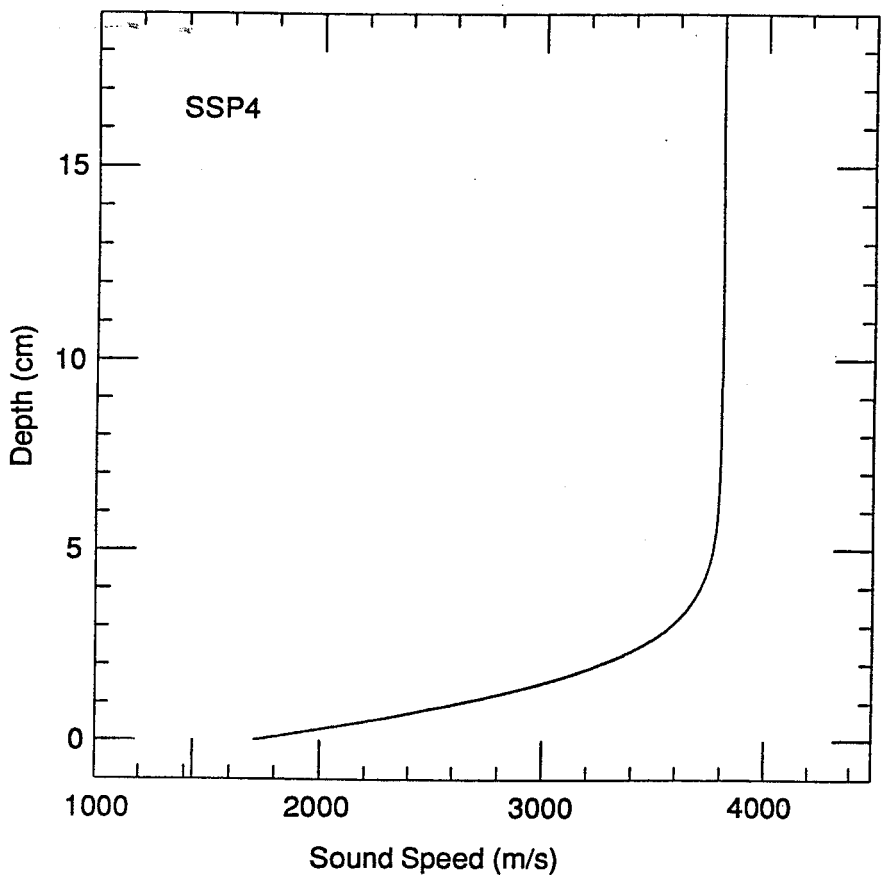

Figure 5.3. Hyperbolic tangent-based sound speed profile for reflection coefficient computation.

Intuitively, it is clear that with increasing wavelength the reflection coefficient must approach that for an abrupt planar interface between two half-spaces in which the sound speeds are those for seawater and for sea ice well above the transition layer. To compute the reflection coefficients at low frequencies ($\lesssim$ 20 kHz) requires special consideration because the transition layer in the sound speed profile is comparable to or thin compared with the wavelength; this makes the differential equation for V difficult to integrate numerically. A specialized computation for transition layers that are thin compared with the radiation wavelength using $\rho = 1$, $R = 0$, and $\theta_i = 0°$ is outlined in Appendix 5A. This computation is also adapted from Brekhovskikh [1980].

In the high-frequency limit, one would expect that the effect of any smooth profile of sound speed will tend toward zero because the change of sound speed on the scale of the wavelength vanishes near this limit. In this case, the reflection coefficient should be determined only by the impedance mismatch between seawater and the bottom of the

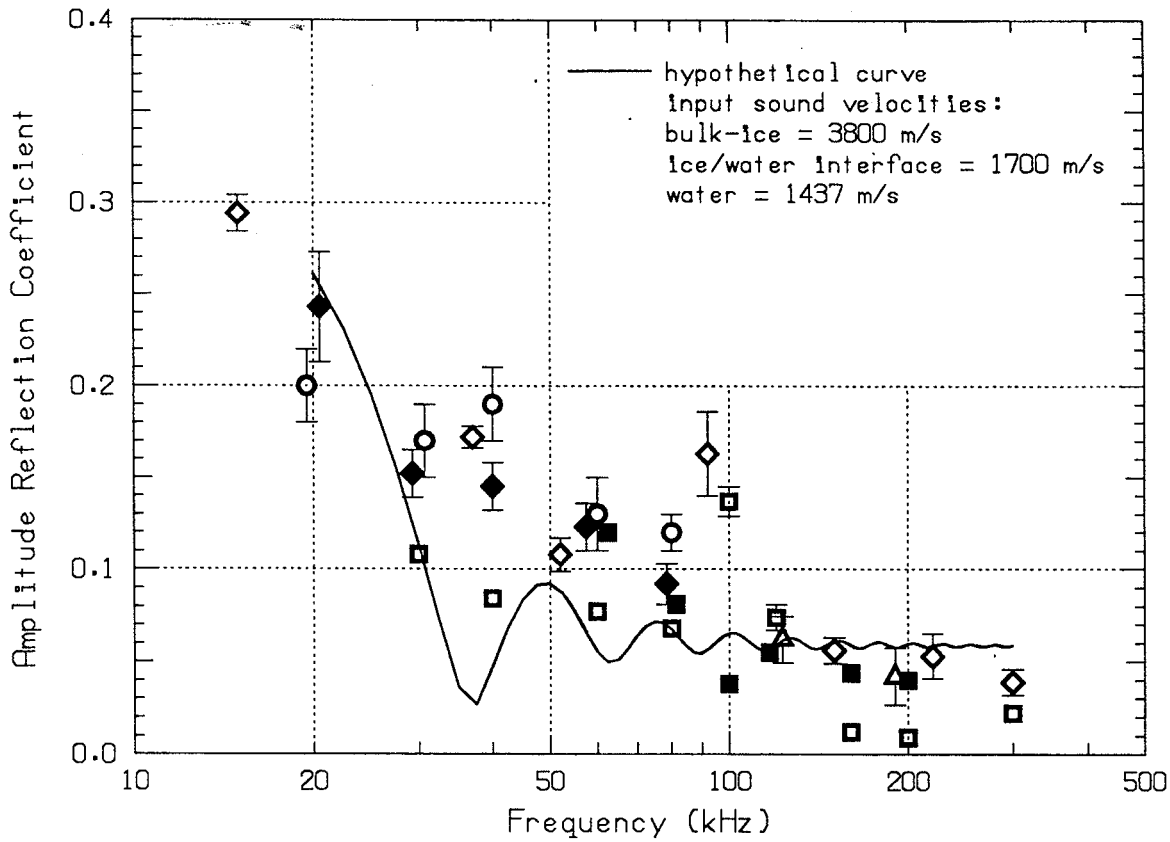

Figure 5.4. Comparison of data with theory for cosine-based sound speed profile.

transition layer. For intermediate frequencies, impedance gradients reflect energy back in a continuous fashion as the frequency changes. The particular shape of $V(\omega)$ depends on the shape of the sound speed profile.

Plots of the computed vertical-incidence reflection coefficients versus acoustic frequency for the profiles in Figures 5.2 and 5.3 are shown in Figures 5.4 and 5.5, respectively. The reflection coefficients for the two profiles differ in their curvatures (as functions of frequency) in the low-frequency limit. Perhaps the most striking difference, however, is that the cosine profile oscillates as a function of frequency while the hyperbolic tangent profile does not. However, this is due largely to the choice of parameters; smaller values of δ_o produce oscillatory reflection coefficients for the hyperbolic tangent profile as well. Thus multiple discrete layer interfaces are not the only possible source of oscillatory reflection coefficients; they can be produced even by continuous-profile transition layers with a single abrupt sound speed change (cf. comments at the end of Section 5.2). Note that the high frequency limit discussed above occurs for both profiles at approximately 200 kHz.

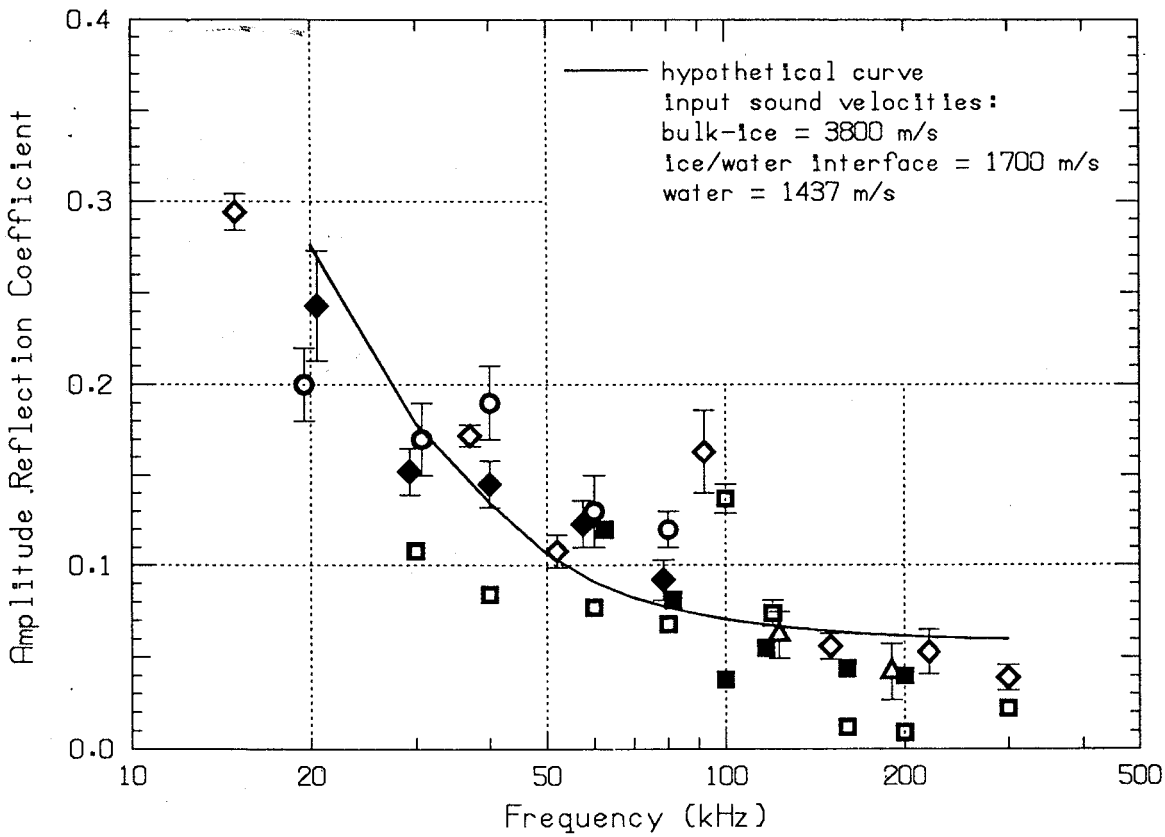

Figure 5.5. Comparison of data with theory for hyperbolic tangent-based sound speed profile.

The available data show no oscillation and thus favor a model such as equation 5.40 for the transition layer (with the choice of parameters above) over that of equation 5.39. Figure 5.6 shows data from the ice block experiment discussed above [Francois et al., 1990] for the reflection coefficient versus frequency. The best theoretical fit is from the sound speed profile/reflection coefficient pair given in Figures 5.3 and 5.5. This theoretical sound speed profile has the same monotone $c'(z)$ as in the observed $c(z)$, although it reaches 99% of the bulk sound speed value at about 5 cm whereas the observed profile does this at about 10 cm (given unquantified errors).

This exercise suggests that future experiments should include measurements at frequencies at or above 200 kHz to infer directly the discontinuity in sound speed at the bottom of the transition layer. Measurements at frequencies at or below 20 kHz should be compared with the reflection coefficient expected for a medium with a sound speed typical of solid ice. Finally, a denser sampling of intermediate frequencies would more conclusively indicate the presence or absence of oscillatory behavior in the reflection coefficient and thus constrain the shape of the sound speed profile. The desired spacing of frequencies can be inferred from further computations like those shown in Figure 5.4.

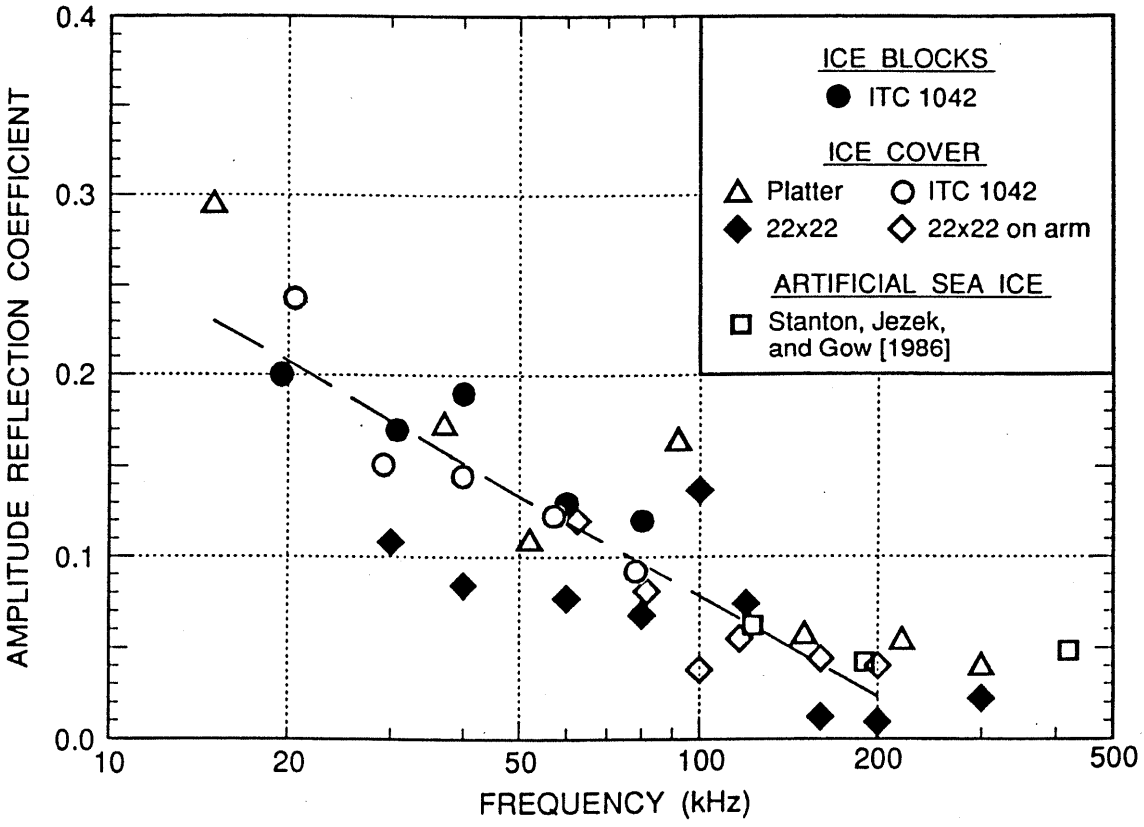

Figure 5.6. Summary of means of the amplitude reflection coefficient.

Section 5.5: Conclusions

It is clear that the continuous-profile transition layer model developed in this chapter can be usefully applied to sea ice at frequencies of tens to hundreds of kilohertz. One surprising and interesting result is that reflection coefficients that oscillate as functions of acoustics frequency can result from layers with only one abrupt interface and otherwise continuous sound speed profiles, as well as from layers with multiple discrete layers. The results given above show that different plausible sound speed profiles for the transition layer produce acoustically distinguishable reflection coefficients. Furthermore, differences in the behavior of model reflection coefficients for various profiles can be used quantitatively to focus future experimental efforts and resolve key questions about the transition layer.

However, the model developed above is effectively limited to vertical incidence and provides information about only the compressional wave speed in the vertical direction. To apply the model at nonzero incidence angles with confidence and obtain information

on shear wave speeds and any anisotropy in wave speeds, a series of significant extensions to the present model would be required. There appears to be no fundamental theoretical barrier to such extensions, though the details may become rather complicated. I would recommend that the series of extensions be undertaken in the following order.

First, the model should address reflection from an isotropic elastic solid with profiles of the elastic profiles given by independent functions of z. The result should be a set of three coupled differential equations for generalized reflection coefficients for the compressional wave and each of two orthogonal shear waves. It should be possible to integrate these numerically using standard methods. This seems likely to be relatively straightforward but might actually be rather involved. At this stage, one might want to use a theory of porous media such as that of Biot [1956, 1962] to compute effective elastic parameters for the model as functions of material properties such as porosity. The considerable body of relevant work on Biot models for porous rocks should be useful in this connection (see, for example, Berryman [1981] and Korringa [1981]). The slow compressional wave in the Biot model might simply be modeled as an attenuation of the usual, fast compressional wave. This would be much simpler than a reflection coefficient model based rigorously on a Biot-type model that allowed for profiles.

With an isotropic elastic model in hand, it would be possible to address the issue of wave speed anisotropies. I would expect ordinary and extraordinary waves to appear for each of the compressional and shear modes in the isotropic problem, perhaps doubling the size of the system of equations. This extension probably involves considerable theoretical work because conversions between various modes are likely to be permitted only under specified circumstances. The results and allowed couplings will surely be much simpler under the assumption of a vertical optic axis for the material properties.

Carrying out the extensions just described would provide invaluable insight for any attempt to build a reflection coefficient model based from first principles on a Biot-type model for porous media. In fact, whether such a model would be worthwhile is, I think, only possible to decide based on experience gained with the simpler elastic models. Though further development is beyond the scope of this report, I hope that this discussion will be useful to those beginning such work.

APPENDIX 5A

Consider again the problem presented in Section 5.3.1. Set the absorption r equal to zero and suppose that the density is constant for all z. Suppose further that the sound speed c is a constant c_o below some level z_o, is an arbitrary function of z between z_o and some $z_1 > z_o$, and is constant at some new value c_1 for all $z \geq z_1$. Brekhovskikh [1980, Section 25.4] has constructed a series approximation for the reflection coefficient in powers of layer thickness, $L = z_1 - z_o$, over radiation wavelength, λ, that is useful when the ratio L/λ is small.

The reflection coefficient V at z can be represented in the form

$$V(z) = \frac{q(z)\,v(z) - q_1\,u(z)}{q(z)\,v(z) + q_1\,u(z)} \quad , \tag{5A.1}$$

where u and v are unknown functions of z and where, at vertical incidence and under the conditions stated above, $q(z) = c^{-1}(z)$. The desired reflection coefficient is just $V(z_o)$. Brekhovskikh shows that approximations for $u(z_o)$ and $v(z_o)$ yielding an estimate for $V(z_o)$ good to first order in $k_o L$ are given by

$$v(z_o) = 1 - ik_o \frac{c_o}{c_1} L \quad \text{and} \quad u(z_o) = 1 - ik_o\, c_o\, c_1 \int_{z_o}^{z_1} dz\, c^{-2}(z) \quad . \tag{5A.2}$$

For the sound speed profile given by equation 5.39, one obtains

$$u(z_o) = 1 - 4k_o c_o c_1 \int_0^L dz \left[(c_a + c_o) - (c_1 - c_a) \cos\left[\frac{\pi z}{L} \right] \right]^{-2} \quad . \tag{5A.3}$$

This integral is amenable to contour integration (in the fashion discussed, for example, in section 74 of Churchill et al., 1976), with the result

$$u(z_o) = 1 - k_o L\, c_o c_1 \frac{c_a + c_1}{2(c_a c_o)^{3/2}} \quad . \tag{5A.4}$$

The desired result is thus obtained using the first of equations 5A.2 and equation 5A.4 in equation 5A.1.

For the sound speed profile given by equation 5.40, layer thickness is formally infinite since the hyperbolic tangent approaches its final value only asymptotically. Practically, however, one finds that the effective layer thickness is that change in z required for the sound speed to come within some small percentage of its asymptotic value.

Chapter 6: CONCLUSIONS

In this report, I have proposed breaking down the high-frequency, underice acoustic backscattering problem into three main components. The first is direct backscattering from ice keels, the second is forward reflection and/or scattering from undeformed ice, and the third is reflection from transition layers between water and ice. The roles of each component can be briefly summarized as follows. At grazing angles away from vertical, the ice that is responsible, directly or indirectly, for virtually all backscattered energy is deformed ice, i.e., ice in keels. However, some of the backscattered acoustic energy may be reflected or forward-scattered from undeformed (hence, "relatively flat") ice. Reflection or scattering from either deformed or undeformed ice will be affected by a frequency-dependent modification of the reflection coefficient when an ice–water transition layer occurs. It appears that this is nearly always so at the bottom of undeformed ice, and may often be the case on the faces of ice blocks in keels. The change in the reflection coefficient results from impedance matching of compressional waves and influences on compressional to shear mode conversions by the transition layer.

The available experimental data indicate that direct backscattering from keels often results from areas of ice localized to within approximately 15 m. The proportion of returns from such areas to the total number of returns is unclear. The frequency dependence of backscattering from keels is chaotic over frequency intervals as small as 2 kHz. Results from one experiment suggest that the localized backscattering areas of ice are in fact clusters of spatially smaller, more elemental scatterers. This would make sense, at least qualitatively, of many of the long-range observations. The characteristics of scatterer clustering, such as the distribution of the number of scatterers per cluster and sizes of clusters, could well be the dominant controlling factors in modeling the acoustic environment. However, this idea can presently be regarded as no more than a hypothesis for lack of definitive experimental data. The nature of the elemental scatterers is essentially unknown, though they are often assumed to be ice blocks oriented to produce backward reflection.

Experiments on forward reflection/scattering from undeformed ice strongly indicate that scattering occurs from long (meter to ten meter scale) spatial-wavelength undulations on the underside of the ice. The best present model for such scattering is physical optics, though this theory may be insufficient at the low grazing angles sometimes encountered in underice acoustics. It appears that surface scattering is the dominant mechanism in forward scattering, but roles for other mechanisms such as lateral variations in acoustic impedance cannot be ruled out based on present evidence. There is little or no evidence for the importance of volume scattering in scattering from this ice type.

Experimental data on transition layer effects are sparse. Most inferences regarding this part of the problem are based on theory. In this report I have given a formulation for reflection from a continuous transition layer based on earlier work by Brekhovskikh [1980]. Model results show that different plausible sound speed profiles in the transition layer produce acoustically distinguishable behavior for the reflection coefficients as a

function of frequency. Results from one profile in particular appear to be consistent with experimental data to date. Model results are also useful in planning further experiments to resolve key questions.

A great deal of scientific work remains to understand the roles and behavior of each of the three components of the backscattering problem. In the case of keel backscattering, the crucial experiment is one in which simultaneous short- and long-range acoustic observations are combined to test the cluster hypothesis. If clusters prove to be a real part of the problem, a knowledge of their characteristics will greatly advance acoustic modeling, whatever the nature of the elemental scatterers. The experiments proposed in Chapter 3 would require development of sled-mobile multi-frequency sonar. As for forward scattering, a much greater volume of forward scattering and underice roughness measurements would be required to quantitatively test rough surface scattering theory (and to confirm or rule out the need for theories involving other mechanisms). The forward scattering measurements could conceivably be made by drilling enough holes in the ice through which transducers are lowered. However, the adequacy of this methodology depends sensitively on certain assumptions. A more (theoretically) robust methodology would use a programmable, free-swimming vehicle as a transmitter. It appears that there is no means to obtain sufficient underice roughness information without a similar vehicle. Thus investigation of forward scattering would require a great deal of work on equipment development. Finally, work on the theory of transition layers has helped to define the relevant range and resolution in frequency needed in experiments to test specific profile-hypotheses. The experiments can be conducted using L-shaped arms to deploy transducers and sample disjoint areas of ice, as has already been done. A considerable amount of theoretical development remains to be done on this topic as well.

Concurrent investigation of each topic discussed above would obviously require a very large, extensive, and expensive program. Such a program may not be realistic in the foreseeable future, and so choices must be made as to the relative importance of topics and the order in which to proceed. Such choices are at most only partially based on scientific considerations. From a purely scientific standpoint, the transition layer problem is probably most widely relevant and offers the most immediate, least risky opportunity for investigating new physics. As noted above, transition layers may be important in scattering from both deformed and undeformed ice. The subject is a fairly clean physics problem that has received relatively little theoretical attention to date. A straightforward extension of the theory given in this report to an isotropic elastic case begs to be done, and would display a good deal of intrinsically new physics in the form of mode conversions. It may be useful to link parameters in the theory to porous medium theory. Extensions to anisotropic elastic solids could be carried out to study the change in mode conversions. The experiments required to pursue this topic are quite modest compared with those required for the other topics. From the standpoint of applications, the study of transition layers is most immediately relevant to sonars operating near vertical incidence, including those operating at hundreds of kilohertz (somewhat above the nominal range of interest in this report).

However, the study of transition layers will not lead directly to an improved ability to simulate the acoustic environment for sonars operating at smaller grazing angles. For such sonars, the most relevant topics are evidently direct backscattering from keels and forward scattering from undeformed ice, in that order. Direct backscattering is the source of most of the scattered acoustic energy. Surface bounces could lead to highly significant effects on angle of arrival estimation (glint), pulse elongation, and signal statistics (see Section 4.4). Variations in the reflection coefficient may be important in modulating these processes, but are probably not central.

Thus a final choice of priorities for further study can be made only by reference to a wide variety of practical and application-oriented considerations, the scope of which lies outside this report.

7. REFERENCES

Barrick, D.E., *A More Exact Theory of Backscattering from Statistically Rough Surfaces*, Report 1388-8, The Ohio State University Research Foundation, 1965. (Ph.D. thesis, available from National Technical Information Service, Springfield, VA)

Barrick, D.E., "Rough surface scattering theory based on the specular point theory," *IEEE Transactions on Antennas and Propagation*, vol. AP-16, no. 4, pp. 449–454, 1968a.

Barrick, D.E., "Relationship between the slope probability density function and the physical optics integral in rough surface scattering," *Proceedings of the IEEE*, vol. 56, no. 10, pp. 1728–1729, 1968b.

Barrick, D.E., and B.J. Lipa, "Analysis and interpretation of altimeter sea echo," in *Advances in Geophysics*, vol. 27, B. Saltzman, ed., Academic Press, New York, 1985.

Barton, D.K., "Low-angle radar tracking," *Proceedings of the IEEE*, vol. 62, no. 6, pp. 687–704, 1974.

Beckmann, P., and A. Spizzichino, *The Scattering of Electromagnetic Waves from Rough Surfaces*, Pergamon Press, Oxford, 1963.

Bell, B.M., and T.E. Ewart, "Separating multipaths by global optimization of a multidimensional matched filter," *IEEE Trans. on Acoustics, Speech, and Signal Processing*, vol. ASSP-34, no. 5, pp. 1029–1037, 1986.

Bennington, K.O., "Desalination features in natural sea ice," *Journal of Glaciology*, vol. 6, no. 48, pp. 845–857, 1967.

Berkson, J.M., C.S. Clay, and T.K. Kan, "Mapping the underside of arctic sea ice by backscattered sound," *Journal of the Acoustical Society of America*, vol. 53, no. 3, pp. 777–781, 1973.

Berryman, J.G., "Elastic wave propagation in fluid-saturated porous media II," *Journal of the Acoustical Society of America*, vol. 70, no. 6, pp. 1754–1756, 1981.

Biot, M.A., "Theory of propagation of elastic waves in fluid-saturated porous solid," *Journal of the Acoustical Society of America*, vol. 28, no. 2, pp. 168–191, 1956.

Biot, M.A., "Mechanics of deformation and acoustic propagation in porous media," *Journal of Applied Physics*, vol. 33, no. 4, pp. 1482–1498, 1962.

Blackman, R.B., and J.W. Tukey, *The Measurement of Power Spectra*, Dover Publications, New York, 1959.

Bogorodskii, V.V., V.P. Gavrilo, and V.A. Nikitin, "Sound propagation in ice crystallized from salt water," *Soviet Physics – Acoustics*, vol. 22, no. 2, pp. 158–9, 1976.

Brekhovskikh, L.M., *Waves in Layered Media*, 2nd ed. (translated from Russian by R.T. Beyer), Academic, New York, 1980.

Brown, J.R., "Reverberation under arctic ice," *Journal of the Acoustical Society of America*, vol. 36, no. 3, pp. 601–603, 1964.

Brown, J.R., and D.W. Brown, "Reverberation under arctic sea-ice," *Journal of the Acoustical Society of America*, vol. 40, no. 2, pp. 399–404, 1966.

Brown, J.R., and A.R. Milne, "Reverberation under arctic sea-ice," *Journal of the Acoustical Society of America*, vol. 42, no. 1, pp. 78–82, 1967.

Chapman, R.P., and H.D. Scott, "Backscattering strength of young sea ice," *Journal of the Acoustical Society of America*, vol. 34, pp. 2417–2418, 1964.

Chin-Bing, S.A., "The effect of the physical properties of ice on the high frequency acoustic backscatter from an ice keel model," *Proceedings of the Arctic Oceanography Conference and Workshop* (June 11-14, 1985), Naval Ocean Research and Development Activity, 1985.

Churchill, R.V., J.W. Brown, and R.F. Verhey, *Complex Variables and Applications*, 3rd ed., McGraw-Hill, New York, 1976.

Clay, C.S., and H. Medwin, "Dependence of spatial and temporal correlation of forward-scattered underwater sound on the surface statistics. I. Theory," *Journal of the Acoustical Society of America*, vol. 47, no. 5 (part 2), pp. 1412–1418, 1970.

Clay, C.S., H. Medwin, and W.M. Wright, "Specularly scattered sound and probability density function of a rough surface," *Journal of the Acoustical Society of America*, vol. 53, no. 6, pp. 1677–1682, 1973.

Cox, G.F.N., and W.F. Weeks, "Salinity variations in sea ice," *Journal of Glaciology*, vol. 13, no. 67, pp. 109–120, 1974.

Dainty, J.C., "The statistics of speckle patterns," in *Progress in Optics*, vol. XIV, E. Wolf, ed., North-Holland, Amsterdam, 1976.

Dunn, J.H., D.D. Howard, and A.M. King, "Phenomenon of scintillation noise in radar-tracking systems," *Proceedings of the IRE*, pp. 855–863, 1959.

Eide, L.I., and S. Martin, "The formation of brine drainage features in young sea ice," *Journal of Glaciology*, vol. 14, no. 70, pp. 137–154, 1975.

Ellison, W.T., "Simulation Studies of Under-Ice Acoustic Scattering (U)," Cambridge Acoustical Associates, Inc. Report C-714-270, 1980. (CONFIDENTIAL)

Ewart, T.E., and D.B. Percival, "Forward scattered waves in random media — The probability distribution of intensity," *Journal of the Acoustical Society of America*, vol. 80, no. 6, pp. 1745–1753, 1986.

Francois, R.E., "High resolution observations of under-ice morphology," APL-UW 7712, Applied Physics Laboratory, University of Washington, Seattle, 1977.

Francois, R.E., and W.E. Nodland, "Arctic acoustic measurements at 50 kHz," APL-UW 7313, Applied Physics Laboratory, University of Washington, Seattle, 1973.

Francois, R.E., G.R. Garrison, E.W. Early, T. Wen, and J.T. Shaw, "Acoustic measurements under shore-fast ice in summer, 1977 (U)," APL-UW 7825, Applied Physics Laboratory, University of Washington, Seattle, 1981. (CONFIDENTIAL)

Francois, R.E., K.L. Williams, G.R. Garrison, P.D. Mourad, and T. Wen, "Ice keels I: Intrinsic physical/acoustic properties of sea ice and scattering from ice surfaces (U)," *U.S. Navy Journal of Underwater Acoustics*, vol. 39, no. 4, 1203–1228, 1989.

Garrison, G.R., E.A. Pence, E.W. Early, and H.R. Feldman, "Studies in the marginal ice zone of the Bering Sea — Analysis of the 1973 Bering Sea data (U)," APL-UW 7410, Applied Physics Laboratory, University of Washington, Seattle, 1974. (CONFIDENTIAL)

Garrison, G.R., E.A. Pence, and E.W. Early, "Acoustic studies from an ice floe near Barrow, Alaska in April, 1974," APL-UW 7514, Applied Physics Laboratory, University of Washington, Seattle, 1976a.

Garrison, G.R., R.E. Francois, and E.W. Early, "Acoustic studies from an ice floe in the Chukchi Sea in April, 1975," APL-UW 7608, Applied Physics Laboratory, University of Washington, Seattle, 1976b.

Garrison, G.R., R.E. Francois, E.W. Early, and T. Wen, "Measurements of short range sound propagation in arctic waters 1979–1980," APL-UW 3-83, Applied Physics Laboratory, University of Washington, Seattle, 1983.

Garrison, G.R., R.E. Francois, and T. Wen, "Acoustic returns from ice keels, 1982 (U)," APL-UW 8311, Applied Physics Laboratory, University of Washington, Seattle, 1984. (CONFIDENTIAL)

Garrison, G.R., R.E. Francois, T. Wen, and R.P. Stein, "Acoustic reflections from a newly formed ice keel (U)," APL-UW 8507, Applied Physics Laboratory, University of Washington, Seattle, 1986a. (CONFIDENTIAL)

Garrison, G.R., R.E. Francois, T. Wen, and R.P. Stein, "Measurements of the acoustic reflection from the end of a cylindrical block of arctic ice," APL-UW 8506, Applied Physics Laboratory, University of Washington, Seattle, 1986b.

Garrison, G.R., R.E. Francois, T. Wen, and R.P. Stein, "Reflections from ice keels, 1984 (U)," APL-UW 3-86, Applied Physics Laboratory, University of Washington, Seattle, 1987. (CONFIDENTIAL)

Garrison, G.R., R.E. Francois, T. Wen, and R.P. Stein, "Acoustic reflections from cylindrical blocks of arctic ice, 1986," APL-UW 8707, Applied Physics Laboratory, University of Washington, Seattle, 1988a.

Garrison, G.R., R.E. Francois, T. Wen, and W.J. Felton, "Acoustic reflections from cylindrical blocks of arctic ice, 1988," APL-UW 8815, Applied Physics Laboratory, University of Washington, Seattle, 1988b.

Garrison, G.R., R.E. Francois, and T. Wen, "Ice keel reflections measured in spring 1986 (U)," APL-UW 8912, Applied Physics Laboratory, University of Washington, Seattle, 1989. (CONFIDENTIAL)

Goddard, R.P., "REVGEN-4 — High-fidelity simulation of sonar pulses," APL-UW 8505, Applied Physics Laboratory, University of Washington, Seattle, 1986.

Greene, R.R., and A.P. Stokes, "A model of acoustic backscatter from arctic sea ice," *Journal of the Acoustical Society of America*, vol. 78, no. 5, pp. 1699–1701, 1985.

Grishchenko, V.D., "Microrelief of the bottom surface of drifting sea ice," draft translation 694, Cold Regions Research and Engineering Laboratory, 1979.

Gulin, E.P., "Amplitude and phase fluctuations of a sound wave reflected from a statistically uneven surface," *Soviet Physics — Acoustics*, vol. 8, no. 2, pp. 135–140, 1962.

Gulin, E.P., and K.I. Malyshev, "Statistical characteristics of sound signals reflected from the undulating sea surface," *Soviet Physics — Acoustics*, vol. 8, no. 3, pp. 228–234, 1963.

Hagfors, T., "Scattering and transmission of electromagnetic waves at a statistically rough boundary between two dielectric media," in *Electromagnetic Wave Theory*, Part II, J. Brown, ed., Pergamon, New York, 1967.

Hecht, E., and A. Zajac, *Optics*, Addison-Wesley, Reading, MA, 1974.

Henderson, T.L., "Wide-band monopulse sonar: processor performance in the remote profiling application," *IEEE Journal of Oceanic Engineering*, vol. OE-12, no. 1, pp. 182–197, 1987.

Ishimaru, A., *Wave Scattering and Propagation in Random Media*, 2 vols., Academic Press, New York, 1978.

Jackson, D.R., D.P. Winebrenner, and A. Ishimaru, "Application of the composite roughness model to high-frequency bottom backscattering," *Journal of the Acoustical Society of America*, vol. 79, no. 5, pp. 1410–1422, 1986.

Jackson, J.D., *Classical Electrodynamics*, 2nd ed., Wiley, New York, 1975.

Jakeman, E., "On the statistics of K-distributed noise," *Journal of Physics (A)*, vol. 13, pp. 31–48, 1980.

Jakeman, E., and P.N. Pusey, "A model for non-Rayleigh sea echo," *IEEE Transactions on Antennas and Propagation*, vol. AP-24, no. 6, pp. 806–814, 1976.

Jao, J.K., "Amplitude distribution of composite terrain radar clutter and the K-distribution," *IEEE Transactions on Antennas and Propagation*, vol. AP-32, no. 10, pp. 1049–1062, 1984.

Jezek, K.C., "Acoustic waves incident on a sea ice/sea water interface," CRREL Special Report 85-10, 6 p., 1985.

Jones, R.H., "Fitting a continuous time autoregression to discrete data," in *Applied Time Series Analysis II*, D.F. Findley, ed., Academic Press, New York, 1981.

Kan, T.K., C.S. Clay, and J.M. Berkson, "Sonar mapping of the underside of pack ice," *Journal of Geophysical Research*, vol. 79, no. 3, pp. 483–488, 1974.

Kerr, D.E., and H. Goldstein, "Radar targets and echoes," in *Propagation of Short Radio Waves*, D.E. Kerr, ed., McGraw-Hill, New York, 1951.

Kerr, D.E., W.T. Fishback, and H. Goldstein, "Reflections from the earth's surface," in *Propagation of Short Radio Waves*, D.E. Kerr, ed., McGraw-Hill, New York, 1951.

Kodis, R.D., "A note on the theory of scattering from an irregular surface," *IEEE Transactions on Antennas and Propagation*, vol. AP-14, no. 1, pp. 77–82, 1966.

Korringa, J., "On the Biot-Gassmann equations for the elastic moduli of porous rocks (critical comment on a paper by J.G. Berryman)," *Journal of the Acoustical Society of America*, vol. 70, no. 6, pp. 1752–1753, 1981.

Lake, R.A., and E.L. Lewis, "Salt rejection by sea ice during growth," *Journal of Geophysical Research*, vol. 75, no. 3, pp. 583–597, 1970.

Landau, L.D., and E.M. Lifshitz, *Fluid Mechanics*, vol. 6 of *Course of Theoretical Physics*, translated from Russian by J.B. Sykes and W.H. Reid, Pergamon, New York, 1959.

Langleben, M.P., "Reflection of sound at the water–sea ice interface," *Journal of Geophysical Research*, vol. 75, no. 27, 5243–5246, 1970.

Lapin, A.D., "Sound scattering at a rough solid interface," *Soviet Physics – Acoustics*, vol. 10, no. 1, pp. 58–64, 1964.

Lapin, A.D., "Scattering of sound by a solid layer with rough boundaries," *Soviet Physics – Acoustics*, vol. 12, no. 1, pp. 46–51, 1966.

Lapin, A.D., "Reflection of a plane wave at a rough solid surface," *Soviet Physics – Acoustics*, vol. 14, no. 1, pp. 58–60, 1968.

Lapin, A.D., "Applicability of the Kirchhoff principle for calculation of the sound scattering by an uneven surface of a solid," *Soviet Physics – Acoustics*, vol. 15, no. 1, p. 75, 1969.

Lapin, A.D., "Scattering of surface waves propagating over an uneven liquid–solid interface," *Soviet Physics – Acoustics*, vol. 15, no. 3, pp. 336–339, 1970.

Long, M.W., *Radar Reflectivity of Land and Sea*, Lexington Books, D.C. Heath and Co., Lexington, MA, 1975.

Longuet-Higgins, M.S., "The statistical distribution of the curvature of a random Gaussian surface," *Proceedings of the Cambridge Philosophical Society*, vol. 54, part 4, pp. 439–453, 1958.

Longuet-Higgins, M.S., "The distribution of the sizes of images reflected in a random surface," *Proceedings of the Cambridge Philosophical Society*, vol. 55, part 1, pp. 91–100, 1959.

Longuet-Higgins, M.S., "The focusing of radiation by a random surface when the source is at a finite distance," *Proceedings of the Cambridge Philosophical Society*, vol. 56, part 4, pp. 27–40, 1960a.

Longuet-Higgins, M.S., "Reflection and refraction at a random moving surface. I. Pattern and path of specular points," *Journal of the Optical Society of America*, vol. 50, no. 9, pp. 838–844, 1960b.

Longuet-Higgins, M.S., "Reflection and refraction at a random moving surface. II. Number of specular points in a Gaussian surface," *Journal of the Optical Society of America*, vol. 50, no. 9, pp. 845–850, 1960c.

Longuet-Higgins, M.S., "Reflection and refraction at a random moving surface. III. Frequency of twinkling in a Gaussian surface," *Journal of the Optical Society of America*, vol. 50, no. 9, pp. 851–856, 1960d.

Maykut, G.A., "An introduction to ice in the polar oceans," APL-UW 8510, Applied Physics Laboratory, University of Washington, Seattle, 1985.

McCammon, D.F., and S.T. McDaniel, "The influence of the physical properties of ice on reflectivity," *Journal of the Acoustical Society of America*, vol. 77, no. 2, pp. 499–507, 1985.

McDaniel, S.T., "Vertical directivity of scatter from ice keels (U)," Technical Note, File No. TN 86-156, Applied Research Laboratory, The Pennsylvania State University, State College, PA, 1986. (CONFIDENTIAL)

McDaniel, S.T., "Physical optics theory of scattering from the ice canopy," *Journal of the Acoustical Society of America*, vol. 82, no. 6, pp. 2060–2067, 1987.

McDaniel, S.T., "Perturbation theory applied to high-frequency scatter from the arctic ice," Technical Memorandum, File No. 88-003, Applied Research Laboratory, The Pennsylvania State University, State College, PA, 1988.

McDonald, J.F., and R.C. Spindel, "Implications of Fresnel corrections in a non-Gaussian surface scatter channel," *Journal of the Acoustical Society of America*, vol. 50, no. 3 (part 1), pp. 746–757, 1971.

Mellen, R.H., "Underwater acoustic scattering from arctic ice," *Journal of the Acoustical Society of America*, vol. 40, no. 5, pp. 1200–1202, 1966.

Mellen, R.H., and H.W. Marsh, "Underwater sound reverberation in the Arctic Ocean," *Journal of the Acoustical Society of America*, vol. 35, no. 10, pp. 1645–1648, 1963.

Melton, D.R., and C.W. Horton, Sr., "Importance of the Fresnel correction in scattering from a rough surface. I. Phase and amplitude fluctuations," *Journal of the Acoustical Society of America*, vol. 47, no. 1 (part 2), pp. 290–298, 1970.

Middleton, D., "Intermediate and high-frequency acoustic backscattering cross sections for water–ice interfaces: I. Two-component profile models," Report NUSC TD 7375, Naval Underwater Systems Center, Newport, Rhode Island/New London, Connecticut, 1985.

Milne, A.R., "Underwater backscattering strengths of arctic pack ice," *Journal of the Acoustical Society of America*, vol. 36, no. 8, pp. 1551–1556, 1964.

Miyamoto, R.T., "The use of simulators to exercise ship sonar classification algorithms," APL-UW ltr, 10/21/86, Serial 4C7784, Applied Physics Laboratory, University of Washington, 1986.

Moore, R.K., "Ground Echo," chapter 25 in *Radar Handbook*, McGraw-Hill, New York, 1970.

Ostrovityanov, R.V., and F.A. Basalov, *Statistical Theory of Extended Radar Targets*, translated from Russian by W.F. Barton and D.K. Barton, Artech House, Dedham, MA, 1985.

Pierce, A.D., *Acoustics: An Introduction to Its Physical Principles and Applications*, McGraw-Hill, New York, 1981.

Pierce, J.G., and K. Hickox, "A review of the Soviet open literature on acoustic research in the Arctic," report number KFR 423-83, Ketron, Inc., Arlington, VA, 1983.

Posey, J.W., G.H. Branch, S.A. Chin-Bing, and G. Tango, "High frequency acoustic reflection from flat sea ice," *Proceedings of the Arctic Oceanography Conference and Workshop* (June 11–14, 1985), Naval Ocean Research and Development Activity, 1985.

Rice, S.O., "Mathematical analysis of random noise," in *Select Papers on Noise and Stochastic Processes*, N. Wax, ed., Dover, New York, 1954.

Rothrock, D.A., and A.S. Thorndike, "Geometrical properties of the underside of sea ice," *Journal of Geophysical Research*, vol. 85, no. C7, pp. 3955–3963, 1980.

Schwarz, J., and W.F. Weeks, "Engineering properties of sea ice," *Journal of Glaciology*, vol. 19, no. 8, pp. 499–531, 1977.

Sims, R.J., and E.R. Graf, "The reduction of radar glint by diversity techniques," *IEEE Transactions on Antennas and Propagation*, vol. AP-19, no. 4, pp. 462–468, 1971.

Skolnick, M.I., "Sea Echo," chapter 26 in *Radar Handbook*, McGraw-Hill, New York, 1970.

Skolnick, M.I., *Introduction to Radar Systems*, 2nd ed., McGraw-Hill, New York, 1980.

Slepian, D., "On Bandwidth," *Proceedings of the IEEE*, vol. 64, no. 3, pp. 292–300, 1976.

Slepian, D., "Some comments on Fourier analysis, uncertainty, and modeling," *SIAM Review*, vol. 25, no. 3, pp. 379–393, 1983.

Stanton, T.K., K.C. Jezek, and A.J. Gow, "Acoustical reflection and scattering from the underside of laboratory grown sea ice: Measurements and predictions," *Journal the Acoustical Society of America*, vol. 80, no. 5, pp. 1486–1494, 1986.

Stogryn, A., "Electromagnetic scattering from rough, finitely conducting surfaces," *Radio Science*, vol. 2 (new series), no. 4, pp. 415–428, 1967.

Thorsos, E.I., "Surface forward scattering and reflection," APL-UW 7-83, Applied Physics Laboratory, University of Washington, Seattle, 1984.

Thorsos, E.I., "The validity of the Kirchhoff approximation for rough surface scattering using a Gaussian roughness spectrum," *Journal of the Acoustical Society of America*, vol. 83, no. 1, pp. 78–92, 1988.

Tolstoy, I., *Wave Propagation*, McGraw-Hill, New York, 1973.

Ulaby, F.T., R.K. Moore, and A.K. Fung, *Microwave Remote Sensing—Active and Passive*, vol. II, Addison-Wesley, Reading, MA, 1982.

Verrall, R., and J. Ganton, "The reflection of acoustic waves in sea water from an ice covered surface," Technical Memorandum 77-8, Defence Research Establishment Pacific, 31 pp., Victoria, B.C., 1977.

Wakatsuchi, M., and T. Kawamura, "Formation processes of brine drainage channels in sea ice," *Journal of Geophysical Research*, vol. 92, no. C7, pp. 7195–7197, 1987.

Watson, J.G., and J.B. Keller, "Reflection, scattering, and absorption of acoustic waves by rough surfaces," *Journal of the Acoustical Society of America*, vol. 74, no. 6, pp. 1887–1894, 1983.

Weeks, W.F., and S.F. Ackley, "The growth, structure, and properties of sea ice," CRREL Monograph 82-1, U.S. Army Cold Regions Research and Engineering Lab, 1982.

Winebrenner, D.P., "A surface field phase perturbation method for scattering from rough surfaces," Ph.D. thesis, University of Washington, 1985. Available as APL-UW 2-85, informal document series.

Wright, J.W. "Radar glint—a survey," *Electromagnetics*, vol. 4, pp. 205–227, 1984.

Yamamoto, T., and M. Badiey, "Propagator matrix for acoustic wave propagation through anisotropic porous media," in *Ocean Seismo-Acoustics—Low-Frequency Underwater Acoustics*, T. Akal and J.M. Berkson, eds., (vol. 16 in the NATO Conference Series, pp. 463–472), Plenum Press, New York, 1986.

Yew, C.H., and X. Weng, "A study of the reflection and refraction of waves at the interface of water and porous sea ice," *Journal of the Acoustical Society of America*, vol. 82, no. 1, pp. 342–353, 1987.

Yordanov, O.I., and M.A. Michalev, "Distribution of specular points on the ocean surface: Bistatic scattering," in the *Proceedings of the IGARSS '88 Symposium*, Ref. ESA SP-284 (IEEE 88CH2497-6), pp. 1317–1318, ESA Publications Division, 1988.

Zornig, J.G., P.M. Schultheiss, and J. Snyder, "Bistatic surface scattering strength at short wavelengths," Technical Report CS-9, Yale University, New Haven, Connecticut, 1977.